

**Correspondence to:**

Professor W. Henderson,  
Chemistry,  
School of Science,  
University of Waikato,  
Private Bag 3105,  
Hamilton 3240,  
New Zealand  
e-mail w.henderson@waikato.ac.nz

**Coordination chemistry of the isomeric 3- and 4-mercaptobenzoate ligands:  
versatile hydrogen-bonding analogues of the thiosalicylate (2-  
mercaptobenzoate) ligand**

Edward R. T. Tiekink<sup>a</sup> and William Henderson<sup>b,\*</sup>

<sup>a</sup> Research Centre for Crystalline Materials, School of Science and Technology, Sunway University, No. 5 Jalan Universiti, 47500 Bandar Sunway, Selangor Darul Ehsan, Malaysia

<sup>b</sup> Chemistry, School of Science, University of Waikato, Private Bag 3105, Hamilton 3240, New Zealand

\* Corresponding author.

Email address: w.henderson@waikato.ac.nz (W. Henderson)

Received:

## ABSTRACT

This review summarises the coordination chemistry of the isomeric 3- and 4-mercaptobenzoate ligands, derived from  $\text{HSC}_6\text{H}_4\text{COOH}$ , being analogues to the widely-studied 2-mercaptobenzoate (thiosalicylate) ligand. The 3- and 4-mercaptobenzoate ligands show a wide range of coordination modes, including monodentate (through either S or less commonly O), chelation through the carboxylate group alone, as well as a wide range of bridging modes. However, S,O-chelation, which is prevalent for thiosalicylate complexes, is not found in the 3MBA and 4MBA analogues. In the solid-state, complexes of 3MBA and 4MBA ligands containing protonated carboxylic acid groups typically undergo aggregation through formation of classical hydrogen-bonded carboxylic acid dimer motifs, which can be supplemented by additional interactions such as aurophilic ( $\text{Au}\cdots\text{Au}$ ) interactions in the case of gold(I) complexes. The hybrid hard-soft nature of 3MBA and 4MBA ligands facilitates the use of these ligands in the construction of early-late heterobimetallic complexes. These ligands also find numerous applications (such as the protection of metallic gold and silver nanoparticles), which are especially prevalent for 4MBA where the para carboxylate/carboxylic acid group is remote from the sulphur coordination site.

Keywords: Mercaptobenzoate; Thiolate ligand; Carboxylate ligand; Complexes; Structures; Hydrogen-bonding

## List of abbreviations

bipy	2,2'-bipyridine
Cy	cyclohexyl
DFT	Density Functional Theory
DMF	N,N-dimethylformamide
DMSO	dimethylsulphoxide, Me <sub>2</sub> S(=O)
dppb	1,4-bis(diphenylphosphino)butane, Ph <sub>2</sub> P(CH <sub>2</sub> ) <sub>4</sub> PPh <sub>2</sub>
dppe	1,2-bis(diphenylphosphino)ethane, Ph <sub>2</sub> P(CH <sub>2</sub> ) <sub>2</sub> PPh <sub>2</sub>
dppp	1,3-bis(diphenylphosphino)propane, Ph <sub>2</sub> P(CH <sub>2</sub> ) <sub>3</sub> PPh <sub>2</sub>
ESI MS	electrospray ionisation mass spectrometry
Fc	ferrocenyl, (η <sup>5</sup> -C <sub>5</sub> H <sub>5</sub> )Fe(η <sup>5</sup> -C <sub>5</sub> H <sub>4</sub> )
H <sub>2</sub> 3MBA	3-mercaptobenzoic acid
H <sub>2</sub> 4MBA	4-mercaptobenzoic acid
MBA	mercaptobenzoate ligand (generic)
NHC	N-heterocyclic carbene ligand
OTf	triflate, CF <sub>3</sub> SO <sub>3</sub> <sup>-</sup>
phen	1,10-phenanthroline
PPN	bis(triphenylphosphine)iminium, [(Ph <sub>3</sub> P) <sub>2</sub> N] <sup>+</sup>
Py	2-pyridyl group C <sub>5</sub> H <sub>4</sub> N
THF	tetrahydrofuran
tta	thenoyltrifluoroacetate, C <sub>4</sub> H <sub>3</sub> SC(O)CHC(O)CF <sub>3</sub>

## Contents

1. Introduction
2. 3- and 4-Mercaptobenzoic acids
3. Complexes with s-block metals
4. Organotin derivatives
  - 4.1 *Triorganotin complexes*
  - 4.2 *Diorganotin complexes*
5. Complexes of titanium, zirconium and hafnium
6. Complexes of chromium, molybdenum and tungsten
7. Complexes of manganese, technetium and rhenium
8. Complexes of iron, ruthenium and osmium
9. Complexes of cobalt, rhodium and iridium
10. Complexes of nickel, palladium and platinum
11. Complexes of copper, silver and gold
  - 11.1 *Copper complexes*
  - 11.2 *Silver complexes*
  - 11.3 *Gold complexes*
12. Complexes of zinc, cadmium and mercury
13. Complexes of the lanthanide and actinide elements
14. Heterobimetallic coordination compounds containing bridging 3MBA or 4MBA ligands
15. Use of MBA ligands in the functionalisation of metal chalcogenide materials
16. Use of MBA ligands in the functionalisation of metal clusters, nanoparticles and metallic surfaces
  - 16.1 *Metal carbonyl cluster derivatives*
  - 16.2 *Well-defined non-carbonyl metal clusters containing MBA ligands*

*16.3 Metal nanoparticles*

*16.4 Metal surfaces*

17. Conclusions

18. Acknowledgements

## 1. Introduction

Hybrid ligands containing a combination of soft sulphur and hard oxygen donor atoms are of significant interest for their coordination chemistry. This combination of donor groups accommodates a diverse variety of metal ions spanning the entire Periodic Table. While the coordination chemistry of such ligands has been of interest for a number of years, applications in areas such as materials chemistry are increasingly exploiting this heterodifunctional nature as a means of coupling different materials.

Mercaptobenzoic acids are of particular interest in this class of hybrid ligand, due to their availability and stability, combined with their rich coordination chemistry. The coordination chemistry of the 2MBA ligand (often referred to by its common name of thiosalicylate, Chart 1) has been the subject of a recent review.[1] Ligands derived from thiosalicylic acid (by deprotonation of one or both acidic hydrogens) are able to coordinate to a diverse range of metal centres, through one or both of the thiolate-sulphur and the carboxylate group, in a variety of binding modes, including monodentate, chelating and a range of bridging modes. In this review we summarise the coordination chemistry of the isomeric 3MBA and 4MBA ligands (Chart 1), with a particular emphasis on the structural and supramolecular chemistry of the resulting complexes. Due to geometric constraints these ligands do not participate in metal chelation, however this 'deficiency' is replaced by the formation of a significant number of supramolecular structures in coordination complexes of 3MBA and 4MBA where the ligand is S-bonded to one or more metals, and the free COOH group then participates in hydrogen-bonding interactions. Carboxylic acids are well-known to form hydrogen-bonded dimers in the solid-state.[2,3] As a result, the carboxylic acid group is well established as a versatile functionality in supramolecular chemistry, and a wide variety of hydrogen-bonded networks have been described based on coordination compounds [4,5,6] as well as organometallic [7,8,9,10] compounds. Additional interest in 3MBA and 4MBA ligands

comes from their ability to act as bridging ligands between chemically disparate metal centres, e.g. early and later transition metals; this is summarised in Section 14 of this Review.

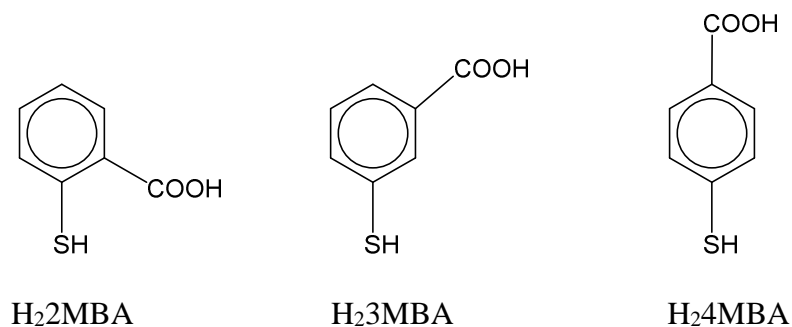


**Chart 1** Structures of the isomeric mercaptobenzoic acids.

Because of space restrictions, the coverage of this review does not include coordination compounds of 3MBA or 4MBA ligands which involve either (i) functionalisation of the carboxylate group into ester or amide derivatives, such as S-bonded technetium [11] or platinum [12] complexes of the  $[\text{SC}_6\text{H}_4\text{CO}_2\text{R}]^-$  ( $\text{R} = \text{Me}, \text{Et}$ ) ligands; or (ii) functionalisation of the thiol group into thioether derivatives such as  $[\text{MeSC}_6\text{H}_4\text{CO}_2]^-$ , such as occurs in O-bonded oxido/hydroxido complexes of iron.[13]

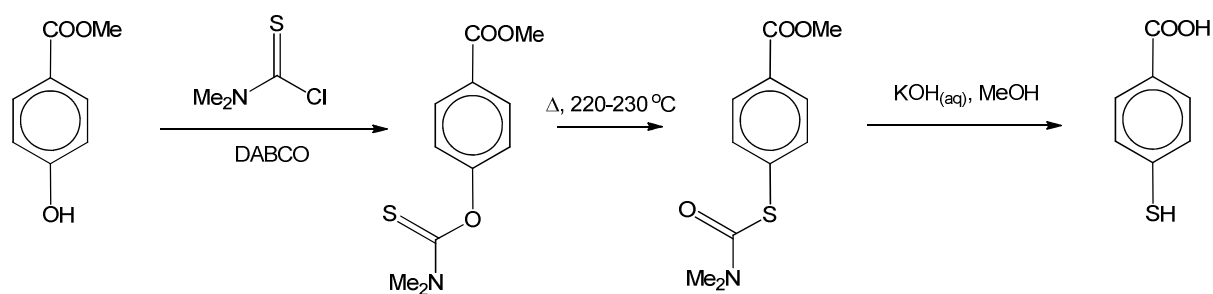
The illustrative molecular structure diagrams herein are original, being drawn with DIAMOND [14] using atomic coordinates obtained from the Cambridge Crystallographic Data Centre [15].

## 2. 3- and 4-Mercaptobenzoic acids

H<sub>2</sub>3MBA and H<sub>2</sub>4MBA are both commercially available in gram-quantities. These compounds can also be synthesised by a variety of methods, some of which are summarised below.

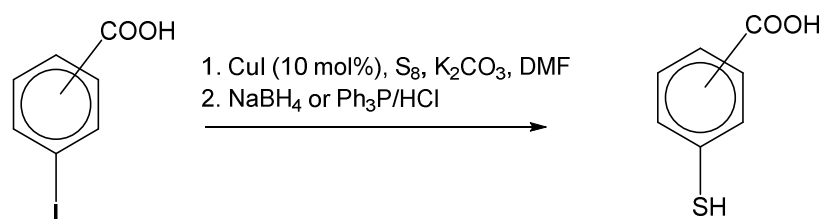
Reaction of m- or p-chlorobenzoic acids with elemental sulphur in a molten salt (NaOH/KOH) medium at 360 °C for 3 min. has been reported to give H<sub>2</sub>3MBA and H<sub>2</sub>4MBA in yields of ca 44 and 61%, respectively.[16] H<sub>2</sub>4MBA can be synthesised as a pale-yellow

solid (m.p. 218 °C) from methyl 4-hydroxybenzoate in three steps, in 57% yield, according to Scheme 1.[17,18]

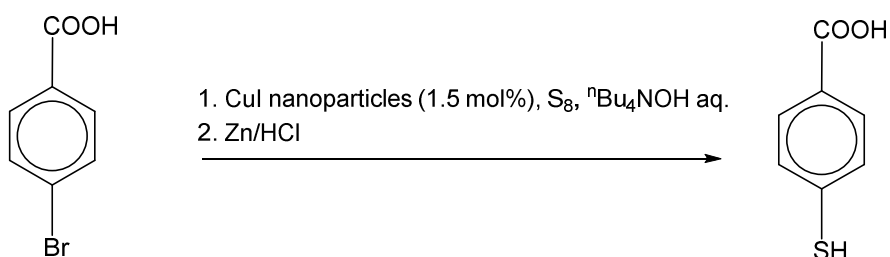


**Scheme 1**

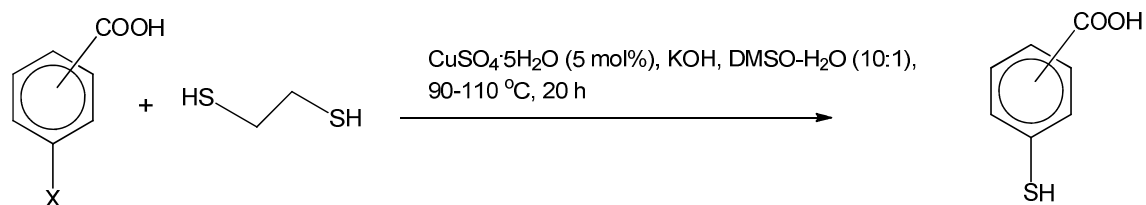
Copper(I) iodide has been employed in the synthesis of mercaptobenzoic acids, together with other related aryl thiols. The reaction of aryl iodides with sulphur powder, catalysed by CuI, followed by reduction of the mixture with NaBH<sub>4</sub> or Ph<sub>3</sub>P/HCl gave H<sub>2</sub>3MBA and H<sub>2</sub>4MBA in 91 and 87% yields, respectively, Scheme 2.[19] This work was subsequently developed using CuI nanoparticles, leading to a synthesis of H<sub>2</sub>4MBA in 87% yield starting from 4-bromobenzoic acid; reaction conditions are summarised in Scheme 3.[20] Ethane-1,2-dithiol has also been used as the thiol source for single-step reactions with aryl halides, catalysed by 5 mol% CuSO<sub>4</sub>·5H<sub>2</sub>O, giving H<sub>2</sub>3MBA and H<sub>2</sub>4MBA, Scheme 4.[21]



**Scheme 2**



### Scheme 3



Compound	X	Yield (%)
H <sub>2</sub> 4MBA	I	94
H <sub>2</sub> 4MBA	Br	91
H <sub>2</sub> 3MBA	I	94

### Scheme 4

Although there have been no X-ray structure determinations on free (thiol-containing) H<sub>2</sub>3MBA or H<sub>2</sub>4MBA, the related disulphides (SC<sub>6</sub>H<sub>4</sub>COOH)<sub>2</sub> have been structurally characterised.[22] Both compounds are 2-fold symmetric and form puckered chains through the formation of hydrogen-bonds between carboxylic acid groups, as shown in Figs. 1 and 2 for the 3- and 4- isomers, respectively.

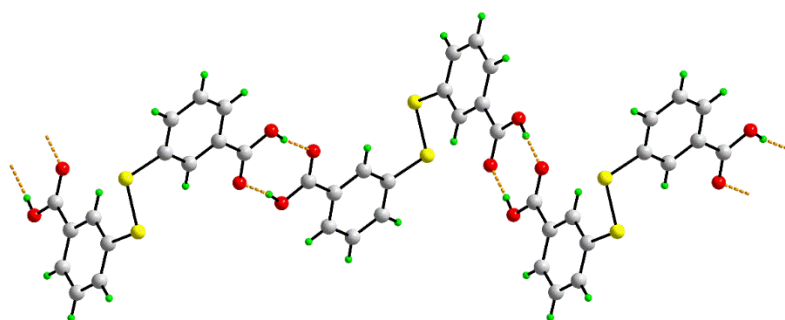


**Fig. 1.** A view of the hydrogen-bonded chain structure formed by the disulphide (SC<sub>6</sub>H<sub>4</sub>COOH-3)<sub>2</sub> (CUVCUS). Colour code in this and subsequent figures: sulphur, yellow; red, oxygen; nitrogen, blue; carbon, grey; hydrogen, bright-green. The O-H $\cdots$ O hydrogen-bonds are shown as orange dashed lines.

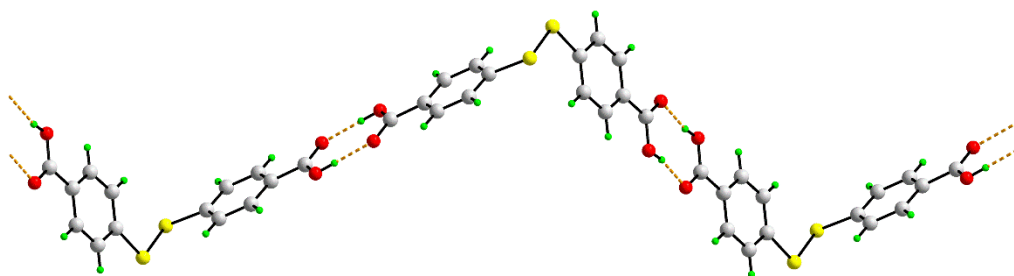


**Fig. 2.** A view of the hydrogen-bonded chain structure formed by the disulphide  $(\text{SC}_6\text{H}_4\text{COOH-4})_2$  (CUVDAZ).

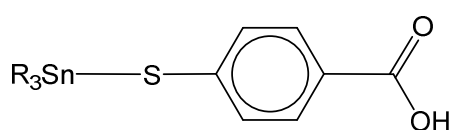
### 3. Complexes with s-block metals

There is only one characterised example of an s-block metal derivative, this being  $[\text{Be}_4\text{O}(\text{O}_2\text{CC}_6\text{H}_4\text{SH})_6]$ , formed by the reaction of H<sub>2</sub>4MBA with  $\text{Be}(\text{OH})_2$ . The compound was proposed to have the same cage structure adopted by basic beryllium acetate  $[\text{Be}_4\text{O}(\text{OAc})_6]$ , with 4  $\text{Be}^{2+}$  ions clustered around a  $\mu_4$ -oxido ligand, and the Be ions of the resulting  $\{\text{Be}_4(\mu_4\text{-O})\}$  tetrahedron bridged by carboxylato ligands, leaving six uncomplexed free thiol groups, consistent with the strongly oxophilic nature of beryllium.[23]

### 4. Organotin derivatives

#### 4.1 Triorganotin complexes

The preparation of organotin(IV) derivatives is readily achieved by simple metathetical reactions starting with the organotin chlorides. A series of 4MBA complexes  $\text{R}_3\text{Sn}(\text{SC}_6\text{H}_4\text{CO}_2\text{H-4})$  ( $\text{R} = \text{Me}, \text{nBu}, \text{Ph}$  or  $\text{CH}_2\text{Ph}$ ) have been prepared by reaction of the respective triorganotin chloride  $\text{R}_3\text{SnCl}$  with H<sub>2</sub>4MBA and NaOEt, to give the complexes **1**. [24]



**1**

The structure of  $\text{Ph}_3\text{Sn}(\text{SC}_6\text{H}_4\text{COOH-4})$  has been determined, and forms a hydrogen-bonded carboxylic acid dimer structure, Fig. 3, where the tin centre is four-coordinate, and bonded to the thiolate-sulphur.[24] Such carboxylic acid dimers are a commonly-repeating structural motif in the solid-state structures of 3MBA and 4MBA complexes, and many other examples are described in subsequent sections of this review. By contrast, in an earlier study, the triphenyltin complex was reported to have an oxygen-bonded ligand, viz.  $\text{Ph}_3\text{SnOC}(\text{O})\text{C}_6\text{H}_4\text{SH-4}$ ; analysis of this complex by  $^{13}\text{C}$  and  $^{119}\text{Sn}$  NMR spectroscopies was used to provide evidence that the complex exists in a monomeric form in solution.[25]

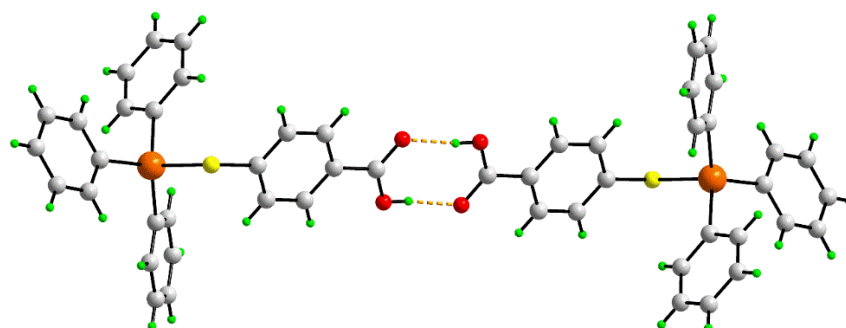


**Fig. 3.** The solid-state structure of  $\text{Ph}_3\text{Sn}(\text{SC}_6\text{H}_4\text{CO}_2\text{H-4})$  (LAVKAV) showing the formation of a carboxylic acid dimer between two centrosymmetrically-related molecules. Additional colour code: key heavy element, orange.

Several compounds with two triorganotin coordinated to a single MBA ligand have also been reported. Reaction of  $\text{H}_2\text{4MBA}$  and the organotin chlorides  $\text{R}_3\text{SnCl}$  ( $\text{R} = \text{Me}, \text{nBu}, \text{PhCH}_2$  and  $\text{Ph}$ ) in the presence of  $\text{NaOEt}$  gives the complexes  $[\text{R}_3\text{SnSC}_6\text{H}_4\text{COOSnR}_3\text{-4}]$ . [24] The bis(triphenyltin) derivative of 3MBA,  $[\text{Ph}_3\text{SnOC}(\text{O})\text{C}_6\text{H}_4\text{SSnPh}_3\text{-3}]$ , has also been prepared by reaction of  $\text{H}_2\text{3MBA}$  with  $\text{Ph}_3\text{SnCl}$  and  $\text{NaOEt}$  in benzene.[26] Crystals of the 3- [26] and 4- [24] isomers of the complex  $[\text{Ph}_3\text{SnOC}(\text{O})\text{C}_6\text{H}_4\text{SSnPh}_3]$  have been characterised by single-crystal X-ray diffraction; the 3-isomer is shown in Fig. 4, and the 4- isomer in Fig. 5. In both structures the tin centre coordinated to the thiolate-sulphur is four-coordinate, while the

other tin centre is coordinated to one oxygen atom of the carboxylate group via a relatively short Sn–O bond [3MBA structure 2.049(2), 4MBA structure 2.055(4) Å] and there is a secondary, weaker interaction to the C=O oxygen, which is somewhat shorter in the 4MBA complex [2.738(4) Å] compared to the 3MBA complex [2.872(3) Å]. This results in a pseudo-five-coordinate, cis-C<sub>3</sub>O<sub>2</sub>, geometry at the carboxylate-bound tin centres. As expected, there are no hydrogen-bonding interactions between molecules of these compounds, due to the absence of free carboxylic acid groups. The 4MBA compound Ph<sub>3</sub>SnOC(O)C<sub>6</sub>H<sub>4</sub>SSnPh<sub>3</sub> has been evaluated for insecticidal activity against early fourth-instar larvae of a resistant strain of the diamondback moth *Plutella xylostella*. [27]

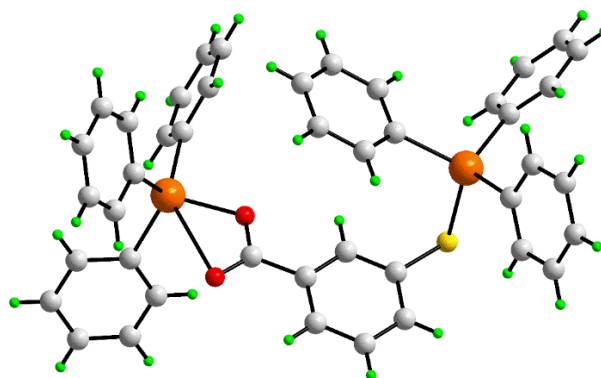


**Fig. 4.** Molecular structure of [Ph<sub>3</sub>SnSC<sub>6</sub>H<sub>4</sub>COOSnPh<sub>3</sub>-3] (JAXWUB).

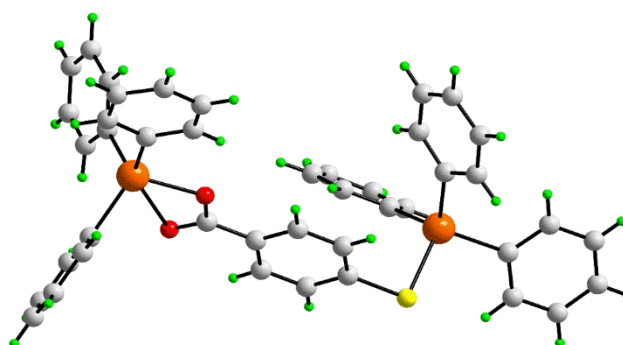
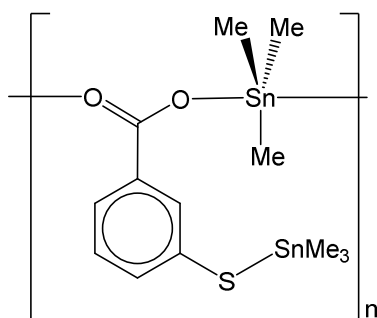


**Fig. 5.** Molecular structure of the 4MBA compound [Ph<sub>3</sub>SnSC<sub>6</sub>H<sub>4</sub>COOSnPh<sub>3</sub>-4] (LAVJUO) as its ethanol solvate (not shown).

The X-ray structure of the bis(trimethyltin) compound derived from 3MBA, viz. **2** (synthesised by reaction of H<sub>2</sub>3MBA with NaOEt in benzene followed by addition of Me<sub>3</sub>SnCl) has been determined, Fig. 6.[28] The structure comprises a tin-carboxylate polymeric chain, with a helical topology and with five-coordinate, trans-C<sub>3</sub>O<sub>2</sub>, tin centres, but with disparate Sn–O bond lengths of 2.153(3) and 2.465(3) Å. Reflecting this disparity, the C–O bond distances of 1.240(5) and 1.273(4) Å are consistent with double and single bonds in the carboxylate group. The thiolate atom is bonded to a SnMe<sub>3</sub> group, resulting in four-coordination at this tin centre as a result of its reduced Lewis acidity. Such interplay between monomeric, cis-C<sub>3</sub>O<sub>2</sub>, Figs 4 and 5, and polymeric, trans-C<sub>3</sub>O<sub>2</sub>, Fig. 7, structures is well documented in triorganotin chemistry and is, to a first approximation, dictated by the size of the tin- and/or organic-bound substituents [29].



**2**

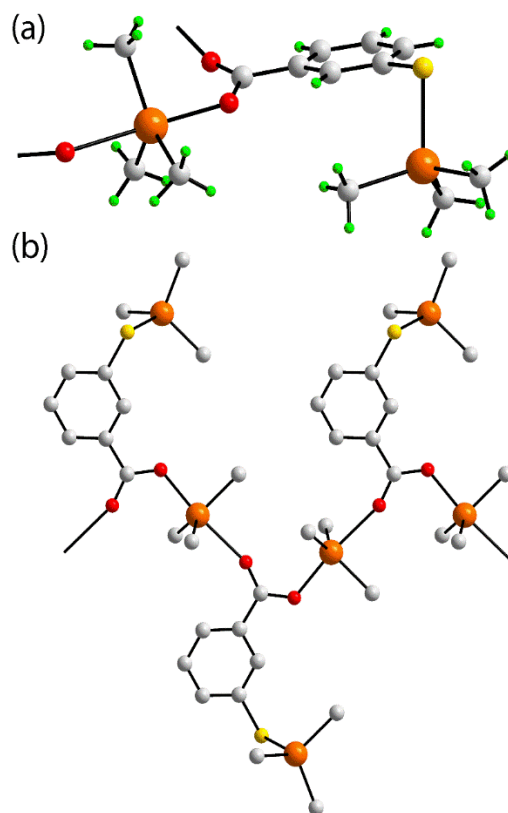


**Fig. 6.** The X-ray structure of  $[\text{Me}_3\text{SnSC}_6\text{H}_4\text{COOSnMe}_3\text{-}3]_n$  (JAYLOL): (a) the bridging of two  $\text{SnMe}_3$  moieties by the 3MBA ligand and (b) formation of the tin-carboxylate chain structure with H atoms omitted.

The structure of the bis(trimethyltin) 4MBA complex  $[\text{Me}_3\text{SnSC}_6\text{H}_4\text{COOSnMe}_3\text{-}4]$  has also been determined, Fig. 7, and shows a similar helical structure to that of the 3-isomer.[24]

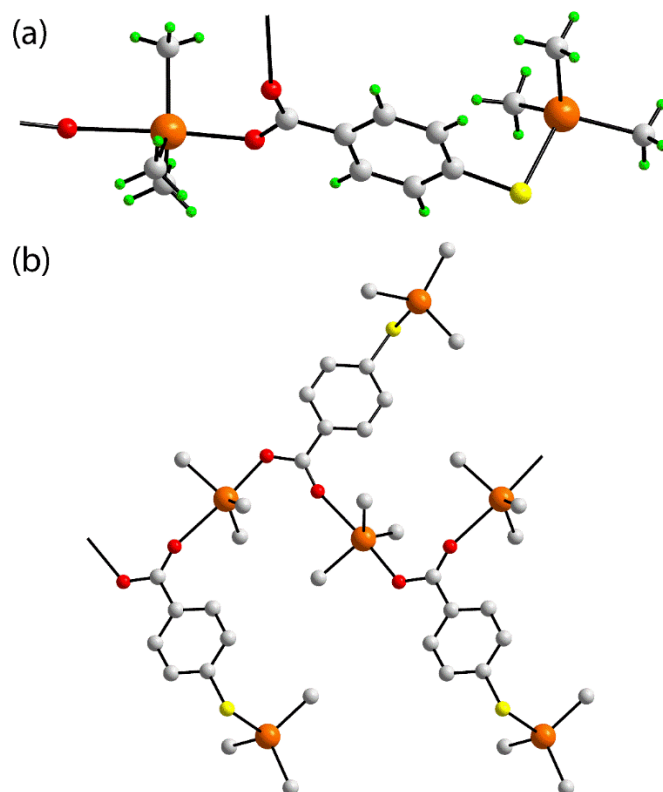
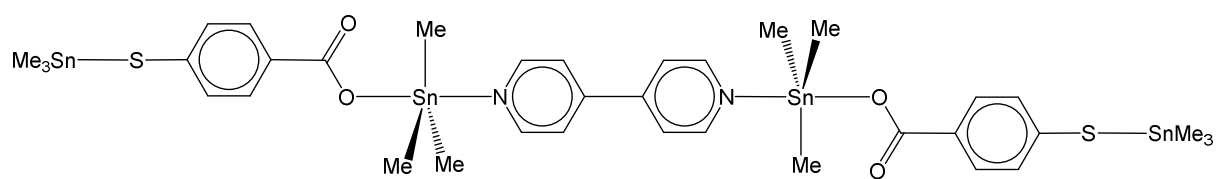


**Fig. 7.** The X-ray structure of  $[\text{Me}_3\text{SnSC}_6\text{H}_4\text{COOSnMe}_3\text{-4}]_n$  (LAVJEY): (a) the bridging of two  $\text{SnMe}_3$  moieties by the 4MBA ligand and (b) formation of the tin-carboxylate chain structure (H atoms are omitted), analogous to the 3MBA analogue shown in Fig. 6.

The bis(trimethyltin) derivative of 4MBA forms an adduct with 4,4'-bipyridine **3**, which was structurally characterised, Fig. 8.[24] This centrosymmetric complex contains four-coordinate tins coordinated to the electron-donating thiolate ligands (giving an  $\text{C}_3\text{S}$  donor set) together with five-coordinate (trigonal bipyramidal) tins bonded to the 4MBA oxygen and a nitrogen atom of the 4,4'-bipy ligand (giving an  $\text{C}_3\text{NO}$  donor set).



**3**

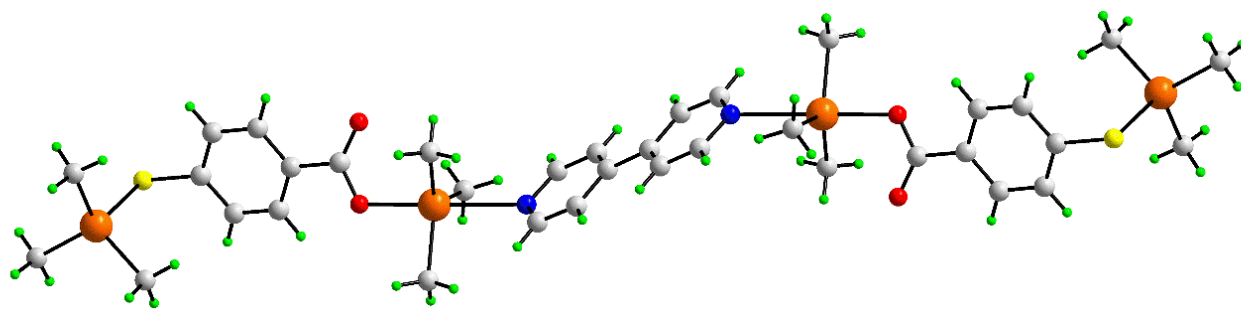
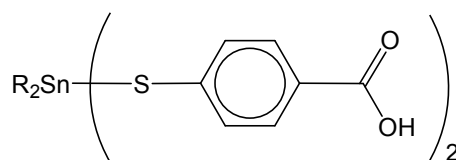


**Fig. 8.** Molecular structure of the 4,4'-bipyridine adduct of the 4MBA derivative  $\text{Me}_3\text{SnSC}_6\text{H}_4\text{CO}_2\text{SnMe}_3$  (LAVKEZ). Additional colour code: nitrogen, blue.

#### 4.2 Diorganotin complexes

The structural chemistry of diorganotin derivatives with 3MBA and 4MBA is considerably more complex than the triorganotin analogues, as a result of: (i) the combination of strong Sn–O and Sn–S bonds, facilitating ligand bridging, (ii) the ability of tin to expand its coordination number from 4 to 5 or 6 and (iii) the ability to form supramolecular structures through extended hydrogen-bonding and  $\pi \cdots \pi$  interactions.

Reactions of the diorganotin dichlorides  $\text{R}_2\text{SnCl}_2$  ( $\text{R} = \text{Me}, n\text{Bu}, \text{Ph}, \text{CH}_2\text{Ph}$ ) with 2 equivalents of  $\text{H}_2\text{4MBA}$  and  $\text{NaOEt}$  in benzene gave the respective bis complexes  $\text{R}_2\text{Sn}(\text{SC}_6\text{H}_4\text{CO}_2\text{H-4})_2$  **4** in good yields.[24] The X-ray structures of the phenyl and n-butyl derivatives were determined and found to be similar;[24] the butyl derivative is shown in Fig. 9. The tin atoms have a tetrahedral geometry, Fig. 9a and the complex dimerises through the formation of two carboxylic acid dimers stacked on top of each other, Fig. 9b. The phenyl rings, separated between their centres by approximately 3.96 Å, are not coplanar.



**4**

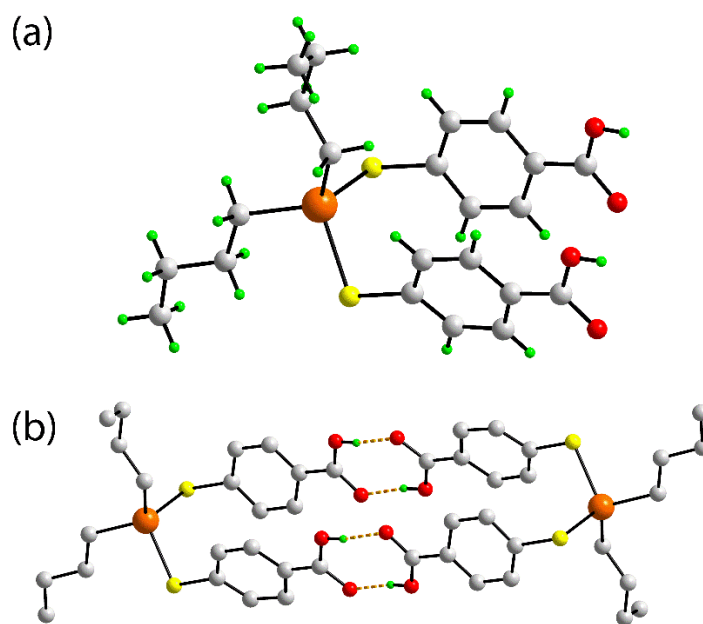


**Fig. 9.** Structure of  $n\text{Bu}_2\text{Sn}(\text{SC}_6\text{H}_4\text{CO}_2\text{H-4})_2$  (LAVJOI): (a) molecular structure and (b) the formation of a centrosymmetric dimer through two pairs of carboxylic acid interactions (non-acidic H atoms are omitted).

Reactions of  $\text{R}_2\text{SnCl}_2$  ( $\text{R} = \text{Me}$  or  $n\text{Bu}$ ) with  $\text{H}_2\text{3MBA}$  in 95% ethanol with added sodium ethoxide gave complexes that can be formulated as  $\{[\text{R}_2\text{Sn}(\text{O}_2\text{CC}_6\text{H}_4\text{S-3})\text{R}_2\text{Sn}(\text{SC}_6\text{H}_4\text{CO}_2\text{-3})\text{SnR}_2]\text{O}\}_2$ , which are centrosymmetric, hexanuclear macrocycles with double-cavity structures. These compounds are soluble in typical organic solvents, including benzene, ether, chloroform and lower alcohols.[30] The structure of the methyl derivative is shown in Fig. 10, while that of the n-butyl analogue is shown in Fig. 11. There are three types of tin in the methyl complex: four-coordinated,  $\text{C}_2\text{S}_2$  (exocyclic) tin atoms, penta-coordinated (exocyclic) tins with a distorted trigonal bipyramidal,  $\text{C}_2\text{O}_3$ , geometry, and hexa-coordinated,  $\text{C}_2\text{O}_4$  tins in the four-membered  $\text{Sn}_2\text{O}_2$  ring system. The n-butyl analogue, with two independent but chemically similar molecules comprising the crystallographic asymmetric unit, is analogous, but not identical, to the methyl complex, because two of the carboxylate

groups in the former have a chelating-bridging mode to two tin centres, giving rise to a tetradentate di-anion.

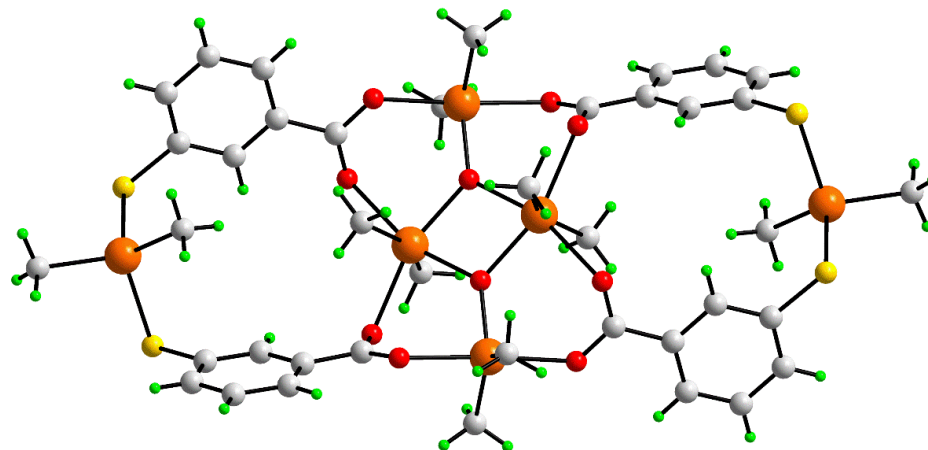


**Fig. 10.** The molecular structure of  $\{[\text{Me}_2\text{Sn}(\text{O}_2\text{CC}_6\text{H}_4\text{S}-3)\text{Me}_2\text{Sn}(\text{SC}_6\text{H}_4\text{CO}_2-3)\text{SnMe}_2]\text{O}\}_2$  (TEBJUG).

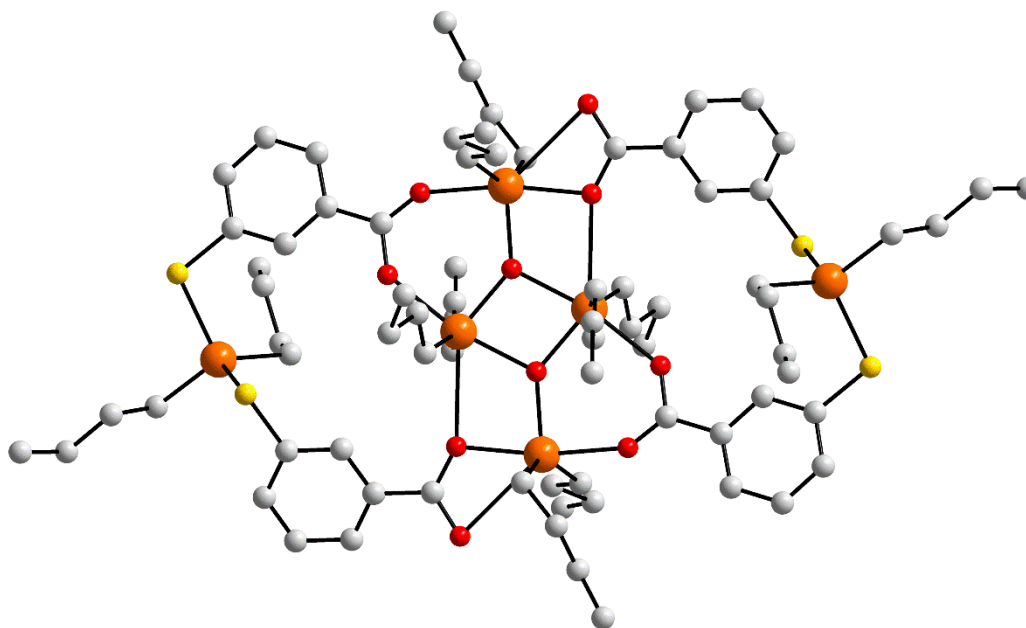
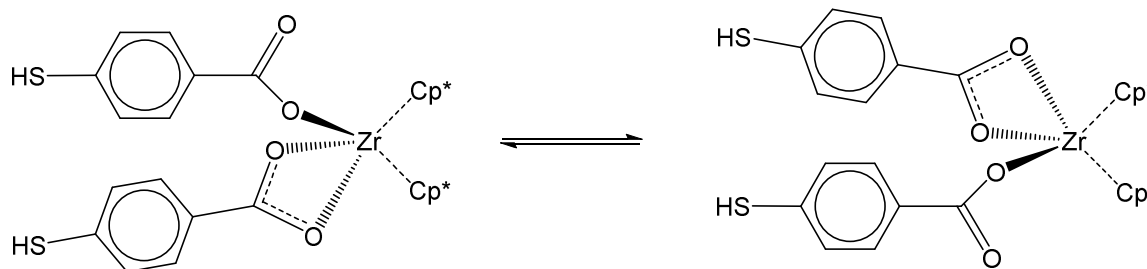


**Fig. 11.** The molecular structures of one of the two independent molecules of  $\{[n\text{Bu}_2\text{Sn}(\text{O}_2\text{CC}_6\text{H}_4\text{S}-3)n\text{Bu}_2\text{Sn}(\text{SC}_6\text{H}_4\text{CO}_2-3)\text{Sn}(n\text{Bu})_2]\text{O}\}_2$  (TEBKAN); H atoms are omitted.

## 5. Complexes of titanium, zirconium and hafnium

Although no hafnium complexes of 3MBA or 4MBA ligands appear to have been reported to date, there is a well-established chemistry of both titanium and zirconium with these ligands.

The reaction of  $\text{Cp}^*_2\text{Zr}(\text{CH}_3)_2$  with 2 mole equivalents of  $\text{H}_2\text{4MBA}$  gives the O-bonded complex  $\text{Cp}^*_2\text{Zr}(\text{O}_2\text{CC}_6\text{H}_4\text{SH})_2$ , with elimination of methane. In solution, the carboxylate ligands of  $\text{Cp}^*_2\text{Zr}(\text{O}_2\text{CC}_6\text{H}_4\text{SH})_2$  are fluxional (Scheme 5), and only one set of signals are observed for the aromatic rings in the room temperature  $^1\text{H}$  NMR spectrum. Upon cooling to low temperature, two signals for the ortho-protons are observed, which coalesce at 175 K. An X-ray structure determination on this complex, Fig. 12a, shows one of the carboxylate groups acting as a bidentate chelating ligand, and the other functioning in the monodentate mode.[31] The complex assembles into a supramolecular chain in the solid-state through the formation of  $\text{S-H}\cdots\text{O}$  hydrogen-bonds, Fig. 12b, with the uncoordinated oxygen of the monodentate carboxylate ligand. The other  $\text{S-H}$  groups form  $\text{S-H}\cdots\text{O}$  hydrogen-bonds to the oxygen atoms of the THF solvate molecules. Two heterobimetallic zirconium(IV)-gold(I) complexes bridged by 4MBA have been prepared from  $\text{Cp}^*_2\text{Zr}(\text{O}_2\text{CC}_6\text{H}_4\text{SH})_2$ , and are described in Section 14.



**Scheme 5**

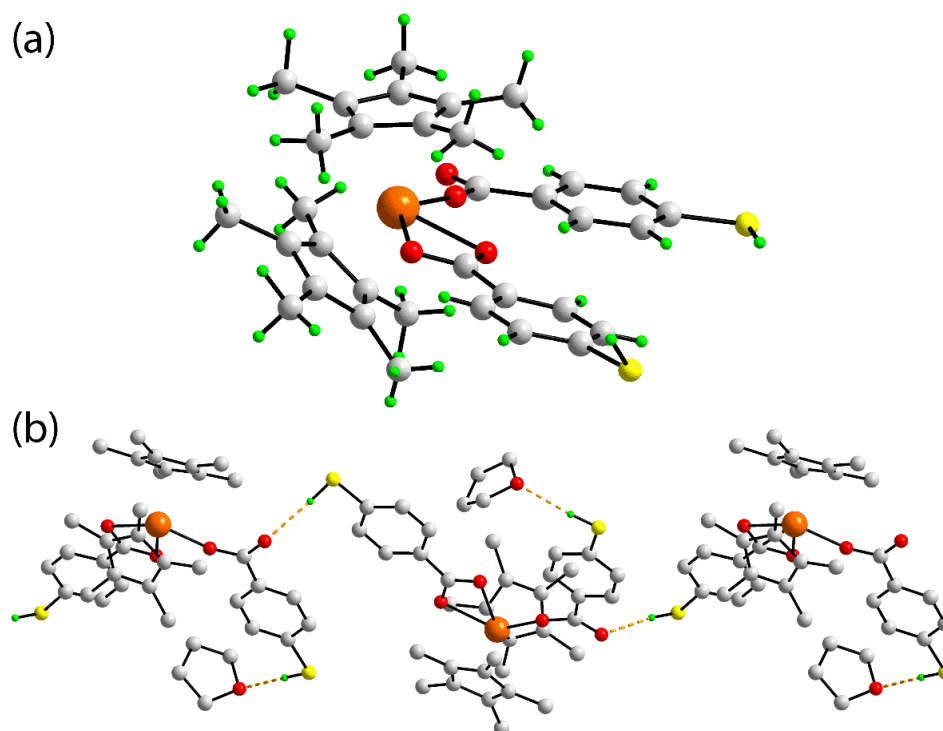
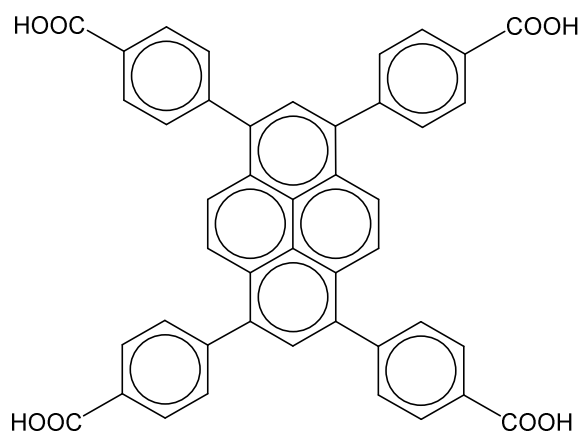


**Fig. 12.** Structure of the complex  $\text{Cp}^*_2\text{Zr}(\text{O}_2\text{CC}_6\text{H}_4\text{SH})_2$  as its THF solvate (BODMOX) showing (a) the coordination complex and (b) hydrogen-bonding interactions involving the thiol-proton (non-acidic H atoms are omitted).

A zirconium-containing Metal-Organic Framework (MOF) material has been constructed using the octahedral  $\text{Zr}_6$  node  $[\text{Zr}_6(\mu_3\text{-OH})_8(\text{OH})]^{8+}$  in conjunction with  $\text{H}_4\text{TBAPy}$  [1,3,6,8-tetrakis(4-benzoic acid)pyrene **5**], giving  $[\text{Zr}_6(\mu_3\text{-OH})_8(\text{OH})_8(\text{TBAPy})_2]$ , which is a mesoporous material with OH-functionalised channels. Secondary derivatisation of the MOF was achieved by reaction with various carboxylic acids, including  $\text{H}_2\text{4MBA}$ . [32,33]

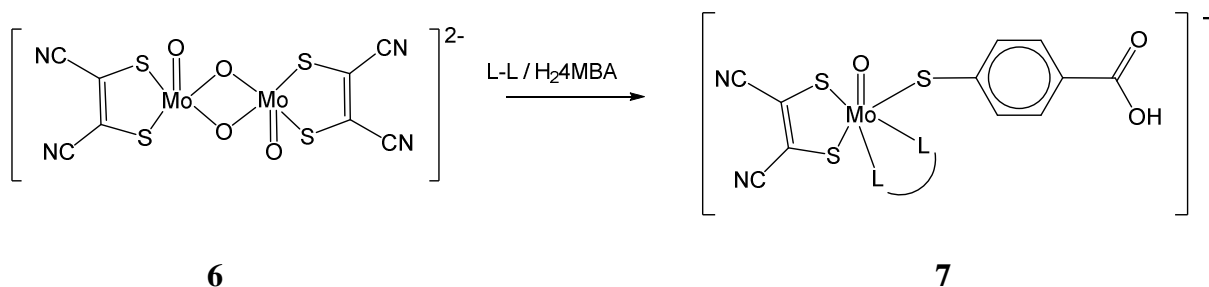


5

## 6. Complexes of chromium, molybdenum and tungsten

Reaction of the molybdenum(V) dimer  $[\text{MoO}_2\{\text{S}_2\text{C}_2(\text{CN})_2\}]_2^{2-}$  **6** with  $\text{H}_2\text{4MBA}$  and a bidentate N-donor ligand L-L (either 2,2'-bipyridine or 1,10-phenanthroline) results in the formation of the mononuclear molybdenum(V) complexes  $[\text{Mo}(\text{O})\{\text{S}_2\text{C}_2(\text{CN})_2\}(\text{SC}_6\text{H}_4\text{CO}_2\text{H-4})(\text{L-L})]^-$  **7** (Scheme 6) which were structurally characterised as their tetra-n-butylammonium salts.[34] The structure of the bipy complex is shown in Fig. 13, showing a slightly distorted octahedral geometry at the metal centre and the formation of a hydrogen-bonded carboxylic acid dimer unit.

No chromium or tungsten complexes of 3MBA or 4MBA ligands have been reported to date.



Scheme 6

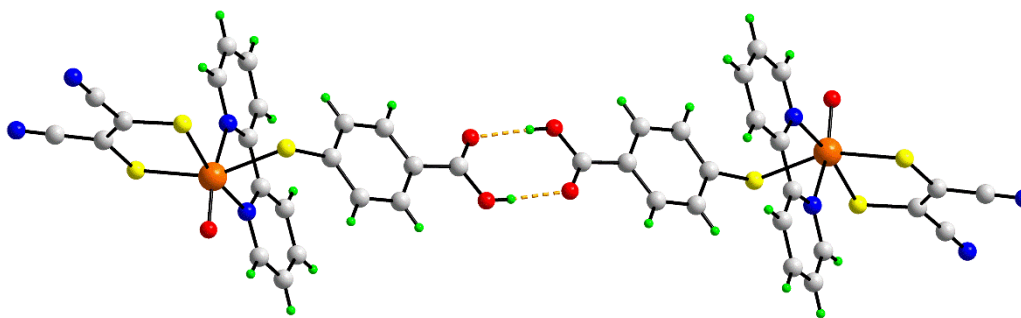
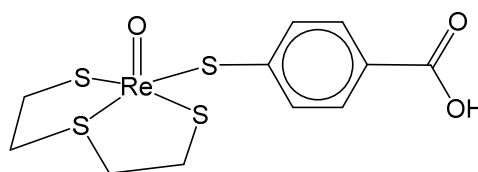


**Fig. 13.** Structure of the hydrogen-bonded dimer of two centrosymmetrically related complex molecules in the crystal of  $n\text{Bu}_4\text{N}[\text{Mo}(\text{O})\{\text{S}_2\text{C}_2(\text{CN})_2\}(\text{SC}_6\text{H}_4\text{CO}_2\text{H}-4)(\text{bipy})]$  as its benzene dichloromethane solvate (DIBROX); cation and solvent molecules are omitted.

## 7. Complexes of manganese, technetium and rhenium

There has been particular interest in 4-mercaptobenzoate ester derivatives of technetium and rhenium for radiopharmaceutical applications. However, fewer complexes containing free acid derivatives have been reported, and are restricted to rhenium; there are no known examples of manganese or technetium complexes. Reaction of  $[\text{Re}(\text{O})\text{Cl}(\text{SCH}_2\text{CH}_2\text{SCH}_2\text{CH}_2\text{S})]$  with  $\text{H}_2\text{4MBA}$  and  $\text{Et}_3\text{N}$  gave complex **8** as an air-stable, red solid, which was soluble only in THF and DMF.[35] The complex showed an  $\text{Re}=\text{O}$  stretch at  $967\text{ cm}^{-1}$  in the IR spectrum. The X-ray structure of the complex, Fig. 14, showed the formation of a hydrogen-bonded carboxylic acid dimer. The coordination geometry about the rhenium(V) centre was considered to be distorted square pyramidal (rather than distorted trigonal bipyramidal). The basal plane of the coordination sphere comprises three sulphur atoms of the tridentate, thioether-thiolate ligand, plus the sulphur of the 4MBA ligand, with the rhenium(V) atom lying above the basal plane.



**8**

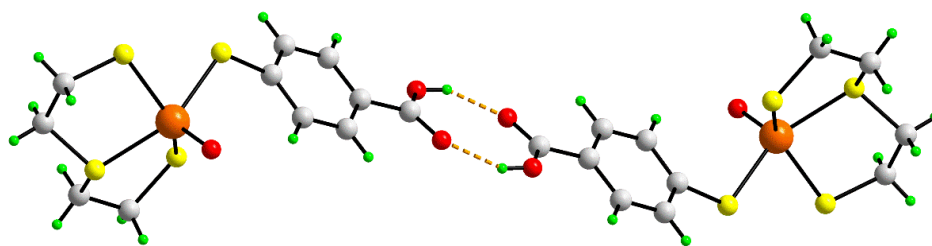


**Fig. 14.** X-ray structure of  $[\text{ReO}(\text{SC}_6\text{H}_4\text{COOH-4})(\text{SCH}_2\text{CH}_2\text{SCH}_2\text{CH}_2\text{S})]$  (RITVIA) showing the formation of a centrosymmetric, carboxylic acid dimer.

## 8. Complexes of iron, ruthenium and osmium

As part of a study into dendritically-encapsulated water-soluble derivatives containing the  $\{\text{Fe}_4\text{S}_4\}$  cubane unit, reaction of  $(\text{Me}_4\text{N})_2[\text{Fe}_4\text{S}_4(\text{S}^t\text{Bu})_4]$  with  $4\text{-HSC}_6\text{H}_4\text{CO}_2^-$  gave the substituted product  $(\text{Me}_4\text{N})_2[\text{Fe}_4\text{S}_4(\text{SC}_6\text{H}_4\text{CO}_2\text{-4})_4]$  as the only known iron complex of 3MBA or 4MBA ligands.[36]

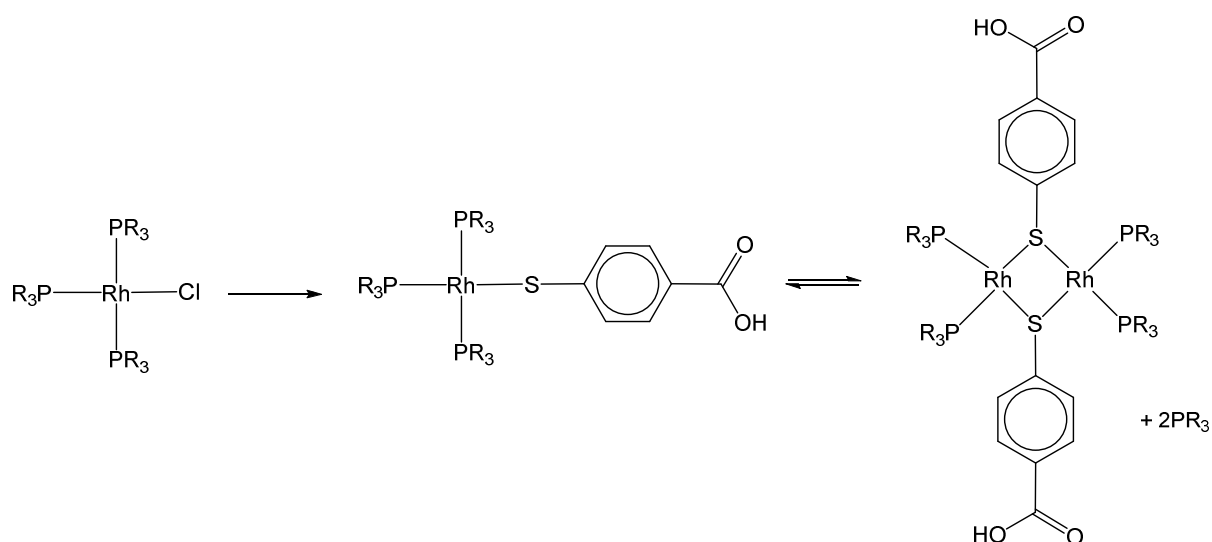
A number of ruthenium and osmium carbonyl cluster derivatives of 3MBA and 4MBA ligands are known and are summarised in Section 15.

## 9. Complexes of cobalt, rhodium and iridium

There is a considerable number of rhodium complexes formed by 3MBA and 4MBA ligands, but none of cobalt or iridium.

Several 4MBA complexes containing rhodium(I) have been synthesised, along with complexes that contain rhodium(III), formed in low yield and identified crystallographically. The rhodium(I) 4MBA complexes are able to act as metalloligands towards other metal centres, and this aspect of their chemistry is described in Section 14. The complexes  $[\text{RhCl}(\text{PR}_3)_3]$  (R = Et or Ph) react with the potassium salt of  $\text{H}_2\text{4MBA}$  giving equilibrium mixtures of  $[\text{Rh}(\text{SC}_6\text{H}_4\text{COOH})(\text{PR}_3)_3]$  and the dimeric complex  $[\{\text{Rh}(\mu\text{-SC}_6\text{H}_4\text{COOH})(\text{PR}_3)_2\}_2]$ , as shown

in Scheme 7.[37] When R = Ph, the dimeric species predominates, however when R = Et the addition of free  $\text{PEt}_3$  shifts the equilibrium in favour of the mononuclear complex. The binuclear complex  $[\{\text{Rh}(\mu\text{-SC}_6\text{H}_4\text{COOH})(\text{PPh}_3)_2\}_2]$  was structurally characterised, Fig. 15a, confirming the presence of a puckered  $\{\text{Rh}_2(\mu\text{-SR})_2\}$  core, Fig. 15a, with a dihedral angle of  $139^\circ$  between the  $\text{Rh}_1\text{S}_1\text{S}_2$  and  $\text{Rh}_2\text{S}_1\text{S}_2$  planes. Puckering in these systems can be explained by the strong tendency of the thiolate-sulphur to adopt  $\text{sp}^3$  hybridisation, and by the tendency for  $d^8$  rhodium(I) centres to mutually interact. The two  $\text{SC}_6\text{H}_4\text{COOH}$  groups of a  $\{\text{Rh}_2\text{S}_2\}$  core show  $\pi\cdots\pi$  stacking, with an average distance of  $3.58 \text{ \AA}$  between neighbouring carbons.  $[\{\text{Rh}(\mu\text{-SC}_6\text{H}_4\text{COOH})(\text{PPh}_3)_2\}_2]$  molecules then interact through the formation of two pairs of carboxylic acid dimers, giving a centrosymmetric, tetrameric aggregate, Fig. 15b.



**Scheme 7** Reaction of  $[\text{RhCl}(\text{PR}_3)_3]$  (R = Et or Ph) with the potassium salt of  $\text{H}_2\text{4MBA}$ , giving equilibrium mixtures of mono- and bi-nuclear rhodium(I) 4MBA complexes.

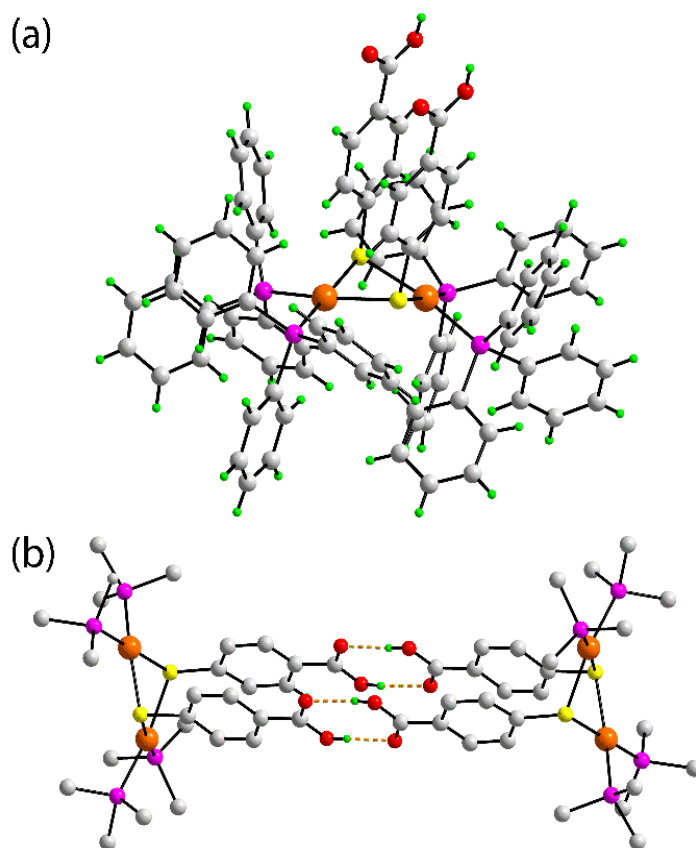
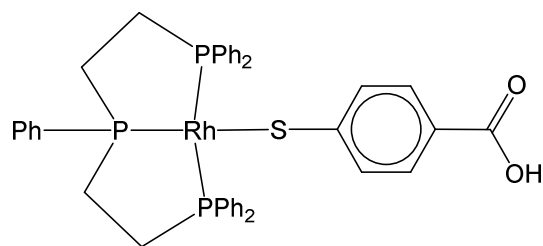


**Fig. 15.** Molecular structure of the binuclear rhodium(I) 4MBA complex  $[\{\text{Rh}(\mu\text{-SC}_6\text{H}_4\text{COOH})(\text{PPh}_3)_2\}_2]$  (NETWEP) showing (a) the structure of one molecule; (b) the cores of two molecules (with only ipso carbon atoms of the  $\text{PPh}_3$  ligands shown and non-acidic H atoms omitted), which dimerise through the formation of two carboxylic acid dimer pairs. Additional colour code: phosphorus, pink.

The reaction of the triphos analogue  $[\text{RhCl}\{\text{PPh}(\text{C}_2\text{H}_4\text{PPh}_2)_2\}]$  with  $\text{H}_2\text{4MBA}$  in the presence of  $\text{nBu}_3\text{N}$  base in THF gave the corresponding complex  $[\text{Rh}(\text{SC}_6\text{H}_4\text{COOH})\{\text{PPh}(\text{C}_2\text{H}_4\text{PPh}_2)_2\}]$  **9** as a highly air- and moisture-sensitive yellow solid. The complex, which was structurally characterised (Fig. 16) is almost insoluble in common organic solvents, but in contrast to the  $\text{PPh}_3$  and  $\text{PEt}_3$  analogues was resistant towards phosphine labilisation and dimerisation.[37]



9

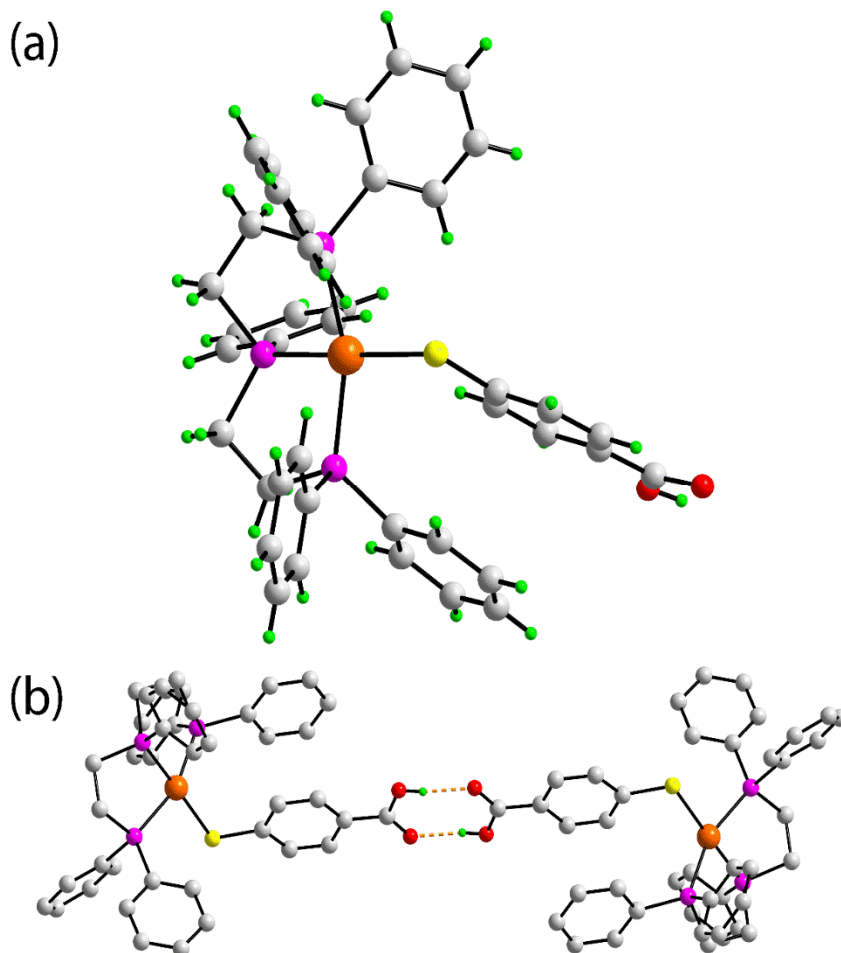
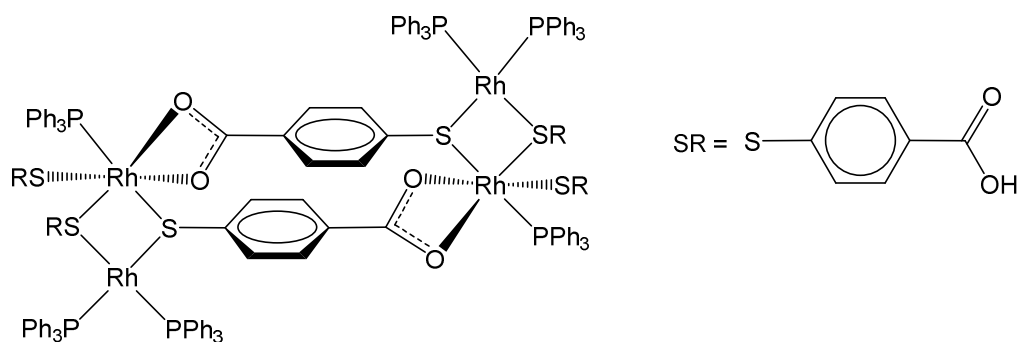


**Fig. 16.** Molecular structure of  $[\text{Rh}(\text{SC}_6\text{H}_4\text{COOH})\{\text{PPh}(\text{C}_2\text{H}_4\text{PPh}_2)_2\}]$  **9** (NETVUE): (a) showing the coordination environment of one molecule and (b) diagram showing the formation of a centrosymmetric carboxylic acid dimer between two molecules (non-acidic H atoms are omitted).

Two rhodium(III) derivatives containing bridging 4MBA ligands have also been isolated. The first product was obtained from the binuclear complex  $[\{\text{Rh}(\mu-$

$\text{SC}_6\text{H}_4\text{COOH}(\text{PPh}_3)_2\}_2]$ . This undergoes decomposition in solution, with one product (dark-brown crystals obtained by diffusion of hexane into a THF solution) identified by X-ray diffraction as the mixed-valence rhodium(I)-rhodium(III) complex  $[\{\text{Rh}^{\text{I}}\text{Rh}^{\text{III}}(\mu\text{-SC}_6\text{H}_4\text{COO})(\mu\text{-SC}_6\text{H}_4\text{COOH})(\text{SC}_6\text{H}_4\text{COOH})(\text{PPh}_3)_3\}_2]$ , shown schematically as **10**.<sup>[37]</sup> The X-ray structure of the complex is shown in Fig. 17. Although solvent loss from the crystals reduced the quality of the data, coupled with disordered phenyl rings and bridging ligands, it allowed the identification of the interesting core of the structure. The rhodium(III) centre is octahedrally coordinated, while the rhodium(I) centre has the usual square-planar geometry. There are two  $\text{SC}_6\text{H}_4\text{COOH}$  groups; one is terminally bonded, while the other bridges the two rhodium(III) centres. In addition, a di-anionic 4MBA ligand  $[\text{SC}_6\text{H}_4\text{COO}]^{2-}$  bridges the two rhodium(III) atoms through the sulphur atom. Two of these units then dimerise through carboxylate groups which chelate the rhodium(III) centre of the other  $\{\text{Rh}_2\text{S}_2\}$  unit. The octahedral coordination at rhodium(III) is completed by a  $\text{PPh}_3$  ligand.<sup>[37]</sup> As in the complex of  $[\{\text{Rh}(\mu\text{-SC}_6\text{H}_4\text{COOH})(\text{PPh}_3)_2\}_2]$  there is  $\pi \cdots \pi$  stacking in **10**, though the phenyl rings of the bridging 4MBA<sup>2-</sup> ligands are somewhat offset due to geometrical constraints. The molecules of **10** also interact through hydrogen-bonding interactions in the solid-state, forming a linear, supramolecular chain by carboxylic acid dimer formation, Fig. 17c, involving the carboxylic acids of the terminal thiolate ligands. Additionally, the remaining  $\text{CO}_2\text{H}$  groups form hydrogen-bonds to the O atoms of the THF solvate molecules.



**10**

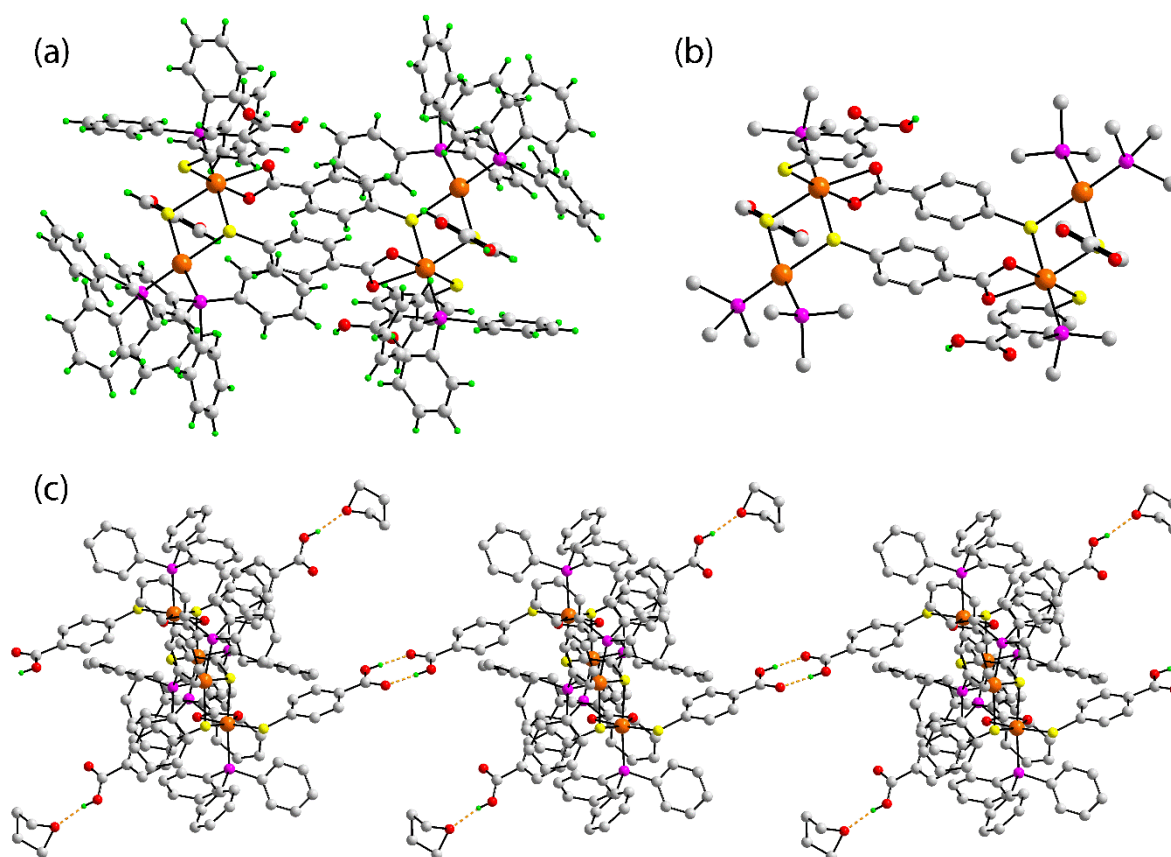
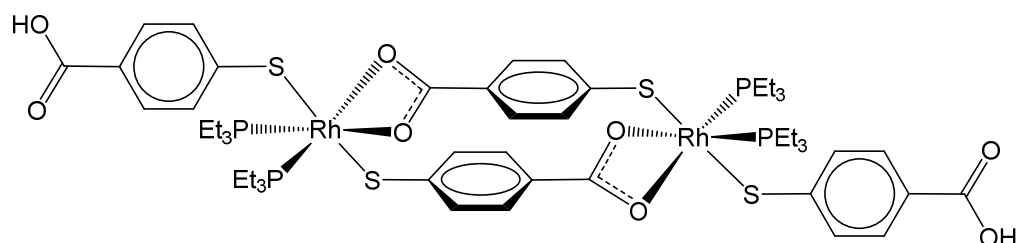


**Fig. 17.** The X-ray structure of the tetranuclear mixed-valence rhodium(I)-rhodium(III) complex  $[\{\text{Rh}^{\text{I}}\text{Rh}^{\text{III}}(\mu\text{-SC}_6\text{H}_4\text{COO})(\mu\text{-SC}_6\text{H}_4\text{COOH})(\text{SC}_6\text{H}_4\text{COOH})(\text{PPh}_3)_3\}_2]$  **10** (NETWAL). (a) shows the complete structure, while (b) shows the core with only ipso carbon atoms of the  $\text{PPh}_3$  ligand and (c) shows the assembly of the tetranuclear aggregates into hydrogen-bonded chains through carboxylic acid dimer formation, together with hydrogen-bonding to the THF solvent molecules. In (b) and (c), non-acidic H atoms are omitted.

The second rhodium(III) 4MBA derivative was formed as a by-product in the synthesis of  $[\text{Rh}(\text{SC}_6\text{H}_4\text{COOH})(\text{PEt}_3)_3]$  upon crystallisation of a concentrated solution, and has the structure **11**. This complex has structural similarities to the mixed-valence complex **10**, in that the rhodium(III) centres are octahedral and the complex contains bridging  $[\text{SC}_6\text{H}_4\text{CO}_2]^{2-}$  dianions (whose carboxylate ligands chelate the rhodium(III) centres) but in this complex the

thiolate ligands are terminally bonded (not bridging). The X-ray structure of this binuclear complex, Fig. 18, confirms the two octahedral rhodium(III) centres; the complex also assembles into hydrogen-bonded zigzag chains through the formation of carboxylic acid dimers.[37]



11

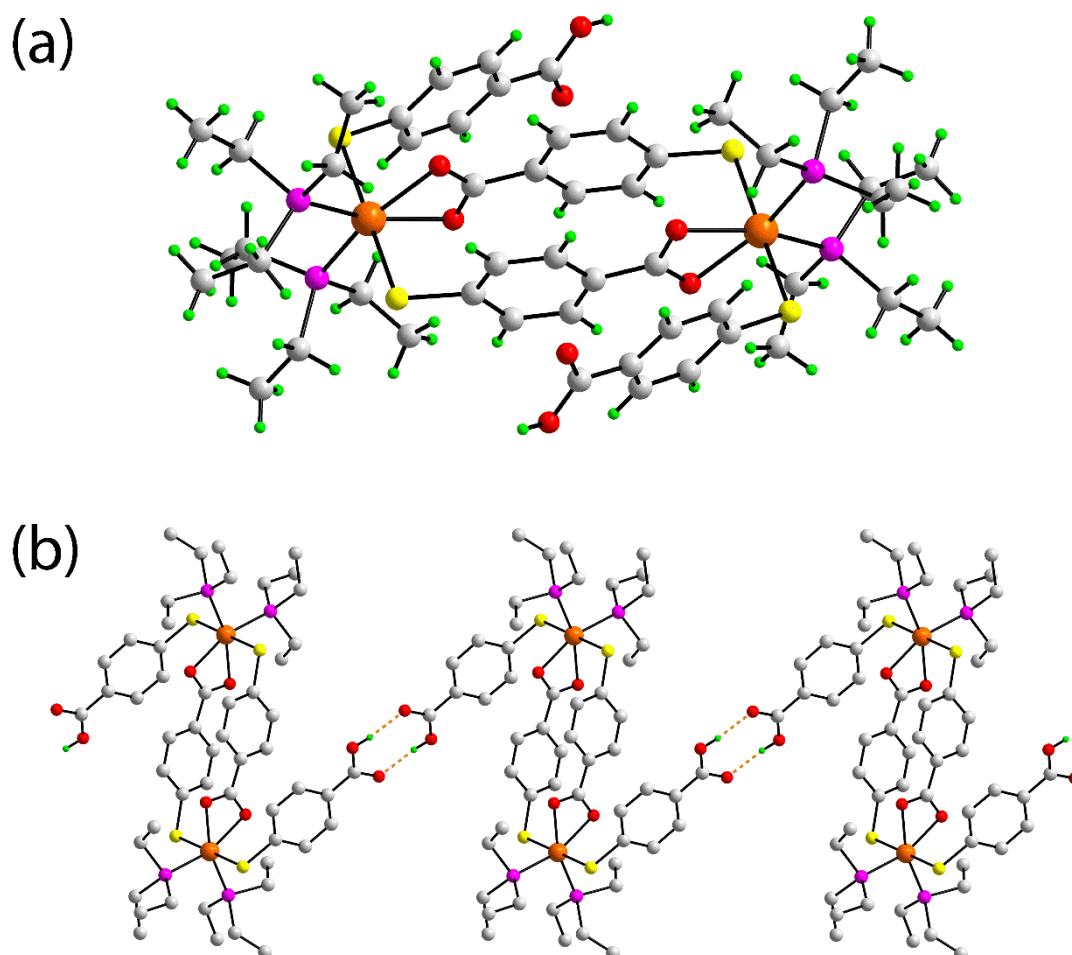
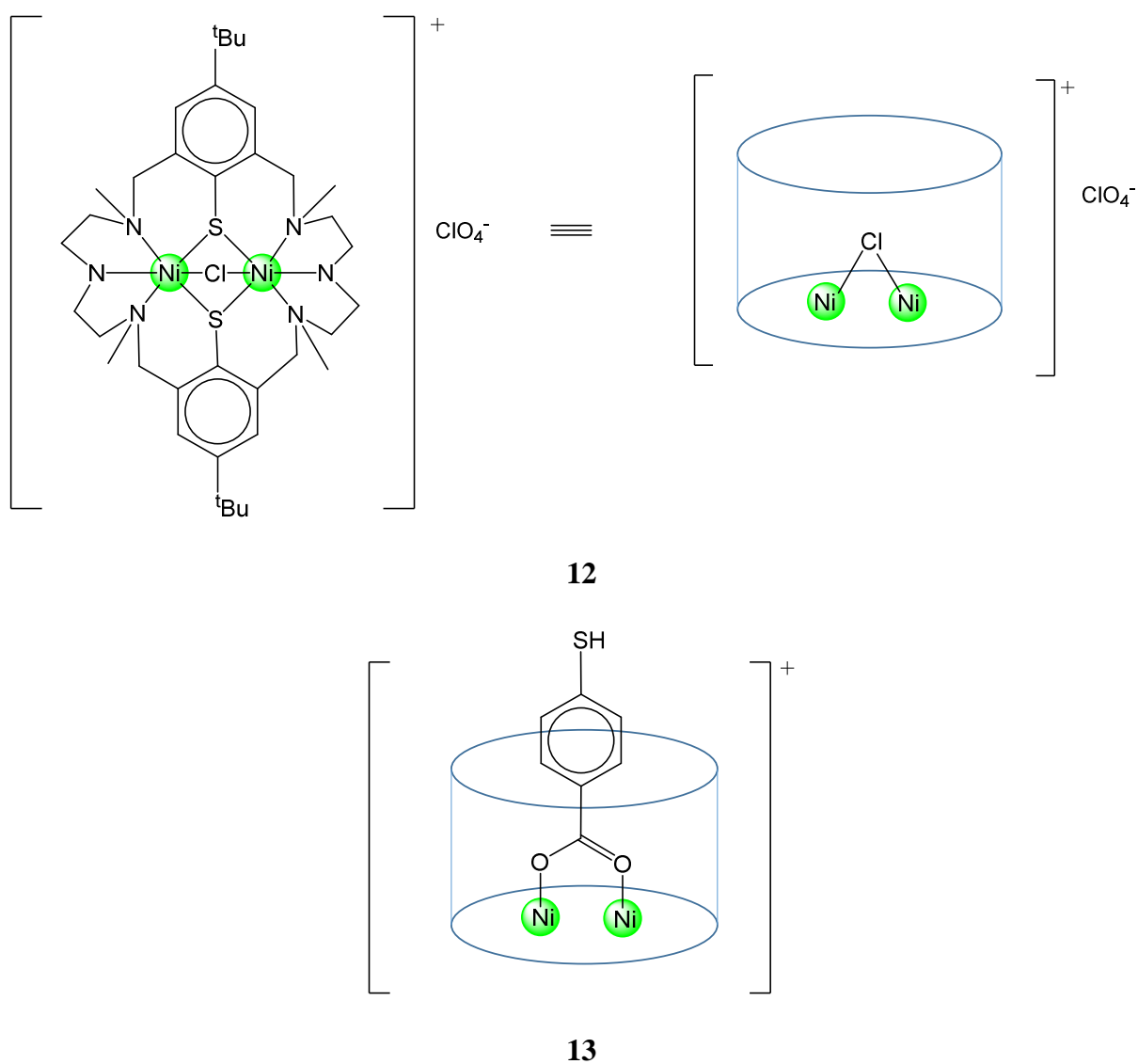


**Fig. 18.** Structure of the centrosymmetric, binuclear rhodium(III) derivative of 4MBA **11** (NETWIT): (a) diagram showing the structure of the dimeric unit with  $[\text{SC}_6\text{H}_4\text{CO}_2]^{2-}$  ligands

bridging rhodium(III) centres and (b) formation of a hydrogen-bonded supramolecular chain involving the S-bound  $\text{SC}_6\text{H}_4\text{COOH}$  groups (non-acidic H atoms are omitted).

## 10. Complexes of nickel, palladium and platinum

The 24-membered macrocyclic dinickel complex **12** has been reacted with  $\text{H}_2\text{4MBA}$  in the presence of  $\text{Et}_3\text{N}$  base, by substitution of the bridging chlorido ligand, to give the 4MBA complex **13** (isolated as the  $\text{ClO}_4^-$  or  $\text{BPh}_4^-$  salts) which has the two nickel centres bridged by the carboxylato ligand.[38]



Complex **13** behaves as a typical thiol, and is for example air-sensitive, undergoing oxidative dimerisation to give a compound with two  $\text{Ni}_2$  macrocycles bridged by a disulphide

bond. The structure of this non-symmetric complex has been determined, Fig. 19.[38] Complex **13** is also able to act as a metalloligand towards the  $\text{Ph}_3\text{PAu}^+$  fragment; further details of this heterobimetallic  $\{\text{NiAu}\}$  complex are given in Section 14.[38]

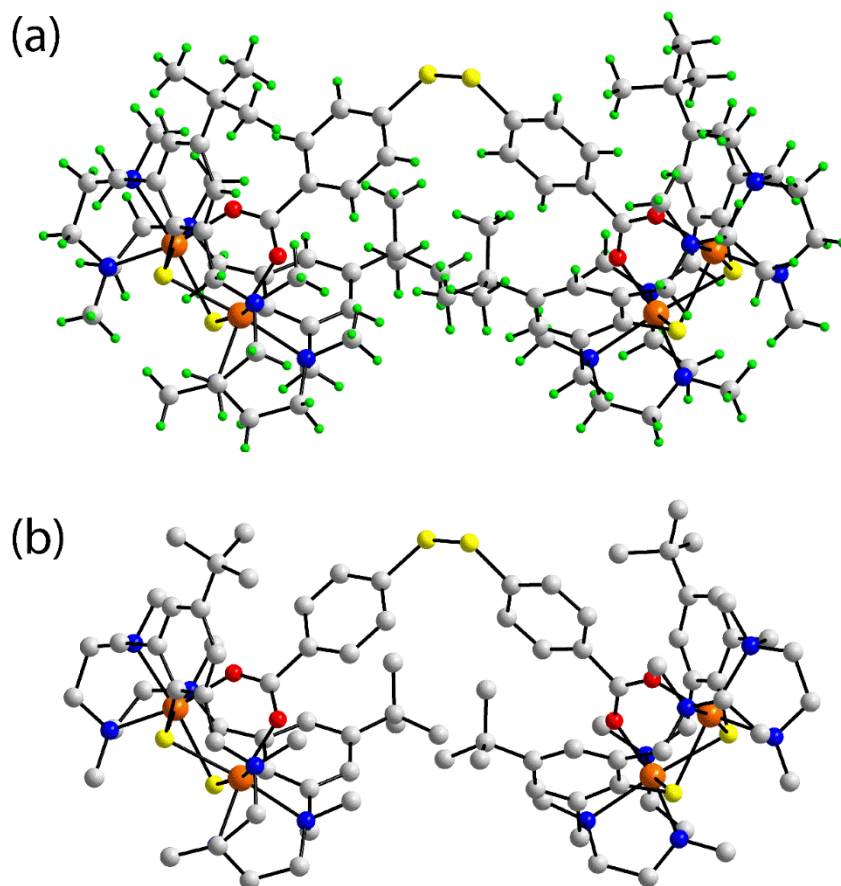
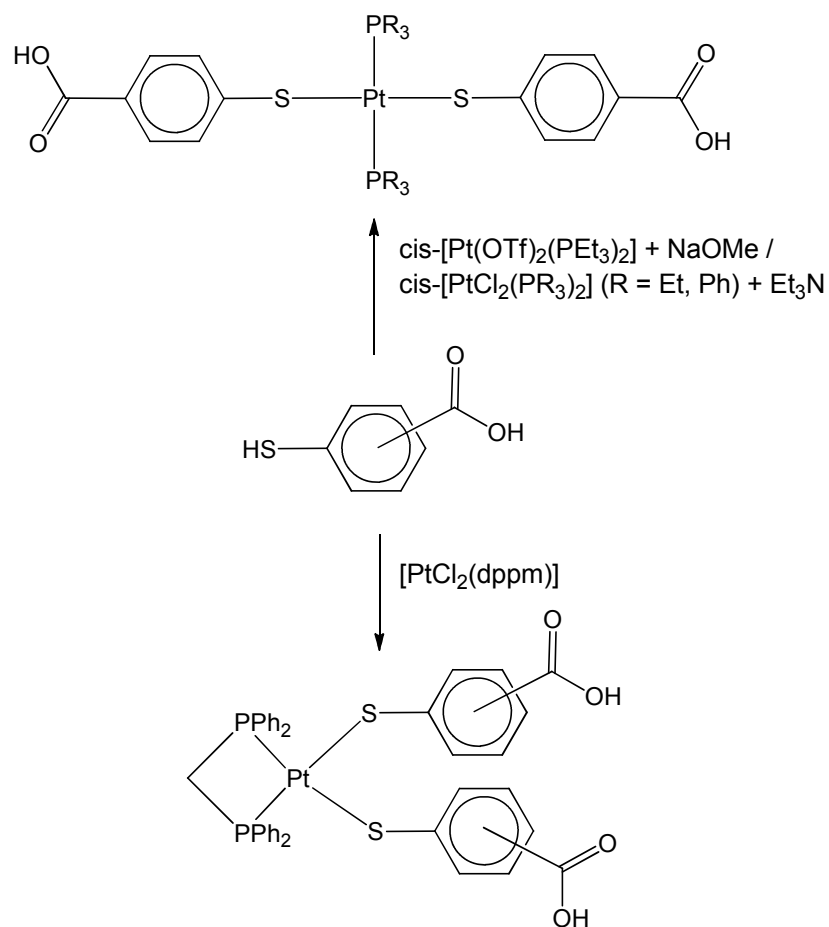


**Fig. 19.** Molecular structure of the MBA disulphide-bridged complex formed by oxidation of the thiol **13** (COYSEQ): (a) full tetra-nuclear di-cation and (b) the di-cation with H atoms omitted. Anions and solvent molecules are omitted.

A number of platinum(II) and palladium(II) complexes containing S-bonded 3- and 4-isomers of MBA have been synthesised, with the denticity of the ancillary phosphine ligand being used to control the geometry. Thus, reaction of  $\text{H}_2\text{4MBA}$  with NaOMe and cis- $[\text{Pt}(\text{OTf})_2(\text{PEt}_3)_2]$ , or with cis- $[\text{PtCl}_2(\text{PR}_3)_2]$  ( $\text{R} = \text{Et}$  or  $\text{Ph}$ ) and  $\text{Et}_3\text{N}$  base in MeOH gives the trans isomers of  $[\text{Pt}(\text{SC}_6\text{H}_4\text{COOH})_2(\text{PR}_3)_2]$ , Scheme 8.[39] Reaction of either  $\text{H}_2\text{3MBA}$  or

H<sub>2</sub>4MBA with [PtCl<sub>2</sub>(dppm)] with Et<sub>3</sub>N base gives the cis isomers [Pt(SC<sub>6</sub>H<sub>4</sub>COOH)<sub>2</sub>(dppm)],

Scheme 8.[39]



**Scheme 8** Synthesis of mononuclear platinum complexes of 3MBA and 4MBA ligands (R = Et or Ph).

The triphenylphosphine complex  $\text{trans-[Pt(SC}_6\text{H}_4\text{COOH)}_2\text{(PPh}_3\text{)}_2\text{]}$  has been structurally characterised, and shows two independent molecules with slightly different bond parameters. The structure of one of the independent molecules is shown in Fig. 20a. In the crystal, the complexes aggregate via the usual carboxylic acid dimer formation; each independent molecule self-assembles to form virtually identical supramolecular chains with the same pitch and a Pt···Pt separation of 18.0 Å, as shown in Fig. 20b. In this structure, the eight-membered hydrogen-bonded rings are puckered due to deviations of the O–H···O angles from linearity. The complex  $\text{trans-[Pt(SC}_6\text{H}_4\text{COOH)}_2\text{(PEt}_3\text{)}_2\text{]}$  has also been structurally

characterised, both as its monohydrate, and as its bis(methanol) solvate. The monohydrate has an analogous structure to the  $\text{PPh}_3$  complex (vide supra); the water molecule is located in the lattice and is not involved in hydrogen-bonding with the carboxylic acid dimer groups. The structure of the complex as its methanol solvate is shown in Fig. 21a, and the hydrogen-bonding network is shown in Fig. 21b. Methanol forms intramolecular hydrogen-bonds between two carboxylic acid groups of two adjacent complexes, forming large hydrogen-bonded rings. Each carboxylic acid group acts as a hydrogen-bond donor to one methanol molecule, and as an acceptor to another methanol. The resulting macrocycle contains a large cavity having the dimensions  $7.5 \times 18.2 \text{ \AA}$ . [39]

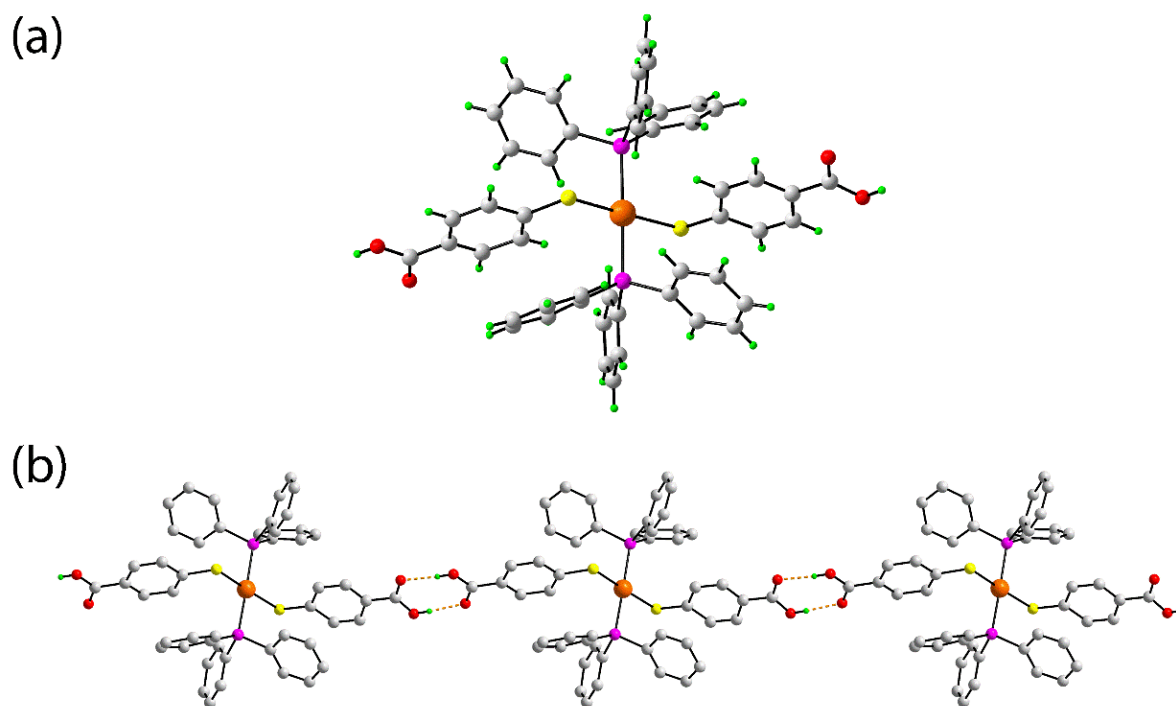


**Fig. 20.** (a) Molecular structure of one of the independent molecules of trans-[Pt(SC<sub>6</sub>H<sub>4</sub>COOH)<sub>2</sub>(PPh<sub>3</sub>)<sub>2</sub>] (WOCCIC) and (b) self-assembled hydrogen-bonded chains of the one independent molecules of trans-[Pt(SC<sub>6</sub>H<sub>4</sub>COOH)<sub>2</sub>(PPh<sub>3</sub>)<sub>2</sub>] (shown in (a)) formed through carboxylic acid dimers.

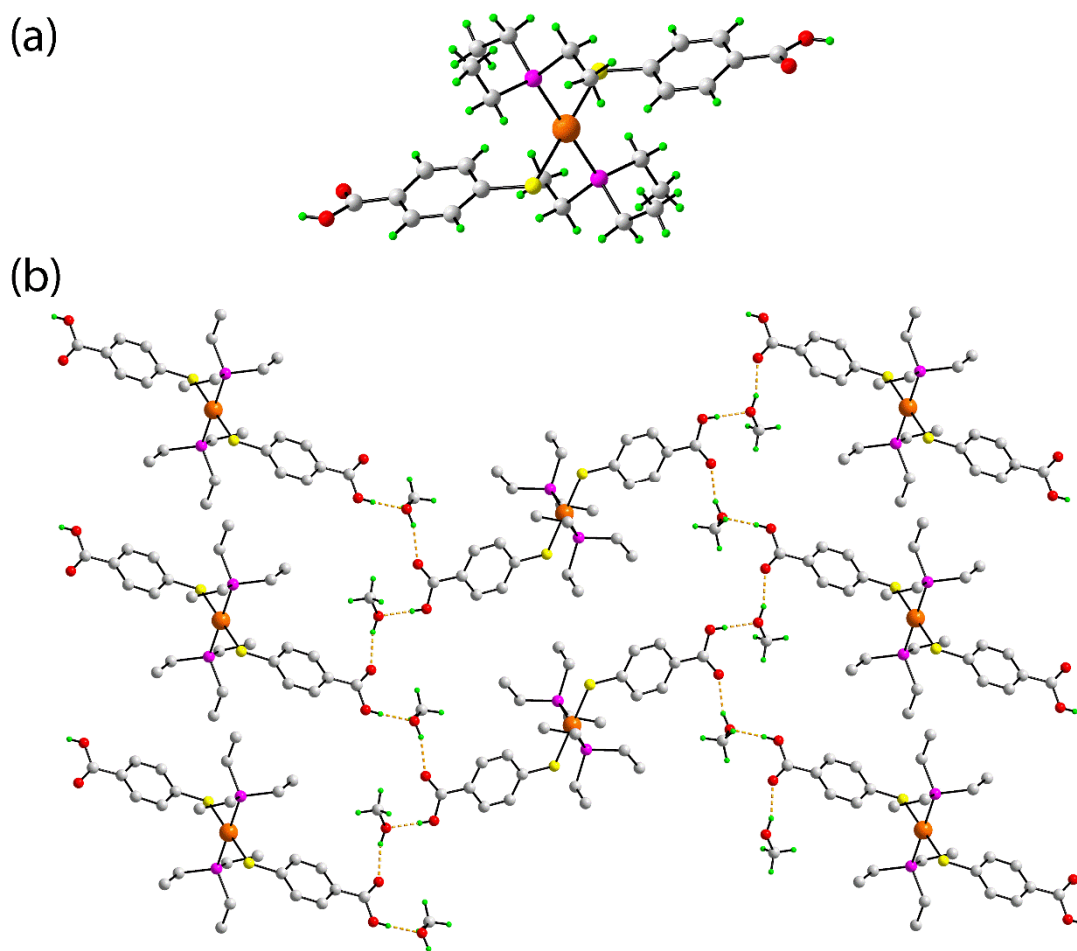
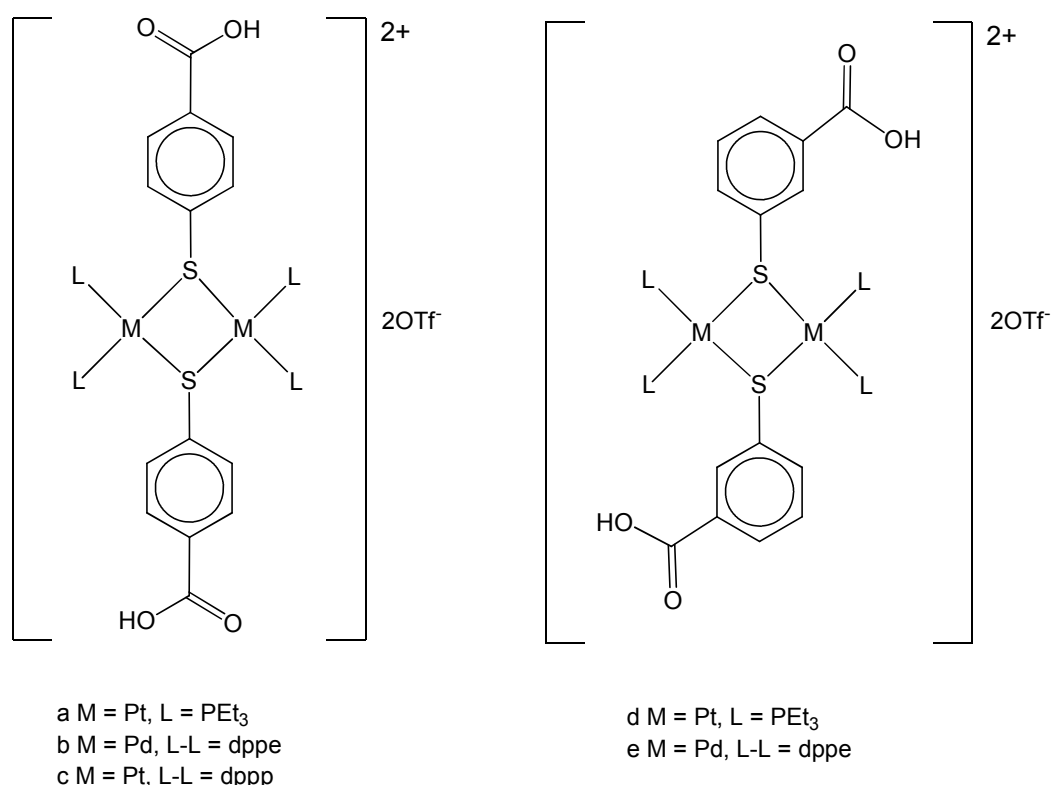


**Fig. 21.** (a) Molecular structure of the 4MBA complex  $\text{trans-}[\text{Pt}(\text{SC}_6\text{H}_4\text{COOH})_2(\text{PEt}_3)_2]$  as its methanol solvate (WOCCOI) and (b) hydrogen-bonding network formed in the 4MBA complex  $\text{trans-}[\text{Pt}(\text{SC}_6\text{H}_4\text{COOH})_2(\text{PEt}_3)_2] \cdot 2\text{MeOH}$ .

Reactions of the complexes  $\text{cis-}[\text{Pt}(\text{OTf})_2(\text{PEt}_3)_2]$  or  $\text{cis-}[\text{M}(\text{OTf})_2(\text{diphos})]$  ( $\text{M} = \text{Pd}$ ,  $\text{Pt}$ ;  $\text{diphos} = \text{dppe}$  or  $\text{dppp}$ ) with  $\text{H}_2\text{3MBA}$  or  $\text{H}_2\text{4MBA}$  in the absence of base resulted in the formation of a series of binuclear thiolate-bridged complexes as shown in Scheme 9.[39] The complexes were characterised by NMR and IR spectroscopies, and by X-ray structure determinations on three derivatives,  $[\text{Pt}(\text{SC}_6\text{H}_4\text{COOH-3})(\text{PEt}_3)_2]_2(\text{OTf})_2$ ,  $[\text{Pt}(\text{SC}_6\text{H}_4\text{COOH-4})(\text{PEt}_3)_2]_2(\text{OTf})_2 \cdot 2\text{H}_2\text{O}$  and  $[\text{Pd}(\text{SC}_6\text{H}_4\text{COOH-3})(\text{dppe})]_2(\text{OTf})_2 \cdot 2\text{H}_2\text{O}$ . The molecular structure of the platinum triethylphosphine 4MBA complex is shown in Fig. 22a. The molecules associate via hydrogen-bonds involving the carboxylic acid groups with water

molecules and triflate (OTf) anions; the C=O and O–H groups form hydrogen-bonded rings of graph set  $R_4^4(12)$  and  $R_4^2(8)$ , and the triflate anions bond to the outside of this ring, as shown in Fig. 22b. The structures of the 3MBA derivatives  $[\text{Pt}(\text{SC}_6\text{H}_4\text{COOH-3})(\text{PEt}_3)_2]_2(\text{OTf})_2$  and  $[\text{Pd}(\text{SC}_6\text{H}_4\text{COOH-3})(\text{dppe})]_2(\text{OTf})_2 \cdot 2\text{H}_2\text{O}$  are somewhat different. The structure of the cation of  $[\text{Pd}(\text{SC}_6\text{H}_4\text{COOH-3})(\text{dppe})]_2(\text{OTf})_2 \cdot 2\text{H}_2\text{O}$  is shown in Fig. 23a. In the crystal, one of the oxygen atoms of the triflate counterion hydrogen-bonds to water molecules, forming an eight-membered ring. The carboxylic acid OH group hydrogen-bonds to the exterior of this ring via a ring oxygen of a water molecule, as shown in Fig. 23b. Finally, in the platinum 3MBA complex  $[\text{Pt}(\text{SC}_6\text{H}_4\text{COOH-3})(\text{PEt}_3)_2]_2(\text{OTf})_2$  the carboxylic acid group is hydrogen-bonded to an oxygen atom of a triflate anion (Fig. 24); there is also a weak noncovalent  $\text{O} \cdots \text{O}$  interaction (2.83 Å), leading to the formation of an infinite chain structure.



**Scheme 9** Structures of the binuclear platinum(II) and palladium(II) phosphine complexes containing bridging 3MBA or 4MBA ligands.

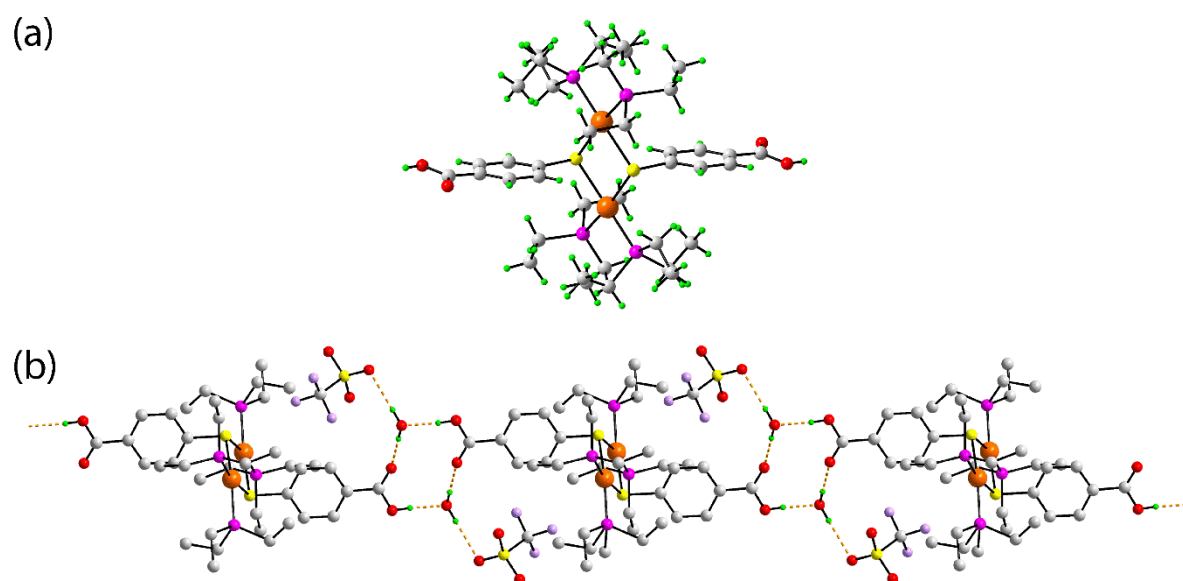


**Fig. 22.** (a) Molecular structure of the cation of  $[\text{Pt}(\text{SC}_6\text{H}_4\text{COOH-4})(\text{PEt}_3)_2]_2(\text{OTf})_2 \cdot 2\text{H}_2\text{O}$  (WOCDD) showing the four-membered  $[\text{Pt}_2(\mu\text{-SR})_2]$  ring and (b) formation of a hydrogen-bonded network in  $[\text{Pt}(\text{SC}_6\text{H}_4\text{COOH-4})(\text{PEt}_3)_2]_2(\text{OTf})_2 \cdot 2\text{H}_2\text{O}$  via hydrogen-bonding of two carboxylic acids and two water molecules; triflate anions hydrogen-bond to the exterior of the resulting 12-membered ring. Non-acidic atoms are omitted.

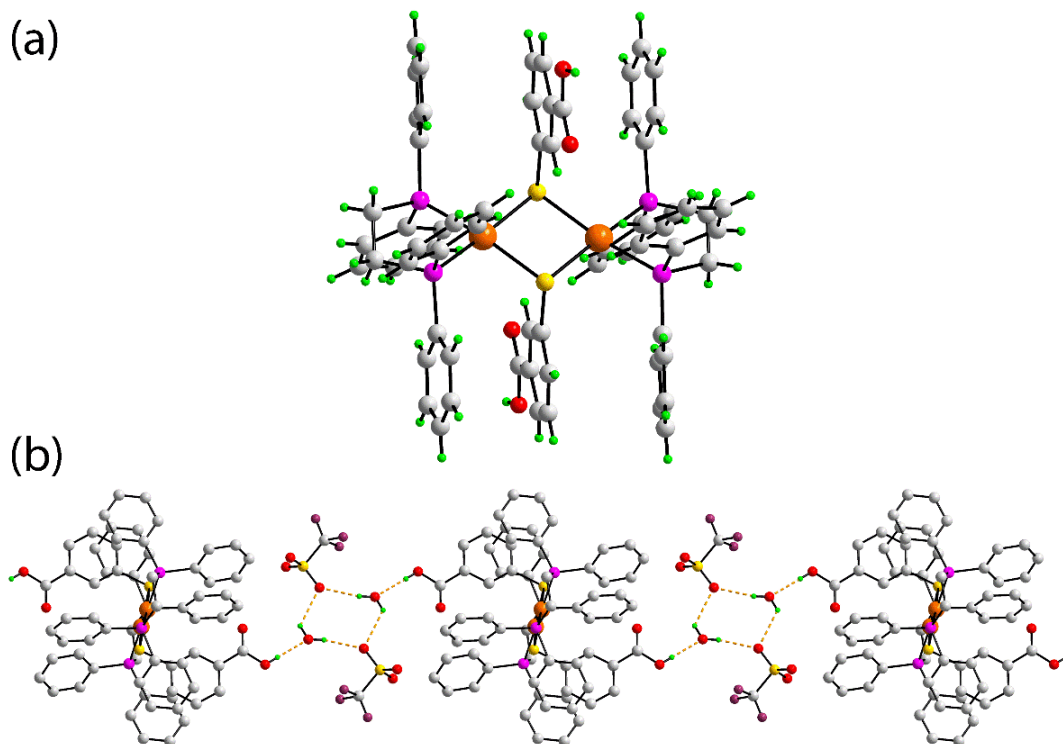


**Fig. 23.** (a) Structure of the coordination complex cation of  $[\text{Pd}(\text{SC}_6\text{H}_4\text{COOH}-3)(\text{dppe})]_2(\text{OTf})_2 \cdot 2\text{H}_2\text{O}$  (WOCDAV) and (b) the hydrogen-bonding in this compound, showing the formation of eight-membered rings involving two triflate anions and two water molecules. Non-acidic atoms are omitted.

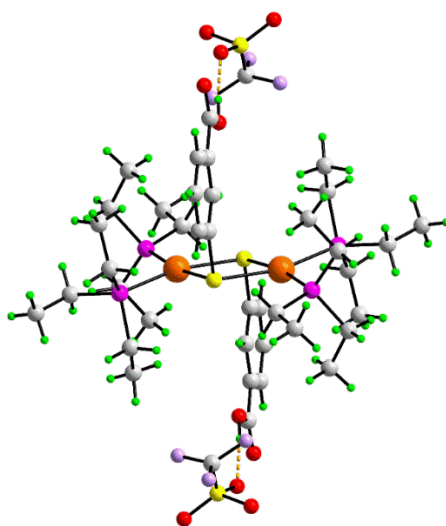


**Fig. 24.** The structure of the cation of  $[\text{Pt}(\text{SC}_6\text{H}_4\text{COOH}-3)(\text{PEt}_3)_2]_2(\text{OTf})_2$  (WOCDEZ), showing hydrogen-bonding interactions with the triflate anions.

## 11. Complexes of copper, silver and gold

This Section describes complexes containing 3MBA or 4MBA ligands with the metal in the +1 oxidation state; cluster compounds of these metals (where the average metal oxidation state is <1) are summarised in Section 16.

### 11.1 Copper complexes

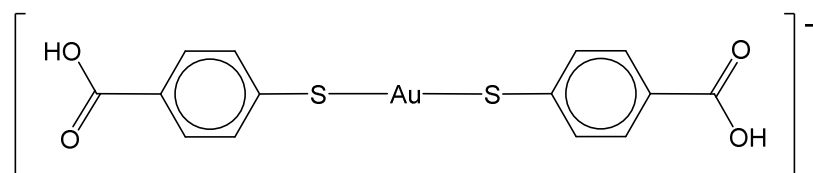
Little work appears to have been carried out regarding copper complexes of 3MBA or 4MBA ligands, though a detailed study reported in 2008 by Che and co-workers described the synthesis and characterisation of the polymeric copper(I) 4MBA compound  $[\text{Cu}(\text{SC}_6\text{H}_4\text{COOH})]_\infty$ , along with a number of other polymeric copper(I) aryl thiolates.[40] Thus, reaction of  $\text{Cu}_2\text{O}$  with  $\text{H}_2\text{4MBA}$  in refluxing ethanol for 48 h gave  $[\text{Cu}(\text{SC}_6\text{H}_4\text{COOH})]_\infty$  in 82% yield as a pale-yellow, insoluble solid. It was found to show considerable thermal stability, being much more stable than the corresponding aliphatic thiolate analogue  $[\text{Cu}(\text{SMe})]_\infty$ . Powder X-ray analysis of  $[\text{Cu}(\text{SC}_6\text{H}_4\text{COOH})]_\infty$  indicated that the compound has a different solid-state structure to  $[\text{Cu}(\text{SC}_6\text{H}_4\text{Me-4})]_\infty$  and  $[\text{Cu}(\text{SC}_6\text{H}_4\text{OMe-4})]_\infty$ , which form infinite polymer chains. Instead, it was proposed that the polymer chains of  $[\text{Cu}(\text{SC}_6\text{H}_4\text{COOH})]_\infty$  are aggregated through hydrogen-bonding interactions between the carboxylic acid groups; the formation of a plate-like crystal habit for  $[\text{Cu}(\text{SC}_6\text{H}_4\text{COOH})]_\infty$  versus rod-like habits for  $[\text{Cu}(\text{SC}_6\text{H}_4\text{X-4})]_\infty$  ( $\text{X} = \text{CH}_3, \text{H}, \text{CH}_3\text{O}, \text{tBu}$  and  $\text{CF}_3$ ) was consistent with this.[40] The C–OH stretching and O–H $\cdots$ O bending modes for  $[\text{Cu}(\text{SC}_6\text{H}_4\text{COOH})]_\infty$  were similar to those of crystalline 4MBA, and the O–H ( $3480 \text{ cm}^{-1}$ ) and C=O ( $1684 \text{ cm}^{-1}$ ) stretches are lower than for a 4MBA SAM on gold ( $3579$  and  $1749 \text{ cm}^{-1}$  respectively).[41] A polycrystalline solid sample of  $[\text{Cu}(\text{SC}_6\text{H}_4\text{COOH})]_\infty$  was found to show low charge mobility.

### 11.2 Silver complexes

In contrast to the extensive coordination chemistry of the 2MBA (thiosalicylate) ligand with silver, forming a wide range of compounds including mononuclear complexes,[1] surprisingly there appears to be no examples of mononuclear silver complexes of 3MBA or 4MBA ligands. However, there is a very extensive chemistry of 3MBA and 4MBA towards silver clusters, nanoparticles and surfaces, which is described in Section 16.

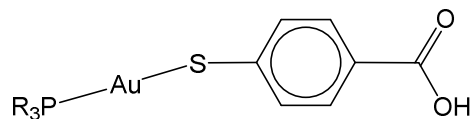
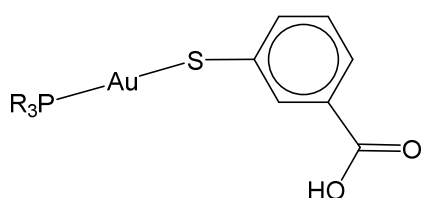
### 11.3 Gold complexes

The chemical softness of gold(I) means that it has a strong affinity for thiolate ligands, so not surprisingly there have been a large number of studies on gold(I) complexes of 3MBA and 4MBA ligands. While the majority of complexes contain a neutral ancillary ligand, there is a single example of a bis(MBA) gold(I) complex without ancillary neutral ligands. Thus, reaction of [PPN][AuCl<sub>2</sub>] with 2 equivalents of H<sub>2</sub>4MBA and NaOMe in methanol gives the gold(I) complex [PPN][Au(SC<sub>6</sub>H<sub>4</sub>COOH-4)<sub>2</sub>] **14** in 77% yield.[42]

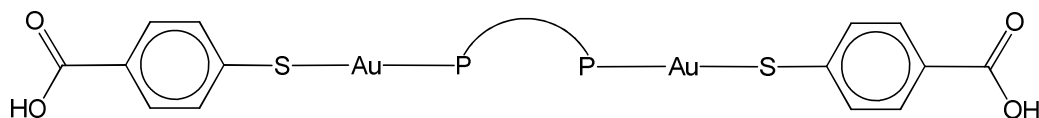


**14**

A wide range of MBA derivatives with ancillary phosphine ligands has been synthesised, as was also the case with the isomeric thiosalicylate (2MBA) ligand.[1] Typically, gold(I) phosphine derivatives of 3MBA and 4MBA of the type **15** can be prepared by a simple metathesis reaction from the phosphine gold(I) chloride complex R<sub>3</sub>PAuCl.[42,43] Thus, reaction of (Ph<sub>3</sub>P)AuCl with either H<sub>2</sub>3MBA or H<sub>2</sub>4MBA with added base (either NaOH or NaOMe) gave the complexes [(Ph<sub>3</sub>P)Au(SC<sub>6</sub>H<sub>4</sub>CO<sub>2</sub>H)] as white powders.[43] In a detailed study by Schmidbaur and co-workers, a series of 4MBA complexes [(R<sub>3</sub>P)Au(SC<sub>6</sub>H<sub>4</sub>COOH-4)] (R<sub>3</sub>P = Me<sub>3</sub>P, Et<sub>3</sub>P, Ph<sub>3</sub>P or Ph<sub>2</sub>PyP) were prepared, along with two examples of compounds containing bisphosphines, namely the dppb and dppf complexes **16**.[42]



15



**16a** P-P =  $\text{Ph}_2\text{P}(\text{CH}_2)_4\text{PPh}_2$  (dppb)

**16b** P-P =  $\text{Fe}(\eta^5\text{-C}_5\text{H}_4\text{PPh}_2)_2$  (dppf)

Alternatively, reduction of  $\text{HAuCl}_4 \cdot 3\text{H}_2\text{O}$  by  $\text{S}(\text{CH}_2\text{CH}_2\text{OH})_2$  followed by addition of  $\text{H}_2\text{4MBA}$  in ethanol gave a light-yellow precipitate of  $[\text{Au}(\text{SC}_6\text{H}_4\text{COOH})]$  that was isolated and characterised, and presumably has a polymeric structure containing thiolate bridges [31], analogous to other gold(I) thiolate compounds of composition  $[\text{Au}(\text{SR})]_n$ . Reaction of this compound with  $\text{PMe}_2\text{Ph}$  gave  $[(\text{PhMe}_2\text{P})\text{Au}(\text{SC}_6\text{H}_4\text{CO}_2\text{H})]$  which was found to have interesting photoluminescence properties (high quantum yield, multi-component emission, large photoluminescence lifetime).

$[(\text{PhMe}_2\text{P})\text{Au}(\text{SC}_6\text{H}_4\text{CO}_2\text{H})]$  has been used as a metalloligand in the synthesis of a heterobimetallic  $\{\text{ZrAu}\}$  complex (vide infra).[31] The ferrocenylphosphine complex  $[(\text{Ph}_2\text{PFc})\text{Au}(\text{SC}_6\text{H}_4\text{CO}_2\text{H})]$  was synthesised by reaction of equimolar quantities of  $\text{H}_2\text{4MBA}$  and  $\text{KOH}$ , followed by addition of  $[(\text{Ph}_2\text{PFc})\text{AuCl}]$ ; this complex (along with the  $\text{PPh}_3$  analogue) were used in the synthesis of 4MBA-bridged  $\{\text{TiAu}\}$  heterobimetallic complexes (vide infra).[44,45]

A considerable number of X-ray structure determinations on phosphine gold(I) derivatives of 4MBA have been carried out. The structures of the 4MBA derivatives

$[(\text{Cy}_3\text{P})\text{Au}(\text{SC}_6\text{H}_4\text{CO}_2\text{H})]$  [ 46 ], the ferrocenylphosphine derivative  $[(\text{Ph}_2\text{PFc})\text{Au}(\text{SC}_6\text{H}_4\text{CO}_2\text{H})]$  [45], the triethylphosphine complex  $[(\text{Et}_3\text{P})\text{Au}(\text{SC}_6\text{H}_4\text{CO}_2\text{H})]$  [42] and the pyridylphosphine complex  $[(\text{Ph}_2\text{PPy})\text{Au}(\text{SC}_6\text{H}_4\text{CO}_2\text{H})]$  [42] show the usual hydrogen-bonded carboxylic acid dimer. As illustrative examples, Figs 25a and b show the structures of the  $\text{Cy}_3\text{P}$  and  $\text{Ph}_2\text{PFc}$  complexes, respectively. In the  $\text{Et}_3\text{P}$ ,  $\text{Ph}_2\text{PFc}$  and  $\text{Ph}_2\text{PPy}$  complexes (but not the  $\text{PCy}_3$  complex) there were additional weak  $\text{Au}\cdots\text{S}$  interactions, forming four-membered  $\text{Au}_2\text{S}_2$  rings, which link the dimers into chains, as shown for the triethylphosphine complex in Fig. 26.

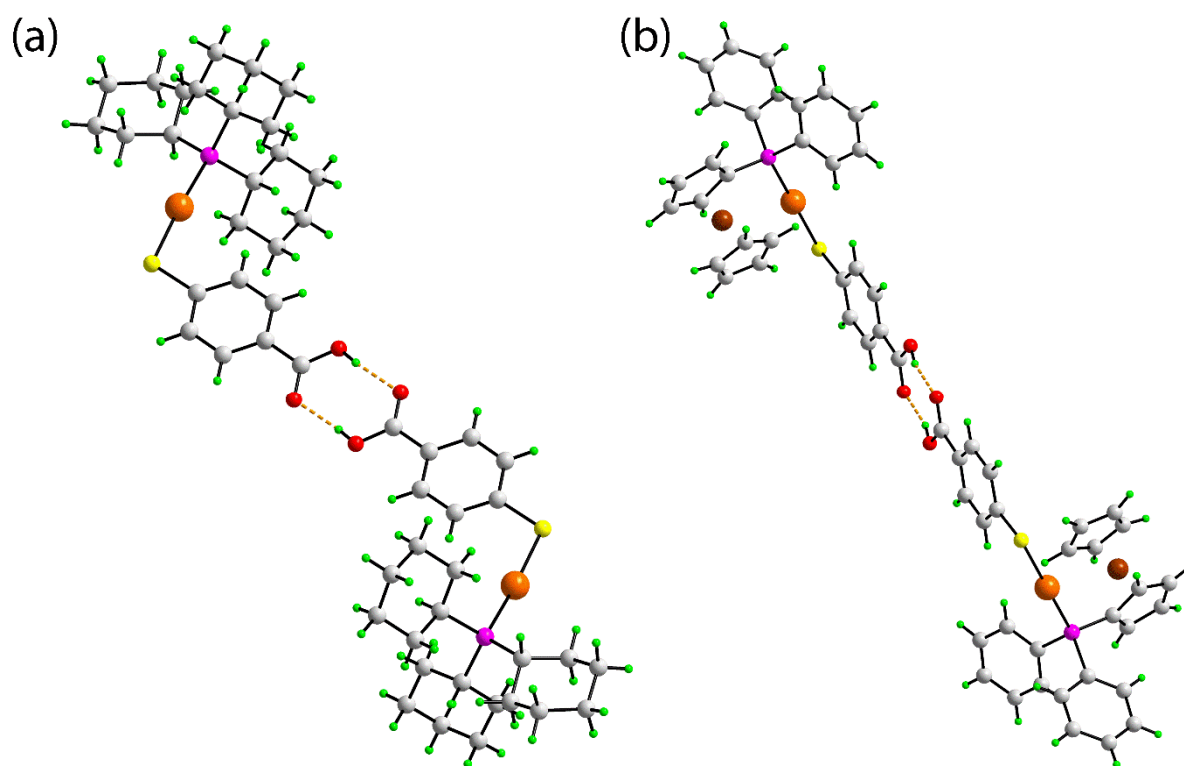


**Fig. 25.** Representative structures of the phosphine gold(I) 4MBA complexes (a)  $[(\text{Cy}_3\text{P})\text{Au}(\text{SC}_6\text{H}_4\text{CO}_2\text{H})_4]$  (DABXIO) and (b)  $[(\text{Ph}_2\text{PFc})\text{Au}(\text{SC}_6\text{H}_4\text{CO}_2\text{H})_4]$  (HUIJIE) showing the formation of a carboxylic acid dimer motif.

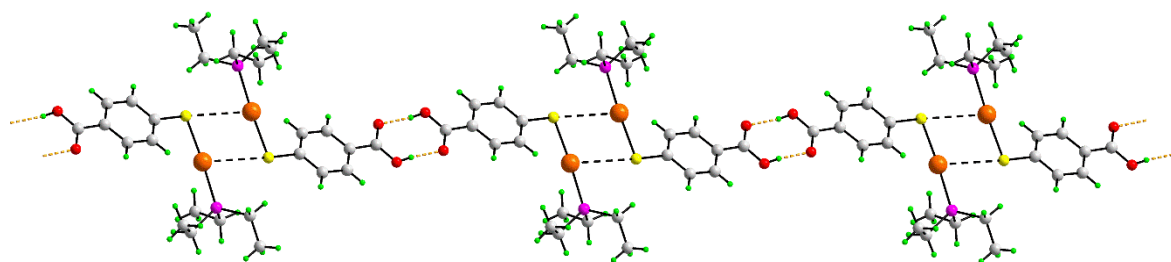


**Fig. 26.** Structure of  $[(\text{Et}_3\text{P})\text{Au}(\text{SC}_6\text{H}_4\text{CO}_2\text{H}-4)]$  (XETNEP) showing the formation of supramolecular chains through carboxylic acid dimer formation coupled with  $\text{Au}\cdots\text{S}$  interactions.

The triphenylphosphine complex  $[(\text{Ph}_3\text{P})\text{Au}(\text{SC}_6\text{H}_4\text{CO}_2\text{H})]$  crystallises as a tetrameric unit; pairs of molecules form dimers through the usual carboxylic acid dimer formation, and these dimers then associate through aurophilic  $\text{Au}\cdots\text{Au}$  interactions, Fig. 30.[42]

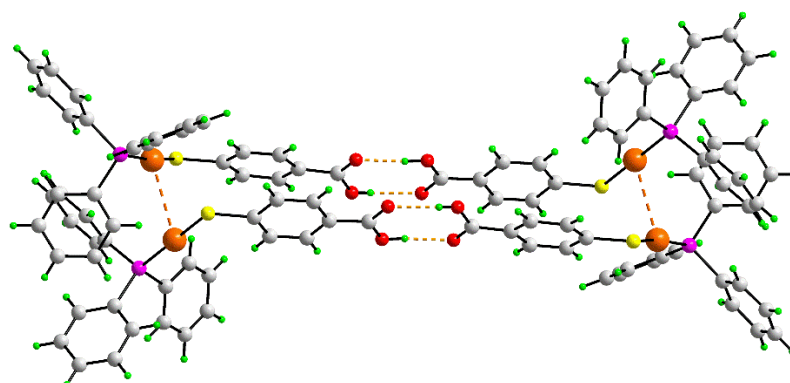


**Fig. 27.** The solid-state supramolecular structure of the 4MBA complex  $[(\text{Ph}_3\text{P})\text{Au}(\text{SC}_6\text{H}_4\text{CO}_2\text{H})]$  (XETNIT) showing the tetrameric assembly of molecules mediated by carboxylic acid dimer formation and via  $\text{Au}\cdots\text{Au}$  aurophilic interactions.

When the phosphine co-ligand is less sterically demanding, such as in  $[(\text{PhMe}_2\text{P})\text{Au}(\text{SC}_6\text{H}_4\text{CO}_2\text{H})]$ , Fig. 28a, additional aurophilic interactions between gold(I) centres are found, Fig. 28b, forming stacks of carboxylic acid dimers.[31]

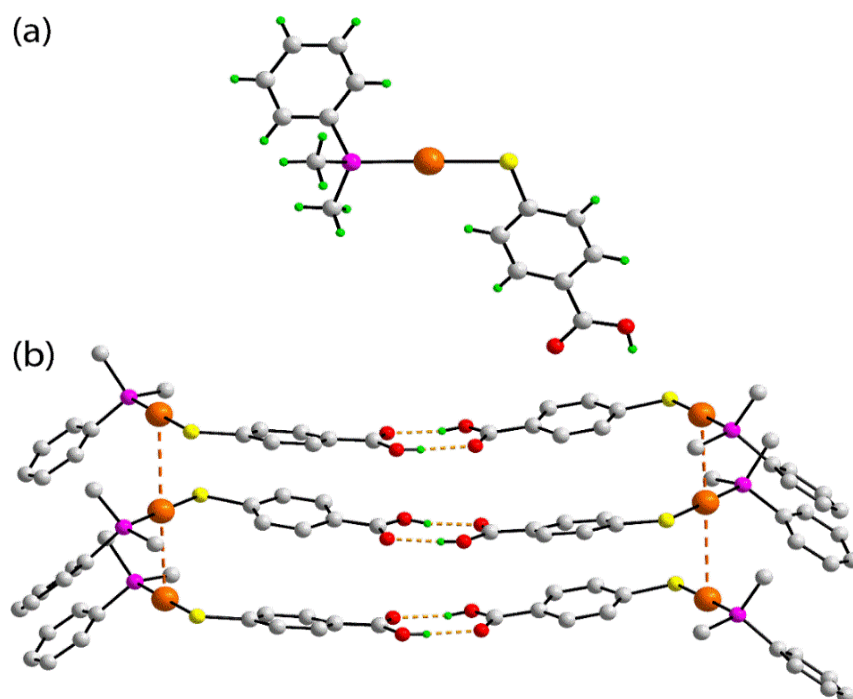


**Fig. 28.** The solid-state structure of the complex  $[(\text{PMe}_2\text{Ph})\text{Au}(\text{SC}_6\text{H}_4\text{CO}_2\text{H})]$  (BODMEN): (a) the molecular structure and (b) the assembly of molecules in the solid-state through carboxylic acid dimer formation and stacking of dimers through  $\text{Au}\cdots\text{Au}$  aurophilic interactions (non-acidic H atoms are omitted).

In comparison, there are only two X-ray structures of gold(I) complexes with 3MBA ligands, namely  $[\text{Au}(\text{SC}_6\text{H}_4\text{CO}_2\text{H}-3)(\text{PR}_3)]$  ( $\text{R} = \text{Ph}$  or  $\text{Cy}$ ).<sup>[47]</sup> The tricyclohexylphosphine complex shows the usual carboxylic acid dimer motif, resembling closely the binuclear aggregate shown in Fig. 25a. By contrast, the triphenylphosphine complex, whose molecular structure is shown in Fig. 29a, shows a more complex solid-state structure, Fig. 29b. The smaller steric bulk of the  $\text{PPh}_3$  ligand compared to  $\text{PCy}_3$  permits a closer aggregation of gold centres in the former complex, via  $\text{Au}\cdots\text{Au}$  aurophilic interactions,  $\text{O}-\text{H}\cdots\text{S}$  hydrogen-bonding interactions, as well as  $\pi\cdots\pi$  interactions between the phenyl ring of the 3MBA ligand and a phenyl ring of the triphenylphosphine. Issues relating to the disparity in the supramolecular aggregation in the isomeric  $[\text{Au}(\text{SC}_6\text{H}_4\text{CO}_2\text{H})(\text{PPh}_3)]$  structures and related systems discussed

herein have been summarised in a very recent bibliographic review of the interplay of conventional hydrogen-bonding interactions on the one hand and aurophilic Au...Au interactions on the other [48].

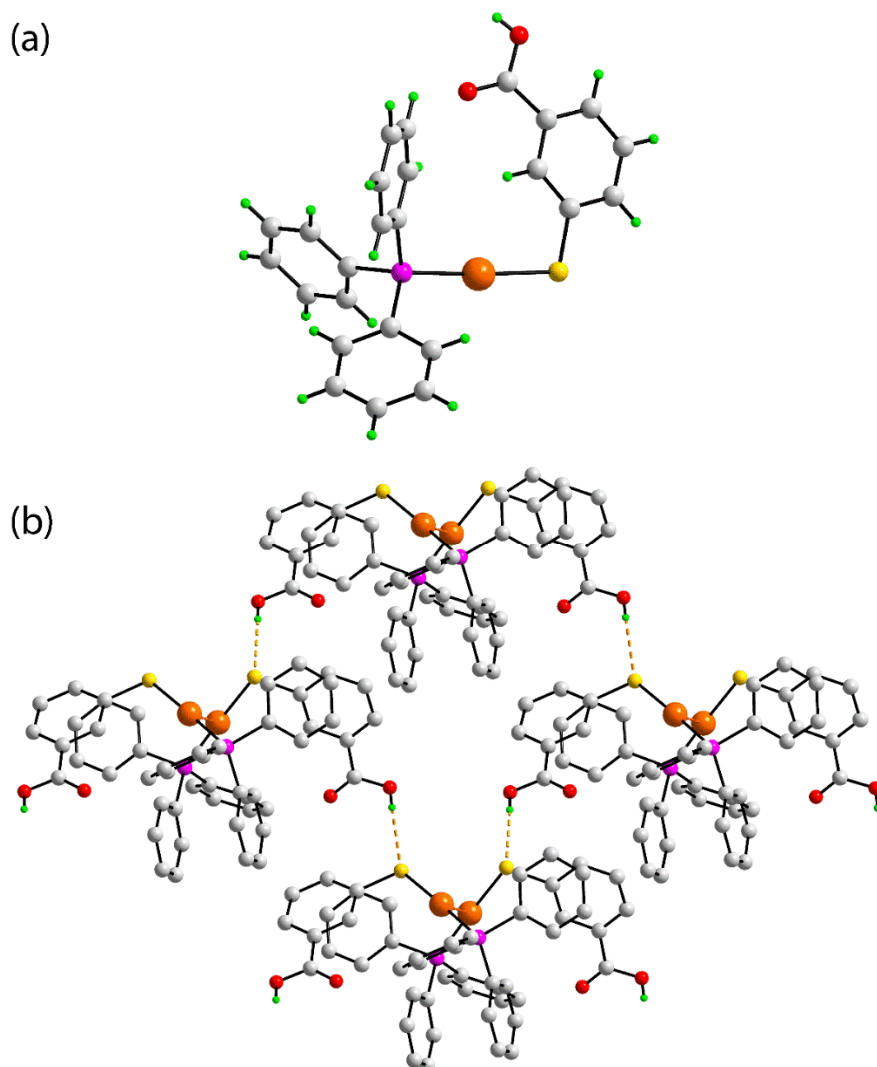
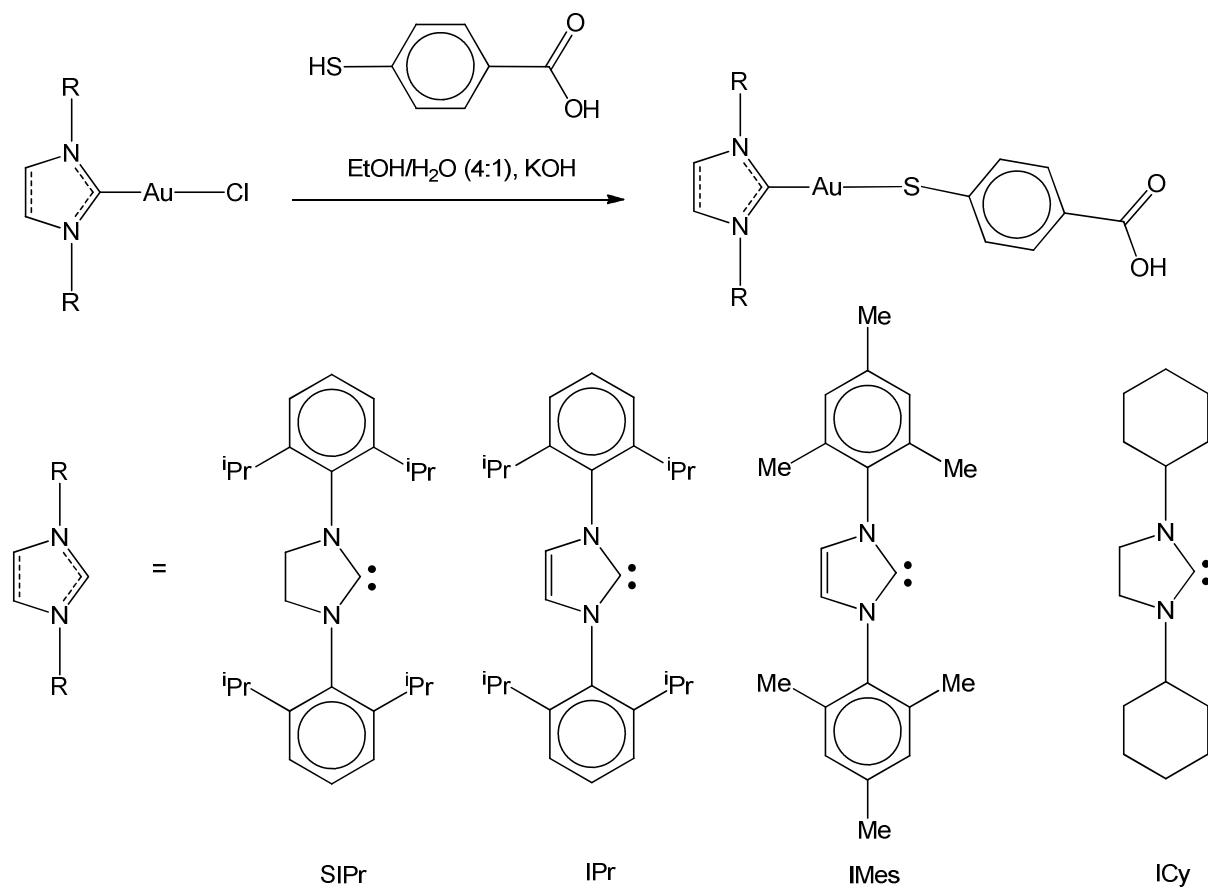


**Fig. 29.** The structure of the 3MBA gold(I) complex  $[\text{Au}(\text{SC}_6\text{H}_4\text{CO}_2\text{H}-3)(\text{PPh}_3)]$  (NENFOB): (a) Molecular structure of the complex and (b) solid-state structure showing the formation of a two-dimensional array formed by Au...Au and O-H...S hydrogen-bonding interactions (non-acidic H atoms are omitted).

A series of triorganophosphine gold(I) derivatives of 3MBA  $[(\text{R}_3\text{P})\text{Au}(\text{SC}_6\text{H}_4\text{CO}_2\text{H}-3)]$  (R = Cy, Ph) and 4MBA  $[(\text{R}_3\text{P})\text{Au}(\text{SC}_6\text{H}_4\text{CO}_2\text{H}-4)]$  (R = Cy, Ph, Et) have been tested against

a panel of seven human cell lines and the compounds found to show somewhat reduced cytotoxicity compared to isomeric thiosalicylate (2MBA) complexes.[46] The anti-microbial activity of the triphenylphosphine 3MBA and 4MBA derivatives  $[(\text{Ph}_3\text{P})\text{Au}(\text{SC}_6\text{H}_4\text{CO}_2\text{H})]$  against a range of organisms has been reported,[43,49] including a correction to the original work [43] which reported the activity as against *S. aureus* rather than *B. subtilis*.

Several examples of gold(I) 4MBA complexes with ancillary organometallic ligands in place of the phosphine have also been reported. Reaction of the isonitrile complexes  $\text{LAuCl}$  (where  $\text{L} = \text{tBuNC}$  or  $2,6\text{-Me}_2\text{C}_6\text{H}_3\text{NC}$ ) with  $\text{H}_2\text{4MBA}$  and  $\text{NaOMe}$  gave the complexes  $[\text{LAu}(\text{SC}_6\text{H}_4\text{CO}_2\text{H})_4]$  in good yield; no structure determinations were carried out on these derivatives.[50] In recent work by Contel and co-workers, a series of gold(I) complexes of 4MBA containing ancillary N-heterocyclic carbene (NHC) ligands (Scheme 10) were prepared by reaction of the respective  $(\text{NHC})\text{AuCl}$  complex with  $\text{H}_2\text{4MBA}$  in  $\text{EtOH}/\text{H}_2\text{O}$  using  $\text{KOH}$  base.[51] The IMes complex was structurally characterised (Fig. 30); the complex forms hydrogen-bonded carboxylic acid dimers, but no additional interactions are noted, presumably as a result of the steric bulk of the NHC ligand.[51] These complexes were used in the synthesis of heterobimetallic  $\{\text{TiAu}\}$  complexes (vide infra).



**Scheme 10**

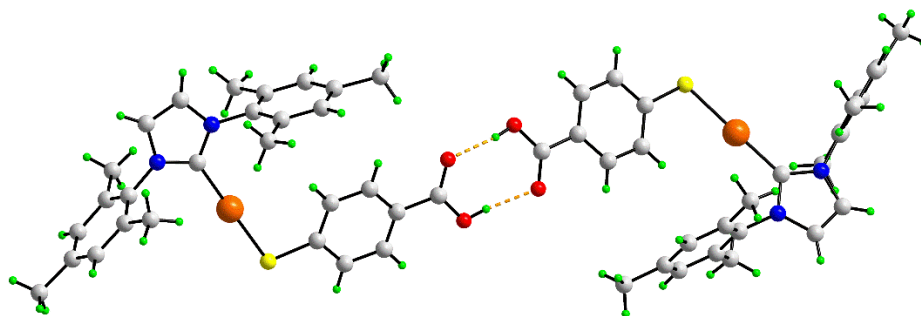
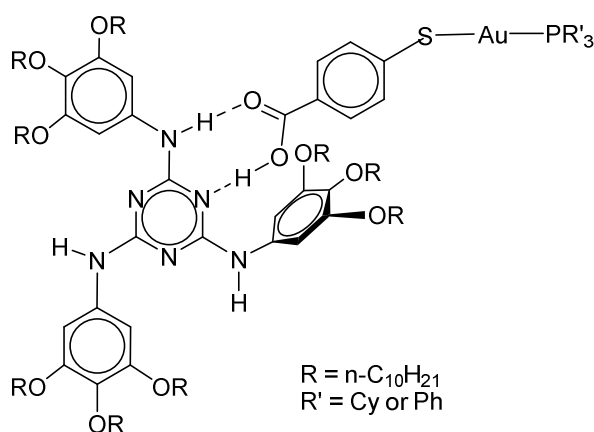


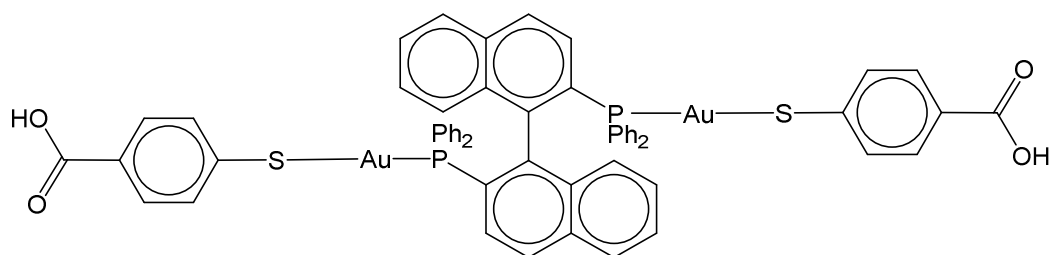
**Fig. 30.** Dimeric supramolecular aggregate involving the assembly of the two independent molecules comprising the asymmetric unit of the N-heterocyclic carbene gold(I) 4MBA complex,  $[(\text{IMes})\text{AuSC}_6\text{H}_4\text{COOH}]_2$  (ref. 51).

Gold(I) phosphine derivatives of 4MBA (as well as 2MBA), viz.  $(\text{R}_3\text{P})\text{AuSC}_6\text{H}_4\text{CO}_2\text{H}$  ( $\text{R} = \text{Ph}, \text{Cy}$ ) have been utilised for their hydrogen-bonding interactions with 2,4,6-

triaryl-amino-1,3,5-triazine, resulting in the formation of supramolecular aggregates **17**, which display a stable columnar hexagonal mesophase at room temperature. Analogous adducts were obtained with the same triazine and the chiral (R)- or (S)-BINAP-derived complexes **18**, which were prepared from BINAP(AuCl)<sub>2</sub> and H<sub>2</sub>4MBA in the same way.[52]

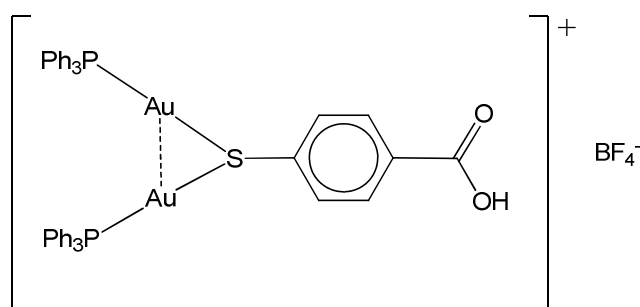


**17**



**18**

Finally, there are two other interesting derivatives of gold(I) with 4MBA ligands. An example of a gold(I) complex with an ancillary phosphine sulphide ligand, [Au(SC<sub>6</sub>H<sub>4</sub>COOH-4)(Ph<sub>3</sub>PS)] was prepared by reaction of [AuCl(SPPH<sub>3</sub>)] with H<sub>2</sub>4MBA and NaOMe.[42] The bis(aurated) complex [(Ph<sub>3</sub>PAu)<sub>2</sub>(SC<sub>6</sub>H<sub>4</sub>COOH)]BF<sub>4</sub> **19** has also been prepared by reaction of H<sub>2</sub>4MBA with the well-known oxonium aurating agent [(Ph<sub>3</sub>PAu)<sub>3</sub>O]BF<sub>4</sub>. [42]



19

## 12. Complexes of zinc, cadmium and mercury

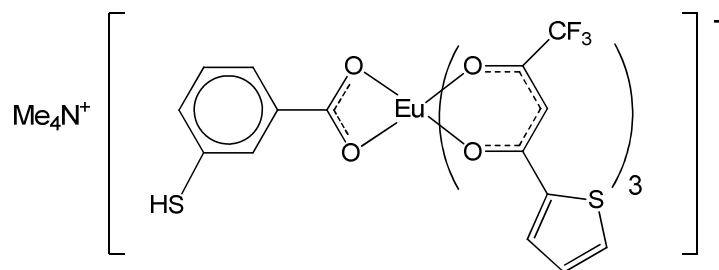
In very early work on mercaptobenzoate complexes of mercury, the ethylmercury derivative  $\text{EtHgSC}_6\text{H}_4\text{CO}_2\text{H}$  was synthesised by reaction of  $\text{EtHgCl}$  with  $\text{H}_2\text{4MBA}$  and added  $\text{NaOH}$ . A series of related compounds including the important ortho-isomer derived from thiosalicylic acid  $\text{EtHgSC}_6\text{H}_4\text{CO}_2\text{H}$  were also prepared in this work.[53] Evaluation of the anti-bacterial activity of these compounds [54] led to the subsequent widespread use of the sodium salt  $\text{EtHgSC}_6\text{H}_4\text{CO}_2\text{Na}$  (Thiomersal®, Thimerosal®) as an anti-bacterial agent (which has been summarised elsewhere [1]); the 3- and 4- isomers of  $\text{EtHgSC}_6\text{H}_4\text{COOH}$  have a lower activity compared to the 2-isomer.

In contrast to the extensive coordination chemistry of 2MBA (thiosalicylate) ligands with zinc and cadmium,[1] there are surprisingly no examples of 3MBA or 4MBA complexes with these metals.

## 13. Complexes of the lanthanide and actinide elements

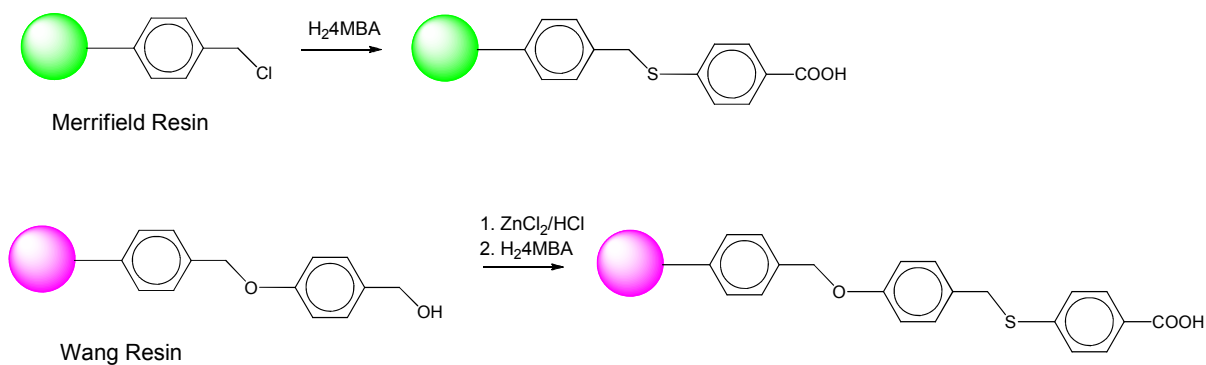
Lanthanide complexes of 4MBA have been obtained by reaction of the complexes  $[\text{M}(\text{tta})_2(\text{H}_2\text{O})_2]$  ( $\text{M} = \text{Eu}$  or  $\text{Gd}$ ;  $\text{tta} = \text{thenoyltrifluoroacetato}$ ) with the mono-sodium salt of  $\text{H}_2\text{4MBA}$ , followed by precipitation with  $\text{Me}_4\text{NCl}$ , to give the anionic europium complexes  $\text{Me}_4\text{N}[\text{Ln}(\text{tta})_3(4\text{-O}_2\text{CC}_6\text{H}_4\text{SH})]$  20.[55] The ground-state geometry of the europium complex was determined by computational methods, which showed the MBA carboxylate ligand to

coordinate to the europium in bidentate chelating fashion. The photophysical properties of the complexes was studied using luminescence spectroscopy and theoretical calculations, and showed high quantum yield.



## 20

4MBA has been used to modify Merrifield and Wang polymeric resins, Scheme 11. These materials were then used, in conjunction with an ionic liquid-modified mesoporous silica (SBA-15), and either hydrated gadolinium or europium nitrates, to encapsulate the europium polytungstate species  $\text{Na}_9\text{EuW}_{10}\text{O}_{36}\cdot 32\text{H}_2\text{O}$ . The ionic liquid was immobilised on the surface of the mesoporous silica through reaction of surface hydroxyl groups with the methylimidazolium (MeIm)-functionalised organosilane  $[(\text{EtO})_3\text{Si}(\text{CH}_2)_3\text{MeIm}]^+\text{Cl}^-$ . It was proposed that the benzoate groups of the modified resins were coordinated to the  $\text{Gd}^{3+}$  or  $\text{Eu}^{3+}$  ions. The emission properties of these hybrid materials was investigated, and many found to show cool-white emission, making them potentially useful in optical devices.[56] A parallel study investigated the introduction and photophysical properties of the corresponding  $\text{Tb}^{3+}$  system.[57]



**Scheme 11** Modification of Merrifield and Wang resins with 4MBA

Although no actinide complexes of 3MBA or 4MBA ligands have been isolated per se, a series of uranyl complexes containing oxidised (i.e. disulphide-containing) ligands ( $\text{SC}_6\text{H}_4\text{COOH}$ )<sub>2</sub> have been reported,[22] in some cases by the in situ oxidation of the thiol to the disulphide; three different compounds were able to be structurally characterised. These compounds, together with the macrocyclic nickel complex **13** (vide supra) [38] are the only structurally characterised examples of complexes derived from the disulphides of 3MBA or 4MBA. The compound  $\text{UO}_2(\text{C}_7\text{H}_4\text{O}_2\text{S})_3 \cdot \text{H}_2\text{O}$  was prepared by hydrothermal reaction of  $\text{UO}_2(\text{NO}_3)_2 \cdot 6\text{H}_2\text{O}$  with  $\text{H}_2\text{3MBA}$  in water with added ammonia base for 3 days at 180 °C. The structure of  $\text{UO}_2(\text{C}_7\text{H}_4\text{O}_2\text{S})_3 \cdot \text{H}_2\text{O}$  contains the 3MBA disulphide ligand coordinated through the bidentate chelating carboxylate ligand to a linear uranyl ( $\text{UO}_2^{2+}$ ) moiety, forming a hexagonal bipyramidal coordination geometry, as illustrated in Fig. 31. There is considerable disorder of the disulphide ligand in the crystal, suffice to mention the authors described the molecular packing as defining a “hexagonal plane net” [22].

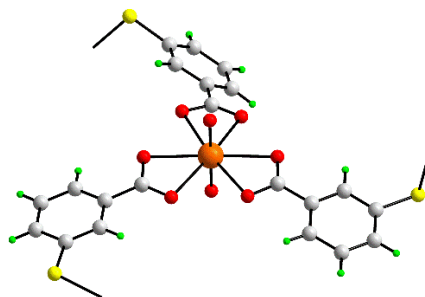


**Fig. 31.** The coordination geometry at uranium in the uranyl derivative containing a 3MBA disulphide ligand,  $\text{UO}_2(\text{C}_7\text{H}_4\text{O}_2\text{S})_3 \cdot \text{H}_2\text{O}$  (CUVCEC); for clarity, only half of each disulphide ligand is shown.

The compound  $[\text{UO}_2(\text{C}_7\text{H}_4\text{O}_2\text{S})_4]$  was prepared by reaction of  $\text{UO}_2(\text{NO}_3)_2 \cdot 6\text{H}_2\text{O}$  with the disulphide of 3MBA and ammonia at 180 °C for 3 days. The structure comprises one-dimensional ribbons constructed by edge-shared, octahedral uranyl centres that are connected via the carboxylate groups of 3MBA disulphide ligands;[22] there are two crystallographically independent but chemically equivalent uranyl groups in the polymeric chain, Fig. 32.

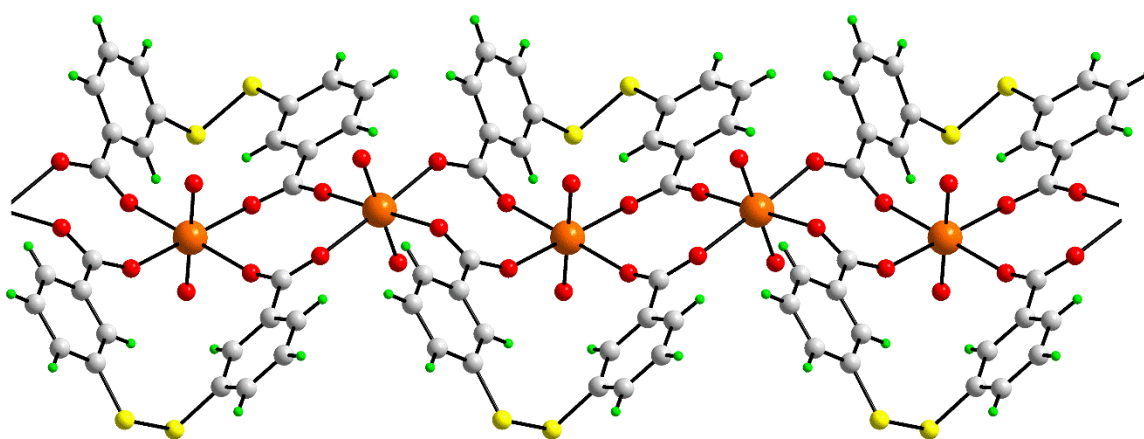


**Fig. 32.** The polymeric chain in  $[\text{UO}_2(\text{C}_7\text{H}_4\text{O}_2\text{S})_4]$  (CUVCOM) formed by bridging of uranyl groups with the carboxylate ligands of 3MBA disulphide ligands.

Finally, the 4MBA disulphide-containing compound  $[\text{UO}_2(\text{C}_7\text{H}_4\text{O}_2\text{S})_2(\text{C}_7\text{H}_5\text{O}_2\text{S})]$  (CUVCIG) was prepared by in situ oxidation of  $\text{H}_2\text{4MBA}$ , in a hydrothermal reaction (180 °C, 3 days) with  $\text{UO}_2(\text{NO}_3)_2 \cdot 6\text{H}_2\text{O}$  in the presence of ammonia. The compound contains uranyl groups bridged by 4MBA disulphide ligands. The coordination geometry about uranium is shown in Fig. 33a which shows one of the carboxylate groups is coordinated in a bidentate chelating mode, another in a monodentate mode and two other positions in the equatorial plane

of the uranyl group is completed by carboxylate-oxygen atoms derived from two bridging ligands, leading to a pentagonal bipyramidal geometry.[22] The bridging 4MBA disulphide ligands and uranyl groups form a two-dimensional net with topology  $4^{13}6^2$ , as illustrated in Fig. 33b.

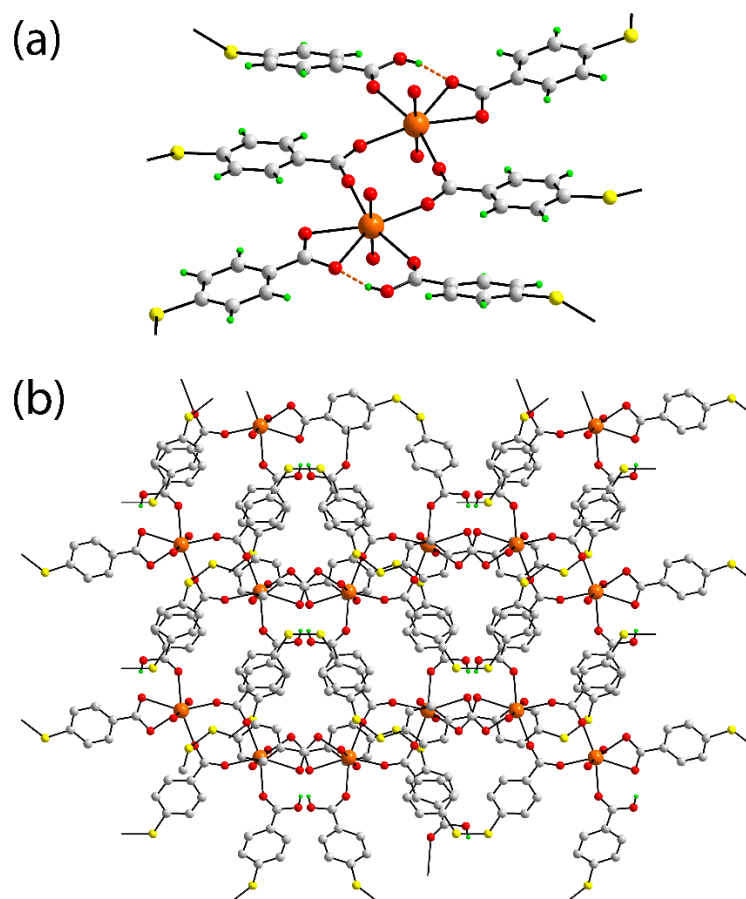


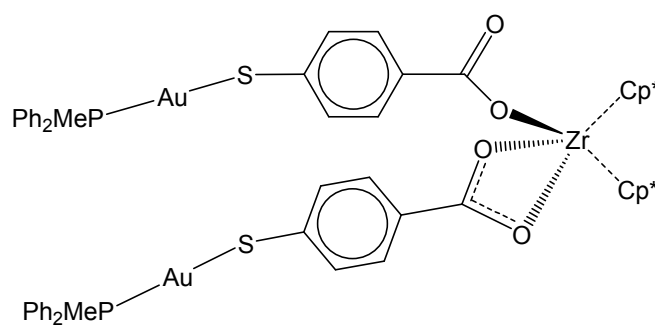
**Fig. 33.** (a) The coordination environment of the uranyl group with 4MBA disulphide ligands in  $[\text{UO}_2(\text{C}_7\text{H}_4\text{O}_2\text{S})_2(\text{C}_7\text{H}_5\text{O}_2\text{S})]$  (CUVCIG); only half of each disulphide ligand is shown and (b) the two-dimensional network (non-acidic H atoms are omitted).

#### 14. Heterobimetallic coordination compounds containing bridging 3MBA or 4MBA ligands

The hybrid hard-soft ligand characteristics of MBA ligands offers much potential for this class of ligand to act as a bridge between hard and soft metal centres, to form heterobimetallic complexes. A number of studies have investigated the potential of these

ligands, and to date, heterobimetallic compounds with metal stoichiometries {ZrAu}, {TiAu}, {ZrRh}, {ZrRh<sub>2</sub>} and {Ni<sub>2</sub>Au} have been synthesised and characterised. In addition, a number of applications of 3MBA and 4MBA ligands in materials chemistry also exploits the heterobifunctional nature of MBA ligands, as described in Sections 15 and 16.

Methane elimination has been extensively used in the synthesis of heterobimetallic compounds containing Ti or Zr, facilitating simple product purification. This is exemplified by the reaction of [Cp\*<sub>2</sub>ZrMe<sub>2</sub>] with 2 mole equivalents of the gold(I) 4MBA derivative [(Me<sub>2</sub>PhP)AuSC<sub>6</sub>H<sub>4</sub>COOH] which results in the elimination of methane and formation of the colourless {ZrAu} heterobimetallic complex [Cp\*<sub>2</sub>Zr{O<sub>2</sub>CC<sub>6</sub>H<sub>4</sub>SAu(PMe<sub>2</sub>Ph)}<sub>2</sub>] **21** in 69% yield.[31] The <sup>1</sup>H NMR spectrum showed a single resonance for the ortho protons, which broadens and splits into two signals between 190-200 K, due to a fluxional process similar to that for [Cp\*<sub>2</sub>ZrMe(O<sub>2</sub>CC<sub>6</sub>H<sub>4</sub>SH)<sub>2</sub>] (vide supra). From a crystallisation trial of this complex some crystals of the Zr-Me intermediate [Cp\*<sub>2</sub>ZrMe{O<sub>2</sub>CC<sub>6</sub>H<sub>4</sub>SAu(PMe<sub>2</sub>Ph)}] were isolated and structurally characterised, Fig. 34, showing the presence of a bidentate carboxylate group.



**21**

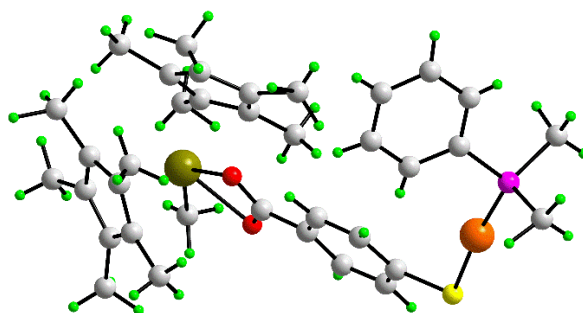
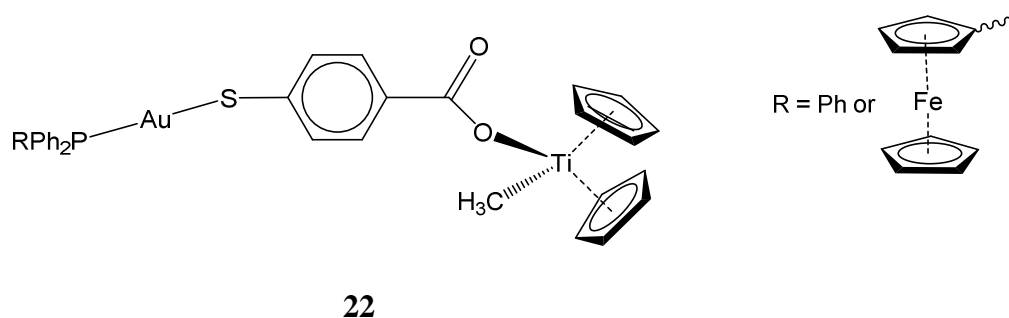


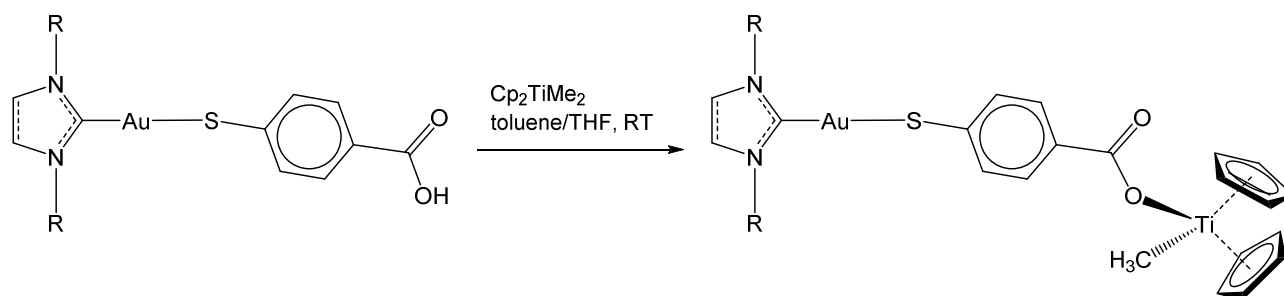
**Fig. 34.** Molecular structure of the 4MBA-bridged heterobimetallic ZrAu intermediate  $[\text{Cp}^*_2\text{ZrMe}\{\text{O}_2\text{CC}_6\text{H}_4\text{SAu}(\text{PMe}_2\text{Ph})\}]$  (BODMIR). Additional colour code: second heavy atom (Zr), dark-yellow.

Because of the biological activities of both titanium(IV) and gold(I) complexes against tumour cells, the two heterobimetallic titanium(IV)-gold(I) complexes **22** were prepared by a methane elimination reaction of the titanocene complex  $[\text{Cp}_2\text{Ti}(\text{CH}_3)_2]$  ( $\text{Cp} = \eta^5\text{-C}_5\text{H}_5$ ) with the 4MBA complexes  $\text{Ph}_2\text{RPAuSC}_6\text{H}_4\text{COOH}$  ( $\text{R} = \text{Ph}$  or ferrocenyl).[44,45] In contrast to the Zr complexes (vide supra), only a single carboxylate group was coordinated to the smaller titanium centre. These compounds, which were air- and moisture-stable, were found to be considerably more toxic when tested against a renal cancer cell line (Caki-1) when compared to reference compounds including cisplatin and titanocene dichloride ( $\text{Cp}_2\text{TiCl}_2$ ). An in vivo study of the  $\text{PPh}_3$  complex against Caki-1 mouse xenografts was also carried out, resulting in a 67% decrease in tumour size. Preliminary mechanistic studies suggested that the complex is active through inhibition of thioredoxin reductase, and titanium and gold were found to co-localise in a 1:1 ratio in the Caki-1 cells.



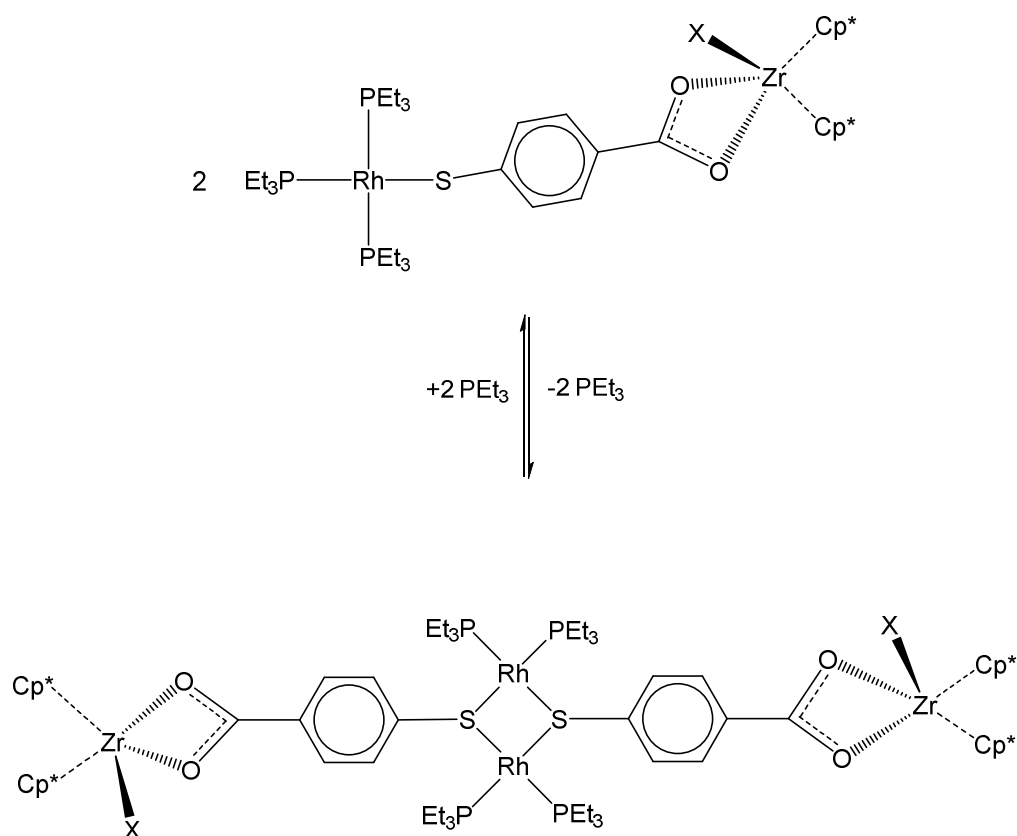
Subsequently, this work was developed to gold(I) complexes containing less labile NHC ligands, via the reaction of the NHC gold complexes (Scheme 10) with  $\text{Cp}_2\text{TiMe}_2$ , giving a series of four new, air- and moisture-stable yellow solids, Scheme 12.[51] These complexes were found to be more soluble than the corresponding phosphine analogues. IR spectroscopy

supported by DFT calculations suggested a monodentate coordination mode of the carboxylate group to Ti, on the basis of a difference of  $>200\text{ cm}^{-1}$  (in the range  $210\text{ to }351\text{ cm}^{-1}$ ) between the  $\text{CO}_2$  symmetric and asymmetric bands. These NHC-containing gold and gold-titanium complexes were evaluated for their biological activity against renal, prostate, colon and breast cancer cell lines. Co-localisation of Ti and Au in a 1:1 ratio was observed for the {TiAu} complex with the SIPr ligand in PC3 prostate cancer cells.



**Scheme 12** Synthesis of heterobimetallic {TiAu} complexes from NHC gold(I) MBA complexes; for the structures of the R groups refer to Scheme 10.

Reaction of the 4MBA complex  $[\text{Rh}(\text{SC}_6\text{H}_4\text{COOH})(\text{PEt}_3)_3]$  with  $\text{Cp}^*_2\text{ZrMe}_2$  in a 1:1 molar ratio (in the presence of excess  $\text{PEt}_3$  to suppress phosphine labilisation) gives the heterobimetallic {RhZr} complex  $[\text{Cp}^*_2\text{ZrMe}(\mu\text{-O}_2\text{CC}_6\text{H}_4\text{S})\text{Rh}(\text{PEt}_3)_3]$ , which reacts with 1 equivalent of water to give the corresponding hydroxido complex  $[\text{Cp}^*_2\text{Zr}(\text{OH})(\mu\text{-O}_2\text{CC}_6\text{H}_4\text{S})\text{Rh}(\text{PEt}_3)_3]$ .<sup>[58]</sup> These complexes dimerise in solution by dissociation of  $\text{PEt}_3$ , giving the {Zr<sub>2</sub>Rh<sub>2</sub>} complexes, as shown in Scheme 13. The molecular structures of these complexes, which are almost identical, are shown in Fig. 34.



**Scheme 13** Dimerisation process in heterobimetallic {ZrRh} complexes; X = CH<sub>3</sub> or OH.

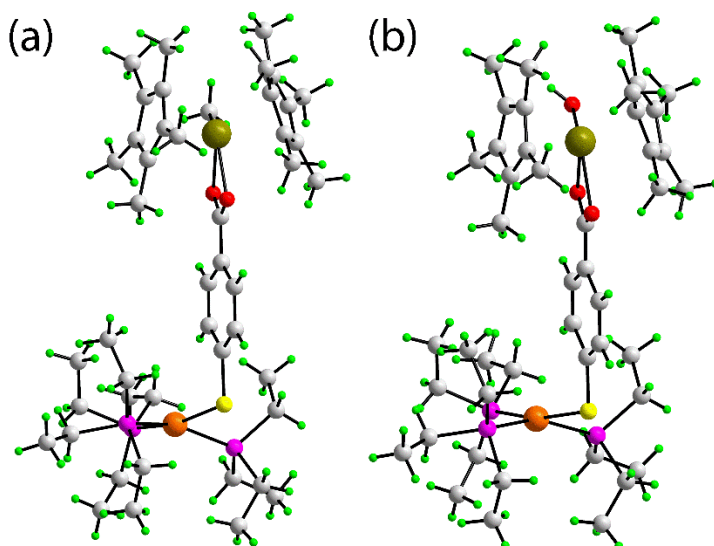
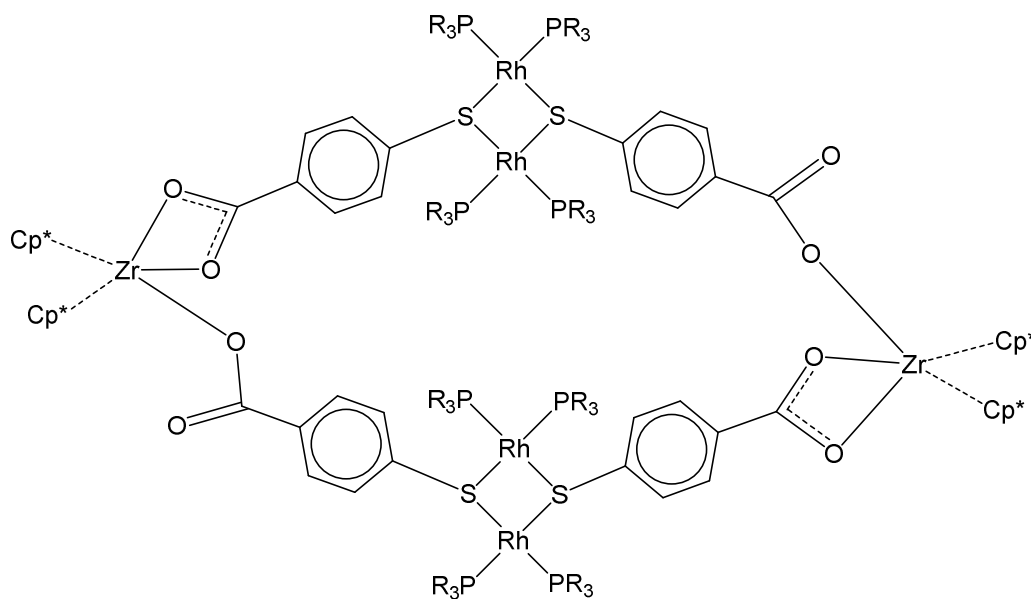


**Fig. 35.** Views of the nearly identical molecular structures of (a) the methyl (WETJEL) and (b) hydroxido (WETJIP) heterobimetallic {RhZr} complexes [Cp\*<sub>2</sub>ZrX(μ-O<sub>2</sub>CC<sub>6</sub>H<sub>4</sub>S)Rh(PEt<sub>3</sub>)<sub>3</sub>] (X = Me, OH).

The reaction of  $[\text{Cp}^*\text{ZrMe}_2]$  with  $[\{\text{Rh}(\mu\text{-SC}_6\text{H}_4\text{COOH})(\text{PPh}_3)_2\}_2]$  or with  $[\text{Rh}(\text{SC}_6\text{H}_4\text{COOH})(\text{PEt}_3)_3]$  (Section 9) gives 32-membered macrocyclic rings having the structure **23**.<sup>[58]</sup> The molecular structure of the  $\text{PPh}_3$  derivative **23a** is shown in Fig. 36, while that of the  $\text{PEt}_3$  analogue **23b** is shown in Fig. 37. In these complexes the zirconium centres are coordinated by one bidentate chelating carboxylate ligand and one monodentate carboxylate ligand. The phosphine group does not alter the overall stoichiometry of the metallomacrocyclic, but the thiolate groups occupy an exo position of the puckered four-membered  $\{\text{Rh}_2\text{S}_2\}$  ring in the  $\text{PPh}_3$  complex, and an endo position in the  $\text{PEt}_3$  derivative. This has a significant effect on the overall geometry of the cavity, which is rhombohedral in the  $\text{PPh}_3$  derivative (with internal cavity edges of 3.31 and 4.70 Å), while in the  $\text{PEt}_3$  complex the cavity comprises two smaller cavities each with dimensions 0.87 x 3.80 Å.



**23a** R = Ph

**23b** R = Et

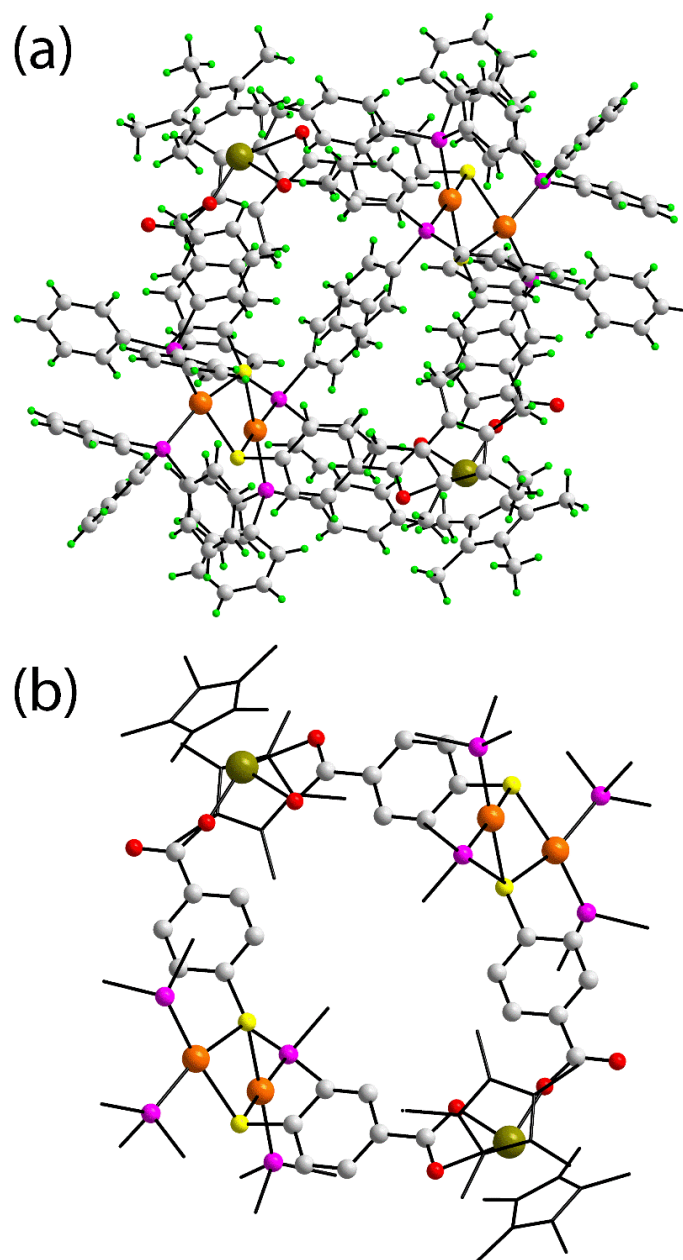


**Fig. 36.** The molecular structure of the metallomacrocyclic  $[(\text{Cp}^*_2\text{Zr}\{\mu\text{-O}_2\text{CC}_6\text{H}_4\text{S}\}\text{Rh}(\text{PPh}_3)_2\}_2)_2]$  **23a** (WETHUZ): (a) the complete molecular structure and (b) the core of the macrocycle with all but the isopropyl carbon atoms of the PPh<sub>3</sub> ligands and all H atoms omitted for clarity, and the Cp\* groups shown as sticks.

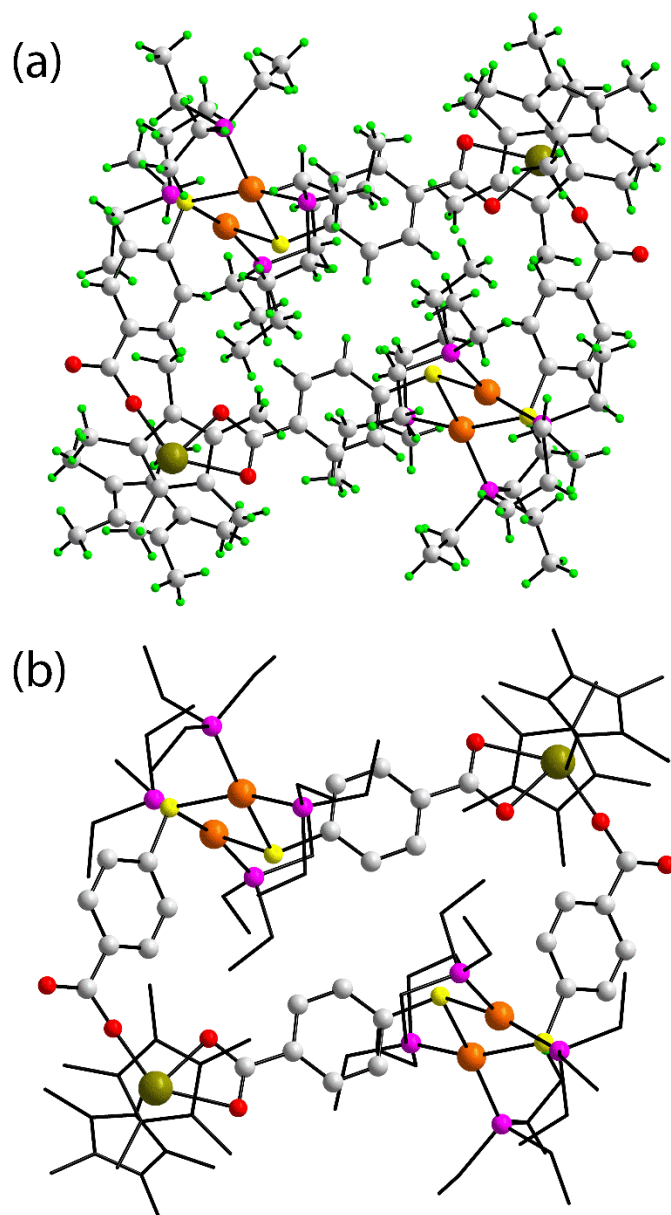
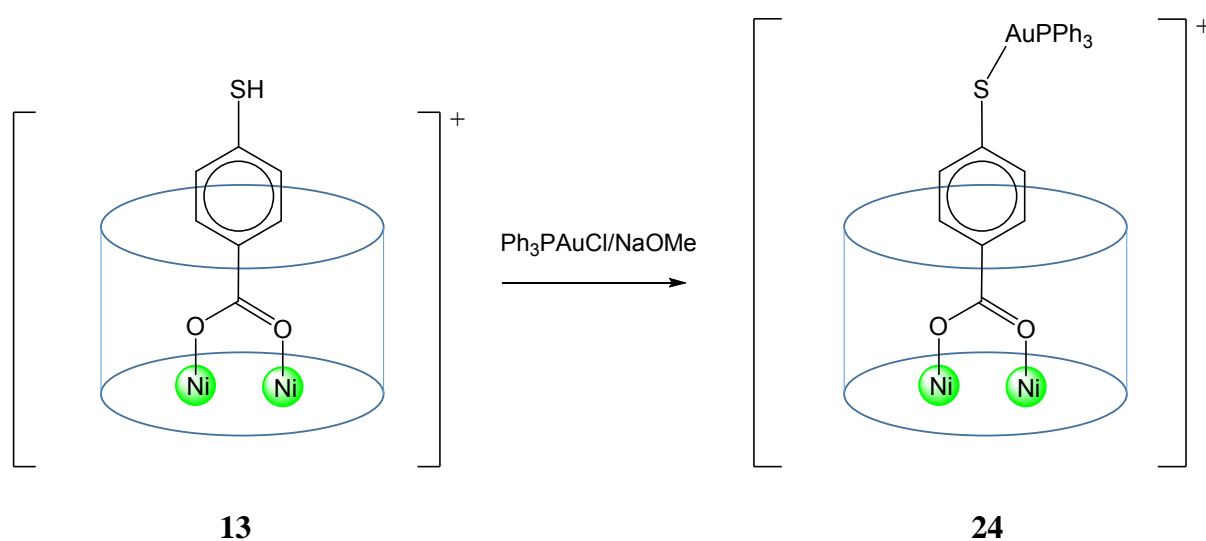


**Fig. 37.** (a) Molecular structure of the metallamacrocycle  $[(\text{Cp}^*_2\text{Zr}\{\mu\text{-O}_2\text{CC}_6\text{H}_4\text{S}\}\text{Rh}(\text{PEt}_3)_2\}_2)_2]$  **23b** (WETJAH): (a) the complete molecular structure and (b) the core of the macrocycle with all H atoms omitted for clarity, and the Et and Cp\* groups shown as sticks.

The macrocyclic dinickel complex **13** containing two nickel centres bridged by the carboxylate group of 4MBA (vide supra) reacts with  $\text{Ph}_3\text{PAuCl}$  in the presence of NaOMe to give the gold(I) thiolate complex **24**, Scheme 14, which was structurally characterised, Fig. 38.

The binding of the thiolate group to gold does not significantly affect the dinickel macrocycle, however the P–Au–S bond angle at  $174^\circ$  is somewhat less linear than in  $\text{Ph}_3\text{PAuSPh}$ , i.e.  $179^\circ$  [59], presumably due to steric effects and/or to the presence of an aurophilic interaction in the latter, i.e.  $\text{Au}\cdots\text{Au} = 3.16 \text{ \AA}$ . The gold complex **24** undergoes a reversible one-electron oxidation process in electrochemical experiments, giving a mixed-valence  $\text{Ni}^{\text{II}}\text{Ni}^{\text{III}}$  species.[38] The redox chemistry of the parent thiol **13** was similar, with additional features ascribed to redox chemistry of the 4MBA ligand.



**Scheme 14** Synthesis of the  $\text{Ph}_3\text{PAu}$  derivative of a macrocyclic dinickel complex **24** from **13**.

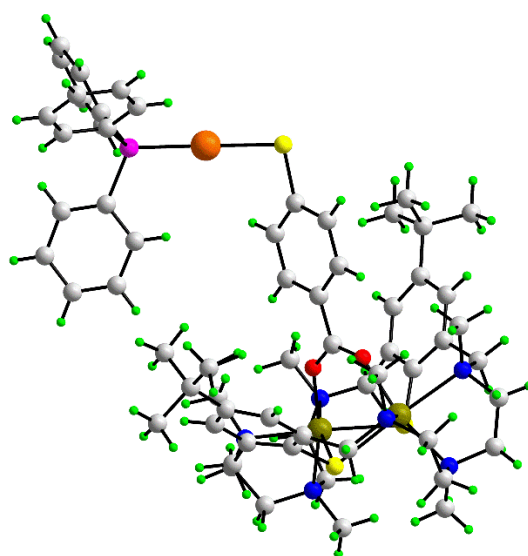
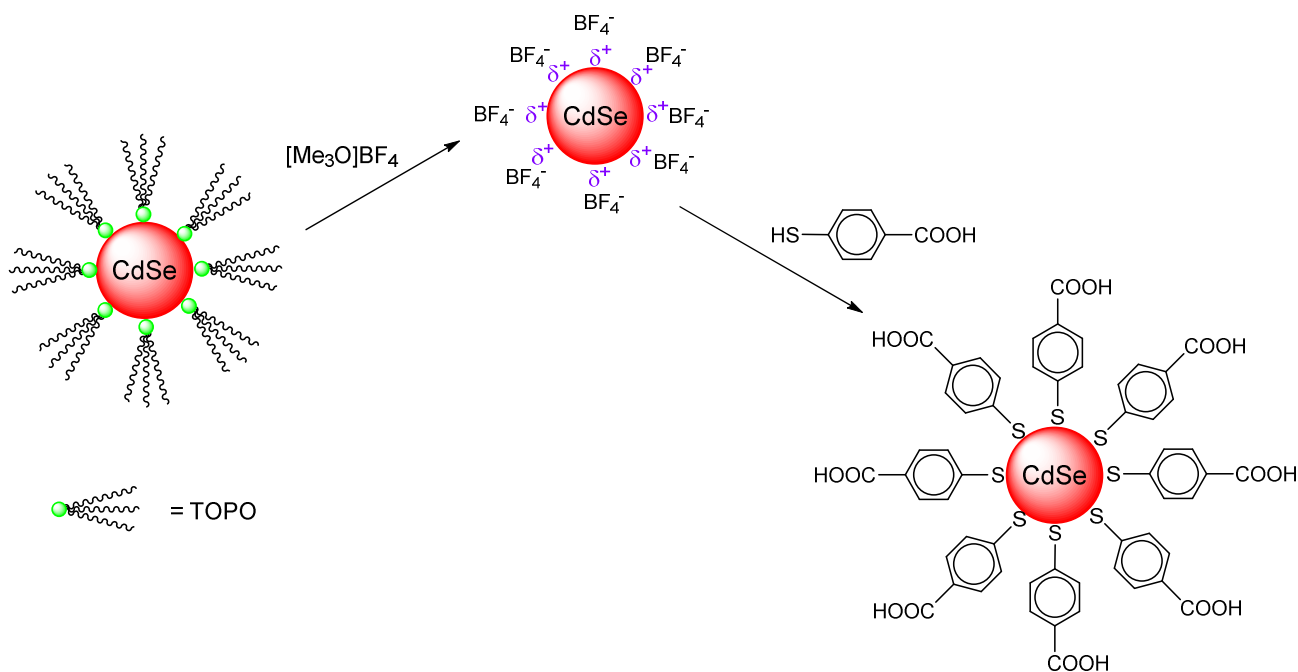


**Fig. 38.** Molecular structure of the  $(\text{Ph}_3\text{P})\text{Au}$  complex of the macrocyclic dinickel complex **24** (COYSAM) containing a 4MBA ligand bridging the two Ni centres through the carboxylate group, and the gold through the thiolate-sulphur.

### **15. Use of MBA ligands in the functionalisation of metal chalcogenide materials**

The bifunctional nature of 4MBA has been utilised in the derivatisation of metal chalcogenide materials, allowing the introduction of carboxylic acid/carboxylate groups onto the surface of the material. This is of interest for imparting water solubilisation, as well as providing a functional group (the carboxylic acid/carboxylate) which imparts further reactivity, allowing coupling to other materials. While we have not attempted to provide a comprehensive coverage of this field, selected examples are given to illustrate the general applicability of this chemistry of MBA groups.

The modification of quantum dots derived from metal chalcogenide materials including CdSe [60,61] and CdTe [62,63,64] has attracted particular interest. As an example, CdSe quantum dots protected with tri-n-octylphosphine oxide (TOPO) were treated with  $[\text{Et}_3\text{O}]\text{BF}_4$  to remove the TOPO protecting groups and provide an activated,  $\text{BF}_4^-$ -stabilised quantum dot. Subsequent treatment with  $\text{H}_2\text{4MBA}$  in THF gave 4MBA-derivatised CdSe quantum dots as shown in Scheme 15.[65]

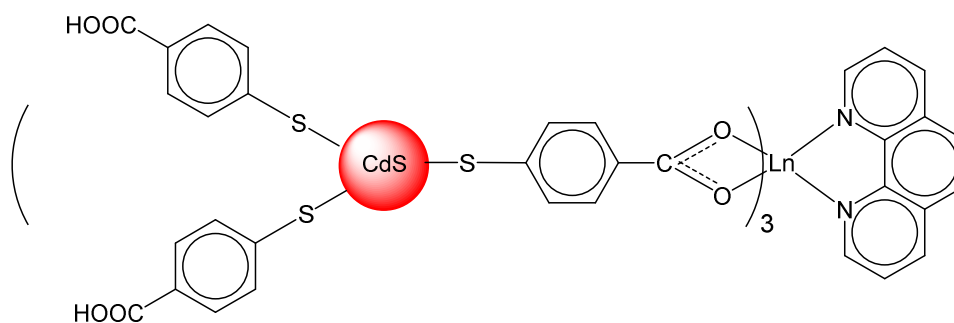


**Scheme 15** Functionalisation of a CdSe quantum dot with 4MBA.

4MBA has been employed as a heterobifunctional linker between metal chalcogenide quantum dots and metal oxides, such as between CdS or CdSe and  $TiO_2$  nanoparticles,[66,67] or between CdSe and ZnO single crystal electrodes [68]; such materials are of significant interest as an electrode in quantum dot-sensitised solar cells. For the same purpose, multi-walled carbon nanotubes have been functionalised with polyaniline, which was then reacted with  $H_2$ 4MBA (resulting in an interaction between the amine groups of the polyaniline and the carboxylic acid) in order to derivatise the resulting composite material with thiol groups that could be used to adsorb CdS-coated CdSe quantum dots.[69]

Lanthanide ions ( $Eu^{3+}$  and  $Tb^{3+}$ ) have been immobilised onto CdS quantum dots immobilised in a zeolite. Firstly, cadmium ion-exchanged zeolite was reacted with sulphide ions to form the CdS quantum dot-loaded zeolite. The CdS was then derivatised through the thiol group of a mercapto carboxylic acid, specifically 4MBA, together with thiosalicylic acid (2MBA) and mercaptoacetic acid ( $HSCH_2COOH$ ). Subsequent reaction with the  $Ln^{3+}$  ion in

the presence of 1,10-phenanthroline (phen) gave the hybrid zeolite-CdS-lanthanide materials, as shown schematically by **25**.<sup>[70]</sup> The luminescence properties of these materials could be changed from white or pink to red upon changing the mercaptocarboxylic acid, attributed to the different electron-transfer abilities of these three acids.



**25**

4MBA has been used as a linker in the construction of a hybrid material containing TiO<sub>2</sub> (which is functionalised by the MBA carboxylate groups), CdS quantum dots, and a polysiloxane material which is used to bind a 1,10-phenanthroline-rare earth element (Eu, Tb) group.<sup>[71]</sup> The use of an MBA-derived linker has also been employed to link gadolinium(III) complexes to InP/ZnS quantum dots for use as MRI contrast agents.<sup>[72]</sup>

## 16. Use of MBA ligands in the functionalisation of metal clusters, nanoparticles and metallic surfaces

### 16.1 Metal carbonyl cluster derivatives

As for the isomeric 2MBA ligand,<sup>[1]</sup> 3MBA and 4MBA are known to form a number of carbonyl cluster derivatives with ruthenium and osmium. Li and Leong have investigated the reactivity of the labilised osmium carbonyl precursor [Os<sub>3</sub>(CO)<sub>10</sub>(NCMe)<sub>2</sub>] with 3MBA and 4MBA, which gave the thiolato-bridged clusters [Os<sub>3</sub>(CO)<sub>10</sub>(μ-H)(μ-SC<sub>6</sub>H<sub>4</sub>CO<sub>2</sub>H)] **26a** and **26b** in 73 and 68% yields for the 3- and 4-isomers, respectively. Additionally, for the 3-isomer the linked cluster **27** was isolated in 3% yield.<sup>[73]</sup> The X-ray structure of the osmium derivative

of the 3MBA ligand **26a** has been reported and exists as a hydrogen-bonded carboxylic acid dimer in the solid, as shown in Fig. 39. The X-ray structure of the bridged compound **27** shows the thiolate-sulphur bridging the Os–Os bond of one Os<sub>3</sub> cluster, while the carboxylate group bridges the Os–Os bond of the second Os<sub>3</sub> cluster, Fig. 40. Reaction of the more reactive [Ru<sub>3</sub>(CO)<sub>12</sub>] with H<sub>2</sub>3MBA and H<sub>2</sub>4MBA gave the trinuclear thiolate-bridged analogues **26c** and **26d** in 61 and 27% yields for the 3- and 4- isomers, respectively. No linked clusters were observed for the ruthenium system.

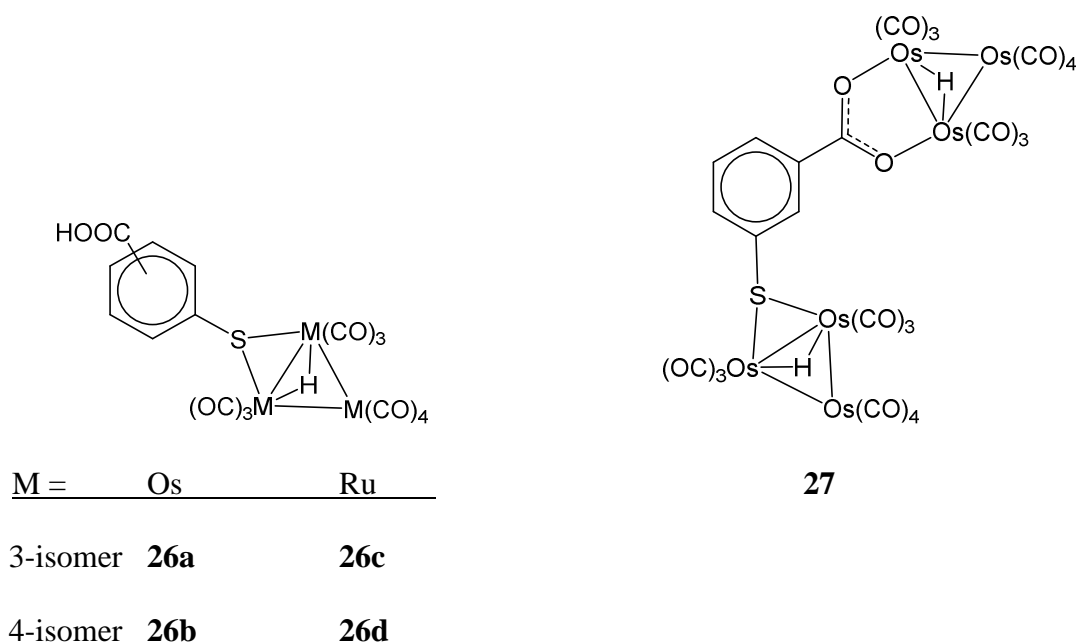


**Fig. 39.** Molecular structure of the 3MBA derivative **26a** (DIZHUQ) showing the formation of a carboxylic acid dimer.

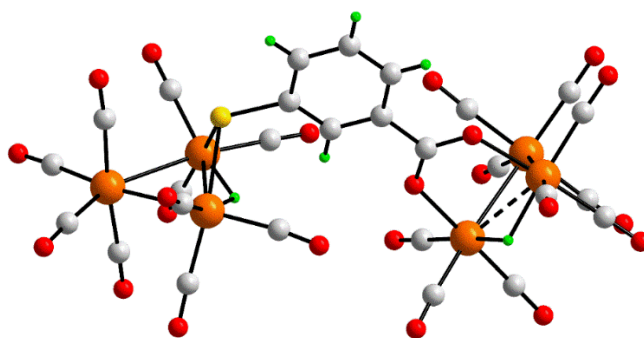


**Fig. 40.** Molecular structure of the 3MBA derivative **27** (DIZJAY) showing the 3MBA ligand bridging two  $\text{Os}_3$  triangles.

### 16.2 *Well-defined non-carbonyl metal clusters containing MBA ligands*

Small clusters of the coinage metals silver and gold can be protected by thiolate ligands, and such materials have attracted considerable attention since their initial development;[74,75] the reader is referred to a number of reviews that have summarised developments in this field,[76,77,78,79,80] and here only a brief overview is given. As a thiol with a para-substituted carboxylic acid group providing further functionality,  $\text{H}_2\text{4MBA}$  is well-known to act as a stabiliser for metal nanoparticles such as gold [81] and silver.[82]

The general methodology for the synthesis of gold clusters involves the reduction of a Au(III) precursor (e.g.  $\text{AuCl}_4^-$ ) to Au(I) using thiol, followed by further reduction to gold(0) using  $\text{NaBH}_4$ . However, poor reproducibility in nanoparticle size distribution has often hampered the development of such materials. In some cases however, well-defined compounds with atomically-precise cores (i.e. with a well-defined number of gold atoms in the metal core) can be obtained. Such materials are described in this Section, with a particular emphasis on compounds that have been crystallographically characterised. However, there is inevitably some overlap with those studies described in the subsequent section, where metal nanoparticles protected by MBA ligands are described. In some cases these may be atomically precise, but are not reported as such.

The earliest synthesis of well-defined gold clusters protected with thiolate ligands concerned the synthesis and structural characterisation of  $[\text{Au}_{25}(\text{SR})_{18}]^-$  ( $\text{R} = \text{PhCH}_2\text{CH}_2$ ).<sup>[83]</sup> A computational study explored the predicted structures and electronic properties of a series of related 4-thiophenolate derivatised clusters of the type  $[\text{Au}_{25}(\text{SC}_6\text{H}_4\text{X})_{18}]^-$  where  $\text{X} = \text{H}, \text{Cl}, \text{NO}_2$  and the 4MBA derivative where  $\text{X} = \text{COOH}$ . The MBA derivative was predicted to have the most distorted  $\text{Au}_{25}\text{S}_{18}$  core geometry; this was correlated with a reduced HOMO-LUMO gap with a consequent effect on the optical absorption spectrum.<sup>[84]</sup> In another computational study, the effects of ligands (including 4MBA) on the stabilities of a range of thiol-stabilised gold nanoclusters of the types  $[\text{Au}_{25}(\text{SR})_{18}]^-$ ,  $[\text{Au}_{38}(\text{SR})_{24}]$  and  $[\text{Au}_{102}(\text{SR})_{44}]$  ( $\text{SR} = \text{SC}_6\text{H}_4\text{COOH}$ ) were explored.<sup>[85]</sup>

The use of CO as a mild reducing agent (in place of the more reactive  $\text{NaBH}_4$ ) has been employed in a study of the reduction kinetics of  $\text{HAuCl}_4$  in the presence of  $\text{H}_2\text{3MBA}$ , giving atomically-precise  $[\text{Au}_{25}(\text{3MBA})_{18}]^-$  nanoclusters in estimated >90% yield. The ESI mass spectrum of the isolated nanoclusters showed two peaks, at approximately  $m/z$  2850 (corresponding to 3- ions) and 3870 (corresponding to 2- ions), with both attributed to the  $[\text{Au}_{25}(\text{3MBA})_{18}]^-$  species. The work also allowed the identification of a total of 29 intermediate gold(I) species of the general composition  $[\text{Au}_M(\text{SR})_N\text{Cl}_P]^{q-}$  using ESI MS, such as  $[\text{Au}_3(\text{SR})_3\text{Cl}]^-$  which is susceptible to reduction by CO. A range of stable nanocluster intermediates, of varying nuclearities, were also observed.<sup>[86]</sup>

4MBA has been used to stabilise  $\text{Ag}_{44}$  nanoparticles, which were obtained on a large (multi-gram) scale as a pure product and found to be highly stable.<sup>[87,88]</sup> The formation of a truly single-sized nanoparticle product is rare in the area of nanoparticle synthesis, and is attributed to the high stability of the nanoparticles' structure. The synthetic methodology involved the reaction of aqueous  $\text{AgNO}_3$  with an ethanol solution of  $\text{H}_2\text{4MBA}$ . Following pH adjustment to pH 9 (preferably using  $\text{CsOH}$ ) to solubilise the Ag thiolate precursor, followed by adjustment to pH 12 to stabilise the product, reduction with  $\text{NaBH}_4$  gave a dark-red solution

containing the  $M_4Ag_{44}(4MBA)_{30}$  with the carboxylate groups in salt form. These were isolated by precipitation with DMF, followed by protonation with acetic acid giving the final  $M_4Ag_{44}(4MBA)_{30}$  product (containing a mixture of alkali metal counter-ions M). It was found that a coordinating solvent (such as DMSO) protected the nanoparticles, which were best stored as damp rather than dry solids. Crystals of the sodium salt  $Na_4Ag_{44}(4MBA)_{30}$  were obtained from its DMF solution, and the X-ray structure of the product is shown in Fig. 41. The silver core of the cluster comprises a hollow icosahedron within a dodecahedron, resulting in 32-silver excavated dodecahedral core, having icosahedral symmetry. The core is capped by the remaining 12 Ag atoms in the form of six  $Ag_2S_5$  ‘mounts’ (three-dimensional decorations of the core). ESI mass spectrometry of the crude product gave various ions consistent with a uniform cluster size, viz.  $[Ag_{44}(4MBA)_{30}]^{4-}$  at  $m/z$  2336 and the fragment ion  $[Ag_{43}(4MBA)_{28}]^{3-}$  at  $m/z$  2975, formed by dissociation of  $[Ag(4MBA)_2]^-$ .

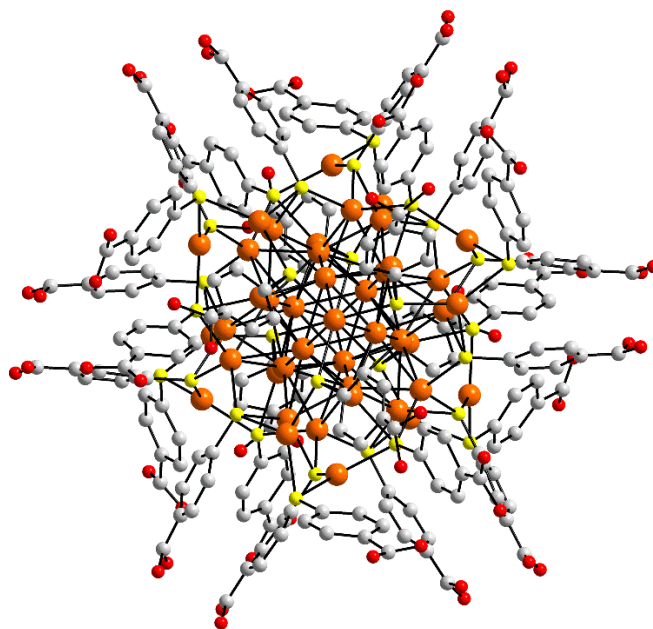
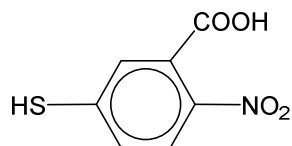


**Fig. 41.** X-ray structure of the sodium salt of the  $Ag_{44}$  cluster,  $Na_4Ag_{44}(4MBA)_{30}$  (XIMHOS).  $Na^+$  cations, H atoms, disordered component and unspecified solvent are not shown.

The 3MBA analogue **28** containing a nitro substituent has been used to stabilise monodisperse silver nanoclusters having the composition  $[\text{Ag}_{44}(\text{SR})_{30}]^n$ , prepared by  $\text{NaBH}_4$  reduction of an  $\text{AgNO}_3$ -thiol mixture. The nanoclusters were characterised by a variety of techniques and found to be stable for at least nine months under ambient conditions.[89]



**28**

Molecular dynamics simulations have been carried out on icosahedral  $\text{Au}_{44}$  nanoclusters that are surface-coated with 60 4MBA groups in eight aqueous solutions containing a range of cations and anions. The behaviour of the nanoclusters was predicted to be alterable by changing the pH and solute ion combinations, which may be an effective way of modulating the tendency for such nanoclusters to aggregate in solution.[90]

The most intensively studied of the discrete gold clusters capped by MBA ligands is the large cluster  $\text{Au}_{102}(\text{4MBA})_{44}$ . This was initially prepared as a minor component of a nanoparticle mixture, and has been obtained as single crystals from a solution containing 40% methanol, 200 mM NaCl and 100 mM NaOAc at a pH of 2.5.[91] An improved procedure by the same research group subsequently gave the compound in high yield (50-70% conversion of  $\text{HAuCl}_4$  to  $\text{Au}_{102}(\text{4MBA})_{44}$ ) and purity; the methodology involves reaction of an aqueous methanol solution of  $\text{H}_2\text{4MBA}$ , NaOH and  $\text{HAuCl}_4$  with  $\text{NaBH}_4$ , followed by a sequence of precipitation-centrifugation-dissolution steps.[92]

$\text{Au}_{102}(\text{4MBA})_{44}$  has been structurally characterised, Fig. 42.[91] The structure has the central gold atoms in a 49-atom Marks dodecahedron, surrounded by layers of gold atoms. Alternatively, the Marks decahedron can be viewed as five twinned fcc or hcc crystallites; the Au–Au distances in the core (2.8 to 3.1 Å) corresponds with the distance in fcc metallic gold (2.9 Å). The gold atoms in the core (which do not interact with the MBA ligands) all have 12

nearest neighbours, but those near the surface have between 2 and 11 nearest neighbours. The 4MBA ligands interact strongly with the gold atoms, and also interact with each other (through  $\pi \cdots \pi$  interactions of phenyl rings, T-stacking of phenyl rings through C–H  $\cdots \pi$  interactions and S  $\cdots$  Ph interactions) forming a rigid surface coating to the nanoparticles. The structure can also be viewed as an Au<sub>23</sub>(MBA)<sub>44</sub> layer (with each gold interacting with two thiolates to form the so-called ‘staple motif’), surrounding a core of 79 gold atoms, and the cluster can therefore be represented as Au<sub>79</sub>[Au<sub>23</sub>(4MBA)<sub>44</sub>].

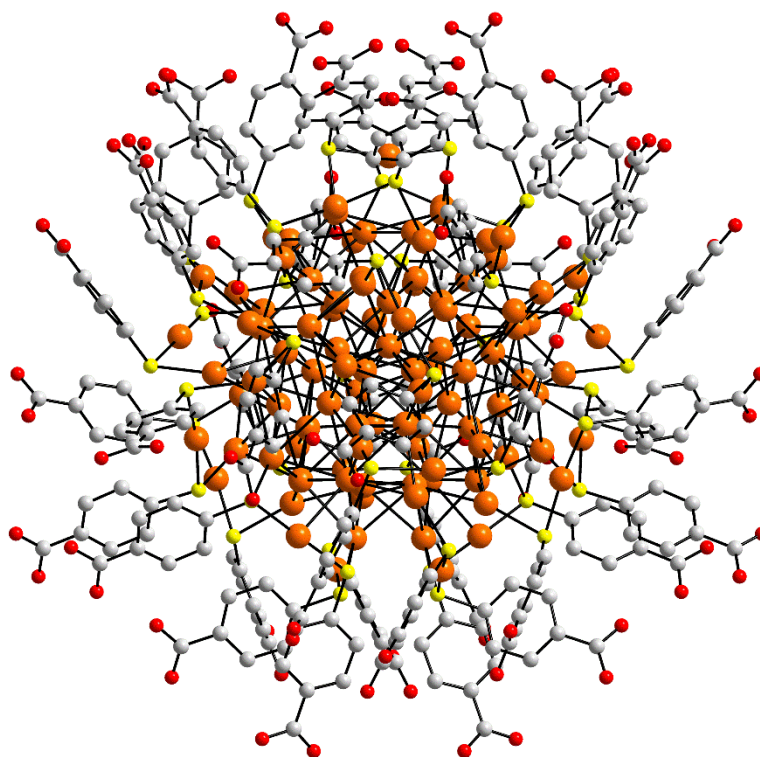
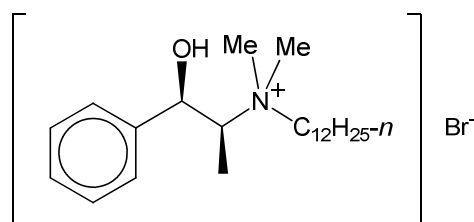


**Fig. 42.** Structure of the 4MBA-protected cluster [Au<sub>102</sub>(4MBA)<sub>44</sub>] (TORDEK). H atoms are omitted.

The structure of Au<sub>102</sub>(MBA)<sub>44</sub> is chiral, with both enantiomers present in the crystal; nanoparticles interact in the crystal through carboxylic acid hydrogen-bonding interactions, in some cases involving water molecules.[91] A partial resolution of the enantiomers has been

achieved using a chiral phase transfer method, whereby the chiral ammonium salt (-)-1R,2S-N-dodecyl-N-methylephedrinium bromide **29** facilitates phase transfer from water into chloroform. At low concentrations (ca 0.5 mg mL<sup>-1</sup>) of the ammonium salt **29**, partial phase transfer of one enantiomer occurs, and the aqueous and chloroform phases both show optical activity with near mirror image relationship, due to the formation of diastereomeric salts. However, at high ammonium salt concentrations, full phase transfer occurs, although the chloroform phase still shows optical activity, which was rationalised by one of the diastereoisomers having very strong optical activity.[93]



**29**

A large number of studies have concerned the properties and potential applications of the Au<sub>102</sub>(4MBA)<sub>44</sub> gold cluster. A number of computational investigations, employing density functional theory (DFT), have explored the structural and electronic properties of Au<sub>102</sub>(SR)<sub>44</sub> clusters, yielding results in agreement with the experimentally determined structure.[94,95] The studies predict an energy gap of approximately 0.5 eV upon adsorption of MBA molecules onto the gold core, and that the stability of these species is due to a combination of the staple motif, stability against dissociation and a significant HOMO-LUMO separation. The stability of this cluster has been described by a “noble gas super-atom analogy”.[96] The relationship between Au<sub>102</sub>(4MBA)<sub>44</sub> and large metalloid clusters of gallium and aluminium has also been explored.[97]

The ESI mass spectrum of Au<sub>102</sub>(4MBA)<sub>44</sub> showed a series of ions having m/z ratios that correspond to a series of ions in different protonation states, while MALDI TOF mass

spectrometry showed a broad peak at around 22,000 Da consistent with a species containing 102 Au and 44 S atoms.[92] The UV-visible spectrum of  $\text{Au}_{102}(\text{4MBA})_{44}$  shows a peak at 269 nm due to the 4MBA ligand, but no surface plasmon resonance band, consistent with other gold clusters < 2 nm in size.[92] A detailed vibrational spectroscopic study of the compound in the mid-IR to UV region has also been carried out.[98]

The  $\text{Au}_{102}(\text{4MBA})_{44}$  cluster undergoes a thiolate-exchange reaction upon reaction with 4-bromobenzene thiol,  $\text{BrC}_6\text{H}_4\text{SH}$ , giving the partly-exchanged cluster  $\text{Au}_{102}(\text{4MBA})_{40}(\text{SC}_6\text{H}_4\text{Br})_4$ . The structure of this compound was determined, which showed that 2 of the 22 symmetry-independent MBA positions undergo rapid exchange.[99] These observations suggested that the  $\text{Au}_{102}(\text{4MBA})_{44}$  cluster should be a very useful substrate for further modifications via thiolate-exchange reactions. For example, the  $\text{Au}_{102}(\text{4MBA})_{44}$  cluster has been successfully conjugated to biological molecules, via thiolate-exchange reactions, to a single chain antibody fragment containing an exposed cysteine group, and to a 14-residue oligodeoxyribonucleotide that had been modified with an SH group.[92]

Larger 4MBA-protected gold nanoparticles containing 144 gold atoms are also known.  $[\text{Au}_{144}(\text{SC}_6\text{H}_4\text{COOH})_{52}]$  was prepared by  $\text{NaBH}_4$  reduction of an aged, alkaline solution of  $\text{HAuCl}_4$  and  $\text{H}_2\text{4MBA}$ , and proposed to be related to the crystallographically-characterised  $[\text{Au}_{102}(\text{SC}_6\text{H}_4\text{COOH})_{44}]$  cluster (vide supra).[100]  $[\text{Au}_{144}(\text{SC}_6\text{H}_4\text{COOH})_{60}]$  is also known and has been isolated as hexagonal-plates, and characterised by MALDI TOF MS.[101] These  $\text{Au}_{144}$  clusters were used in bioconjugation studies, for example to conjugate a thiol-based small molecule SDC-1721 via a simple thiolate ligand-exchange reaction, where the resulting conjugate effectively inhibited HIV-1 fusion to human T cells.[100] Conjugates with proteins and DNA have also been investigated.[102]

### 16.3 *Metal nanoparticles*

As described in the preceding section, 4MBA has been used in the synthesis of thiolate-protected metal clusters that are atomically precise. A significant number of studies have also concerned the synthesis and applications of MBA-protected metal nanoparticles of less well-defined metal nuclearity, such as in the use of 6.6 nm 4MBA-capped gold seeds in the synthesis of gold nanorods.[103]

An improved procedure for the synthesis of Au nanoparticles protected with 3MBA or 4MBA (or other thiols) involved reaction of  $\text{HAuCl}_4$  with the thiol in methanol, giving a white precipitate, which was allowed to equilibrate at pH 13 at room temperature for 16 h, followed by reduction with  $\text{NaBH}_4$  for 4.5 h, which gave uniform-sized, water-soluble gold nanoparticles that were stable for years in water. The ratio of thiol to gold determined the size of the particles.[104] 4MBA-protected gold nanoparticles can also be prepared using ‘size-focusing’. The resulting nanoparticles were separated using gel purification and found to have sizes in the range 1.5-2.5 nm, with three large nanoparticle sizes having masses of 23, 51 and 88 kDa.[105]

The carboxylate groups of MBA ligands affords water-solubility to the nanoparticles, and a study of the interfacial chemistry of 4MBA-protected gold nanoparticles has demonstrated the effect of pH on the properties of these nanoparticles. An aqueous solution of 4MBA-protected gold nanoparticles with a mean size of 6 nm at pH 9 is red; adjustment of the pH to 2 resulted in the formation of a thin-film of nanoparticles at the water-heptane interface, with the film adhering to the hydrophobic wall of the glass vial. Adjustment of the pH of the aqueous phase back to 9 resulted in the re-dispersion of the nanoparticles in the aqueous phase, restoring the red colour. Interestingly, for 4MBA-capped nanoparticles with a larger mean size (16 nm), the interfacial film of nanoparticles formed at pH 2 was not re-dispersed back into the aqueous phase when the pH was adjusted to 9.[106]

Surface-enhanced Raman scattering (SERS) spectroscopy on MBA-functionalised metallic nanoparticles has been an area of considerable interest.[107,108,109] In this

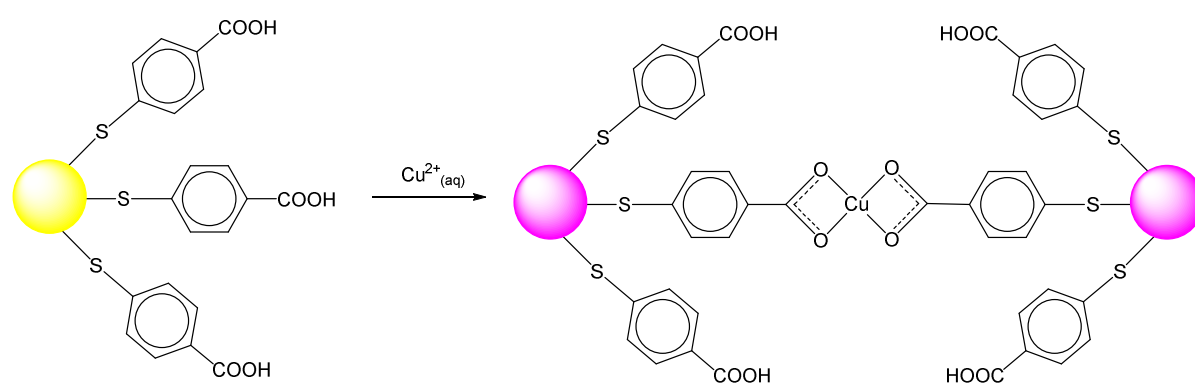
application, the MBA group is used as the Raman-active reporter molecule. MBA-capped metal nanoparticles have also been employed as a component in silica-coated metal nanoparticles which are then further derivatised with quantum dots to provide hybrid SERS and fluorescence dual mode probes, for example in cancer cell targeting.[110,111,112]

As an example, 4MBA-protected gold nanoparticles have been used to develop a “turn-off” bio-sensing method based on SERS for the detection of thrombin.[113] In this work, the synthetic arginine-based oligopeptide, Arg-Arg-Arg-Arg-Arg-Arg-Arg-Arg-Arg (Arg<sub>9</sub>) was used as the thrombin substrate. In the absence of thrombin, Arg<sub>9</sub> induces the aggregation of the 4MBA-modified Au nanoparticles, via electrostatic attractions between the negatively-charged nanoparticles and the positively-charged arginine groups. This results in a large electromagnetic coupling effect produced an enhancement of the SERS activity of the 4MBA. However, when Arg<sub>9</sub> is treated with thrombin, it is hydrolysed into Arg fragments, which have a much weaker interaction with the Au nanoparticles, resulting in reduced aggregation, and a concomitant reduction in SERS intensity. The decrease in SERS intensity can therefore be used as an assay for thrombin. Other morphologies have been MBA-functionalised for SERS applications, including gold nanostars, [ 114 , 115 , 116 ] silver nanowires,[ 117 ] gold nanowires,[ 118 ] silver-gold nanowires [117] and gold nanotubes.[117] 4MBA on silver nanoparticles has been encapsulated in a 30 nm-thick SiO<sub>2</sub> layer having small pores. This functionalised surface allowed pH to be determined through SERS detection of the 4MBA group. An advantage of this methodology was that the SiO<sub>2</sub> encapsulation prevented bovine serum albumin molecules from interfering with the surface 4MBA groups. These functional silver nanoparticles were successfully taken up by living J774A.1 macrophage cells, permitting determination of the pH of the local environment during endocytosis.[119]

As previously described for metal chalcogenide materials, MBA-functionalised metal nanoparticles can also be coupled through the carboxylic acid moiety onto other materials. For example, raspberry-like gold microspheres have been derivatised with 4MBA, and the

consequent particles then immobilised on an indium tin oxide (ITO) surface that had been functionalised with amine groups by derivatisation with  $\text{H}_2\text{N}(\text{CH}_2)_3\text{Si}(\text{OMe})_3$ , with the interaction of the carboxylic acid and amine groups providing the immobilisation pathway.[120]

4MBA-modified metal nanoparticles have been extensively employed in analytical chemistry, for example in the colorimetric determination of metal ions. Here, the aggregation of the nanoparticles mediated by the metal ion results in a colour change, which can be determined spectrophotometrically. For example, 4MBA-modified silver or gold nanoparticles have been used in the determination of  $\text{Cu}^{2+}$  ions; in the case of the Ag nanoparticles the concentration of  $\text{Cu}^{2+}$  could be determined by a colour change from bright-yellow to purple, as represented in Scheme 16.[121] Silver nanoparticles modified with  $\text{H}_2$ 4MBA and melamine have been used in the colorimetric determination of  $\text{Mn}^{2+}$  ions; there the additional use of melamine resulted in additional selectivity over 4MBA alone.[122] Similarly,  $\text{H}_2$ 3MBA-modified Au nanoparticles were shown to aggregate in the presence of  $\text{Cr}^{3+}$ ,  $\text{Pb}^{2+}$ ,  $\text{Cd}^{2+}$  and  $\text{Al}^{3+}$  ions.[123]

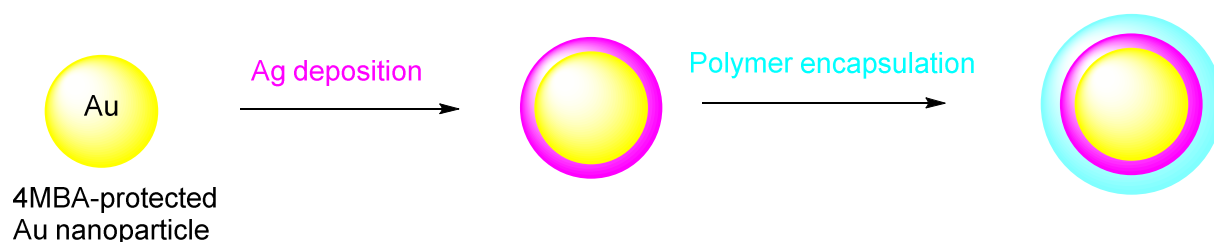


**Scheme 16** Schematic diagram showing the aggregation of 4MBA-functionalised silver nanoparticles in the presence of copper(II) ions.

p-Type silicon (100) wafers have been used as a substrate for deposition of a 4MBA SAM by simple immersion in an ethanolic solution of  $\text{H}_2$ 4MBA. The resulting SAM was used

as a substrate for the deposition of crystalline  $\text{Bi}_2\text{S}_3$  thin films, by reaction of  $\text{Bi}^{3+}$  ions and thiourea in an aqueous acidic solution.[124] The resulting  $\text{Bi}_2\text{S}_3$  crystals were found to have a rectangular parallelepiped shape, with preferential growth in the [001] direction; this contrasted with  $\text{Bi}_2\text{S}_3$  deposited on an unfunctionalised surface, which formed as quasi-spherical polycrystalline particles.

4MBA has also been ‘embedded’ in metal nanoparticles within metal layers. Thus, gold nanoparticles functionalised with 4MBA were used as a substrate for the colloidal deposition of silver. After addition of a thiol-terminated phospholipid (which was considered to replace some of the MBA molecules) and encapsulation of the nanoparticles in polystyrene-block-poly(acrylic acid), core-shell nanoparticles with embedded 4MBA molecules were obtained, as shown in Scheme 17. These materials had a large SERS enhancement as a result of the embedded MBA molecules.[125]



**Scheme 17** Formation of polymer-encapsulated core-shell AgAu nanoparticles.

There are many other applications of MBA-functionalised metal nanoparticles that have been utilised in the analysis of biologically-active molecules through SERS measurements, and developments in this area have been reviewed.[126] Examples include analysis of the neurotransmitter dopamine using ferrocene-capped gold nanoparticle/streptavidin conjugates,[127] identification of anti-biotics [128] and aflatoxin B1,[129] as well as application in live-cell imaging.[130]

The 3MBA-derived Os<sub>3</sub> cluster [Os<sub>3</sub>(CO)<sub>10</sub>(μ-H)(3MBA)] **26a** has been used to modify silver nanoparticles; TEM analysis showed the presence of spherical particles with an average size of 2.9 ± 0.6 nm. Evidence for the cluster-nanoparticle interaction was provided by: (i) a red-shift of the UV-vis absorption band, (ii) EDX spectra, which showed the presence of Os, Ag and S; (iii) IR spectroscopy, which showed a shift in the C≡O stretching band, indicating the surface interaction to be through the carboxylate group; and (iv) ToF-SIMS, which showed ions such as [Os<sub>3</sub>(CO)<sub>n</sub>(μ-H)(μ-S)]<sup>-</sup> (n = 1-10).[131]

#### 16.4 Metal surfaces

The chemistry of H<sub>2</sub>3MBA, and especially H<sub>2</sub>4MBA, on metal surfaces is extensive, and a brief discussion of this field follows on naturally from the applications in cluster and nanoparticle derivatisation. Although no attempt has been made to provide comprehensive coverage herein, the following discussion serves to illustrate the importance of the heterobifunctional MBA ligands in modifying the surface properties of metallic materials, and acting as linkers, affording functional materials having practical applications.

H<sub>2</sub>4MBA is well-known to form stable, self-assembled monolayers (SAM's) on gold and silver surfaces. An IR spectroscopic study of a SAM of 4MBA on gold showed that the carboxylic acid groups show characteristics of isolated gas-phase molecules viz. a sharp O-H stretching band, together with a non-hydrogen-bonded C=O stretch.[41] These conformationally-rigid monolayers contrast with non-rigid SAMs formed by ω-mercaptoalkanoic acids, which showed spectra features typical of hydrogen-bonding involving the carboxylic acid groups. A detailed study by Wells et al. [132] has investigated the formation of SAMs from the three isomeric H<sub>2</sub>MBA molecules on gold. Wells et al.[132] and Creager and Steiger [41] report a main sharp C≡O stretch at 1747 cm<sup>-1</sup>, together with a shoulder at 1710 cm<sup>-1</sup>, corresponding to molecules that are respectively associated and unassociated within the

SAM. This behaviour has been summarised by Zangmeister and van Zee.[133] A comparison with the SAM formed by H<sub>2</sub>3MBA showed a band at 1730 cm<sup>-1</sup> comprising several peaks, indicating that the carboxylic acid is participating in various hydrogen-bonding interactions.[132,133]

A more recent study investigated the surface chemistry of H<sub>2</sub>4MBA self-assembled on Ag(111) surfaces, and on Ag nanoparticles, using X-ray photoelectron spectroscopy, electrochemical methods and high-resolution transmission electron microscopy, coupled with computational methods (DFT). The SAM of H<sub>2</sub>4MBA molecules on the Ag(111) surface assembles in a  $\sqrt{3} \times 4$  lattice with coverage  $\theta = 0.25$ . [134]

Surface-enhanced Raman scattering (SERS) spectroscopy on MBA-functionalised metallic surfaces, like the analogous applications using metallic nanoparticles, has been of considerable interest. Studies of 4MBA monolayers on Ag and Au surfaces gave evidence for the 4MBA molecules adopting a tilted arrangement with respect to the surface when the surface modification is carried out in aqueous solutions at neutral to alkaline pH values, and with low concentrations of H<sub>2</sub>4MBA. In this situation, the MBA molecules were considered to interact with the surface through both S and CO<sub>2</sub> groups. However, at higher 4MBA concentrations (>10<sup>-3</sup> M) and/or use of acidic pHs, the 4MBA molecules have a more perpendicular arrangement, and the carboxylate groups are protonated.[135,136] The bonding of 4MBA to silver was interpreted in terms of multilayer adsorption supported by the Freundlich isotherm model; this multilayer adsorption contributes to the SERS effect.[136]

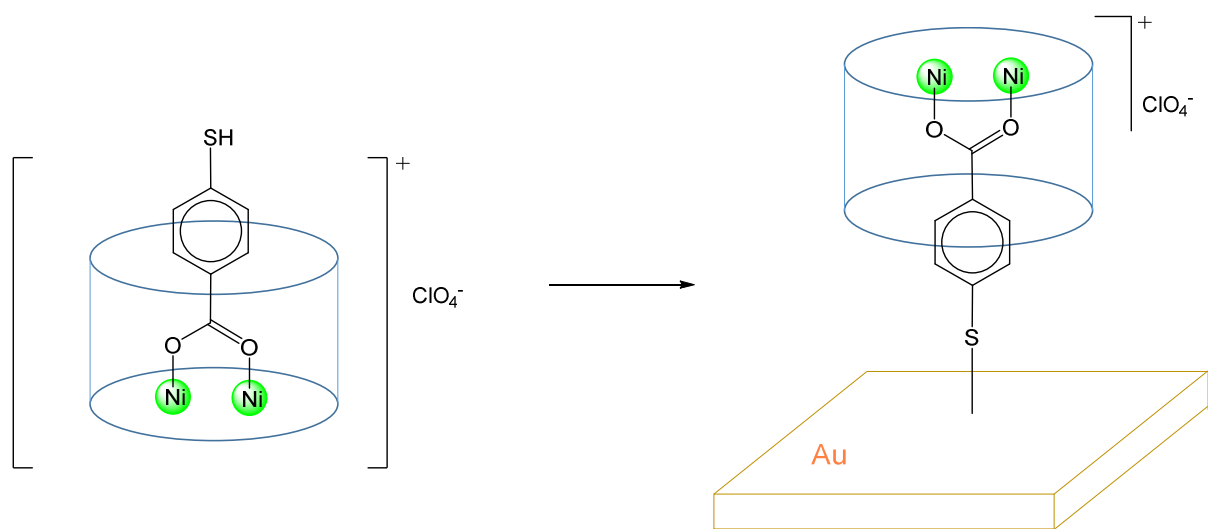
In another study,[137] SAMs formed from H<sub>2</sub>4MBA on gold surfaces have been characterised using cyclic voltammetry and Fourier transform infrared external reflection spectroscopy. The electrochemical studies showed that the application of an electric potential allows the carboxyl group to be protonated or deprotonated, dependent on the pH of the electrolyte. The formation of surface salts (with Na<sup>+</sup>, K<sup>+</sup> or Ca<sup>2+</sup> ions) was explored, with Ca<sup>2+</sup> ions quenching the field-driven protonation/deprotonation, leading to a stable carboxylate salt

thin film. The possibility of using a 4MBA SAM on gold for investigating the surface complexation of Cu(II) was investigated, but were found to be unsuitable because of the orientation of the MBA ligands.[138] SAMs of H<sub>2</sub>3MBA have been prepared using porous alumina membranes that were coated with gold using an electroless process; the resulting SAMs were characterised using SERS.[139]

A 4MBA SAM on gold has been used as a substrate for the electroless deposition of copper metal, using a basic copper sulphate solution in the presence of sodium hydrogentartrate and formaldehyde. In contrast, a bare gold surface, or a SAM derived from 3MBA, did not deposit copper, indicating that the presence and position of the carboxylic acid group is important in facilitating metal deposition. A microcontact printed surface of 4MBA on gold deposited copper only on the printed surfaces.[133]

In an interesting application involving scanning tunnelling microscopy (STM), gold tips were derivatised with MBA. The resulting chemically-modified tips were then used in order to detect the ester group of palmityl palmitate, CH<sub>3</sub>(CH<sub>2</sub>)<sub>14</sub>COO(CH<sub>2</sub>)<sub>15</sub>CH<sub>3</sub>, which was adsorbed at the interface between highly orientated pyrolytic graphite and phenyloctane. Such tips enhanced the contrast between the ester and methylene groups in the compound, due to hydrogen-bond formation facilitating electron tunnelling.[140]

The dinickel(II) macrocyclic compound derived from H<sub>2</sub>4MBA, [Ni<sub>2</sub>L(HMBA)]<sup>+</sup> **13** as its perchlorate salt (see Section 10) has been grafted onto an Au(111) single crystal using a dichloromethane solution, as shown in Scheme 18.[38,141] The resulting grafted macrocyclic complex was investigated using scanning tunnelling microscopy (STM) and X-ray photoelectron spectroscopy (XPS), showing the formation of large monolayers, with additional granular structures, anchored via the usual Au–S interaction, and showing a height of around 1.5 nm.



**13**

**Scheme 18** Schematic diagram showing the immobilisation of the macrocyclic dinickel 4MBA complex **13** onto a gold surface through the 4MBA thiol group.

Finally, H<sub>2</sub>3MBA and H<sub>2</sub>4MBA have been explored (along with a wide range of other organic molecules including organic acids, heterocyclic compounds and thiol-acids) for their applicability as corrosion inhibitors towards the aluminium alloys AA2024-T3 (containing a higher copper content, 5.3% Cu) and AA7075-T6 (containing a higher zinc content, 5.4%). H<sub>2</sub>4MBA was found to be an effective corrosion inhibitor for both alloys, while H<sub>2</sub>3MBA was a poor inhibitor for AA2024-T3 and accelerated corrosion in the case of AA7075-T6.[142,143,144] Experimental work has been supplemented by computational studies, which investigated ionisation and deprotonation energies as indicators of the effectiveness of various small molecules (including H<sub>2</sub>4MBA) as functional coatings.[145]

## 17. Conclusions

The 3MBA and 4MBA ligands have an extensive coordination chemistry, though there are fewer examples of compounds compared to the isomeric 2MBA (thiosalicylate) ligand, and complexes of some elements are not yet represented, in particular for the main group elements.

In part this is due to the inability of the 3- and 4- isomers to chelate metal centres, as is widespread for 2MBA. The 3MBA and especially the 4MBA ligands do however possess a rich structural chemistry when bound to a metal as a mono-anion through sulphur, with the resulting carboxylic acid group(s) participating in extensive hydrogen-bonding interactions in the solid-state. Furthermore, the 4MBA ligand has been shown to act as an effective heterodifunctional linker, bridging soft metal centres (gold, rhodium) with hard centres (titanium, zirconium), and it also finds applications in the functionalisation of both metal clusters, nanoparticles and surfaces, as well as metal chalcogenide and other materials. It is clear that the 3MBA and 4MBA ligands possess a rich coordination chemistry, and many new discoveries can be anticipated using these ligands.

## **18. Acknowledgements**

We thank the University of Waikato and Skim Geran Penyelidikan Trans-Diplin (TRGS; TR002-2014A), Malaysia, for financial support of this work.

## References

---

- [1] T. Wehr-Candler, W. Henderson, *Coord. Chem. Rev.* 313 (2016) 111.
- [2] J.L. Derissen, P.H. Smit, *Acta Crystallogr. A* 34 (1978) 842.
- [3] J. Powell, K. Kalakewich, F. J. Uribe-Romo, J. K. Harper, *Phys. Chem. Chem. Phys.* 18 (2016) 12541.
- [4] *Supramolecular Chemistry*, J.W. Steed, J.L. Atwood, Wiley, Chichester (2000).
- [5] K.T. Mahmudov, M.N. Kopylovich, M.F.C. Guedes da Silva, A.J.L. Pombeiro, *Coord. Chem. Rev.* (2016) in press.
- [6] G. Beobide, O. Castillo, J. Cepeda, A. Luque, S. Pérez-Yáñez, P. Román, J. Thomas-Gipson, *Coord. Chem. Rev.* 257 (2013) 2716.
- [7] D. Braga, S. d'Agostino, F. Grepioni, *Organometallics* 31 (2012) 1688.
- [8] D. Braga, L. Maini, M. Polito, F. Grepioni, *Comprehensive Organometallic Chemistry III* (Eds. D.M.P. Mingos, R.H. Crabtree) 12 (2007) 555.
- [9] D. Braga, L. Maini, M. Polito, E. Tagliavini, F. Grepioni, *Coord. Chem. Rev.* 246 (2003) 53.
- [10] D. Braga, S.L. Giaffreda, F. Grepioni, L. Maini, M. Polito, *Coord. Chem. Rev.* 250 (2006) 1267.
- [11] C. Tsoukalas, I. Pirmettis, G. Patsis, A. Papadopoulos, C.P. Raptopoulou, A. Terzis, M. Papadopoulos, E. Chiotellis, *Nucl. Med. Biol.* 28 (2001) 975; C. Tsoukalas, M.S. Papadopoulos, T. Maina, I.C. Pirmettis, B.A. Nock, C. Raptopoulou, A. Terzis, E. Chiotellis, *Nucl. Med. Biol.* 26 (1999) 297; H.J. Pietzsch, H. Spies, S. Hoffmann, *Inorg. Chim. Acta* 168 (1990) 7; H.-J. Pietzsch, H. Spies, S. Hoffmann, *Inorg. Chim. Acta* 165 (1989) 163.

- 
- [12] H.L. Steel, S.L. Allinson, J. Andre, M.P. Coogan, J.A. Platts, *Chem. Commun.* 51 (2015) 11441.
- [13] G. Jiang, M. Wang, X. Gu, T. Chen, Y. Shang, Y. Tang, G. Jiang, Y. Shi, *CrystEngComm* 16 (2014) 472.
- [14] **K. Brandenburg, DIAMOND. Visual Crystal Structure Information System, version 3.1, Crystal Impact, Bonn, Germany, 2006.**
- [15] **C.R. Groom, I.J. Bruno, M.P. Lightfoot, S.C. Ward, *Acta Crystallogr. B* 72 (2016) 171.**
- [16] T. Kamiyama, S. Enomoto, M. Inoue, *Chem. Pharm. Bull.* 33 (1985) 5184.
- [17] M. Selva, P. Tundo, *J. Org. Chem.* 71 (2006) 1464.
- [18] T.V. DeCollo, W.J. Lees, *J. Org. Chem.* 66 (2001) 4244.
- [19] Y. Jiang, Y. Qin, S. Xie, X. Zhang, J. Dong, D. Ma, *Org. Lett.* 11 (2009) 5250.
- [20] H.-J. Xu, Y.-F. Liang, Z.-Y. Cai, H.-X. Qi, C.-Y. Yang, Y.-S. Feng, *J. Org. Chem.* 76 (2011) 2296.
- [21] Y. Liu, J. Kim, H. Seo, S. Park, J. Chae, *Adv. Synth. Catal.* 357 (2015) 2205.
- [22] C.E. Rowland, N. Belai, K.E. Knope, C.L. Cahill, *Cryst. Growth. Des.* 10 (2010) 1390.
- [23] R.J.F. Berger, M.A. Schmidt, J. Juselius, D. Sundholm, P. Sirsch, H. Schmidbaur, *Z. Naturforsch. B: Chem. Sci.* 56 (2001) 979.
- [24] C. Ma, Q. Zhang, R. Zhang, L. Qiu, *J. Organomet. Chem.* 690 (2005) 3033.
- [25] J. Holeček, K. Handlříř, M. Nádvorník, A. Lyčka, *J. Organomet. Chem.* 258 (1983) 147.
- [26] Q.-F. Zhang, R.-F. Zhang, C.-L. Ma, *Acta Crystallogr. E* 61 (2005) m1923.
- [27] N.W. Ahmad, S.-A. Mohd, S. Balabaskaran, V.G.K. Das, *Appl. Organomet. Chem.* 7 (1993) 583.
- [28] Q.-F. Zhang, R.-F. Zhang, C.-L. Ma, S.W. Ng, *Acta Crystallogr. E* 61 (2005) m2374.
- [29] **E.R.T. Tiekink, *Appl. Organomet. Chem.* 5 (1991) 1.**

- 
- [30] C. Ma, Q. Zhang, R. Zhang, D. Wang, *Chem. Eur. J.* 12 (2006) 420.
- [31] U. Helmstedt, S. Lebedkin, T. Höcher, S. Blaurock, E. Hey-Hawkins, *Inorg. Chem.* 47 (2008) 5815.
- [32] O.K. Farha, J.T. Hupp, P. Deria, *PCT Int. Appl.* (2015) WO 2015117071 A1 20150806.
- [33] P. Deria, W. Bury, J.T. Hupp, O.K. Farha, *Chem. Commun.* 50 (2014) 1965.
- [34] J. Mitra, S. Sarkar, *Inorg. Chem.* 52 (2013) 3032.
- [35] S. Chowdhury, A. Canlier, N. Koshino, Y. Ikeda, *Inorg. Chim. Acta* 361 (2008) 145.
- [36] A.K. Sharma, N. Kim, C.S. Cameron, M. Lyndon, C.B. Gorman, *Inorg. Chem.* 49 (2010) 5072.
- [37] U. Helmstedt, P. Lönnecke, E. Hey-Hawkins, *Inorg. Chem.* 45 (2006) 10300.
- [38] J. Lach, A. Jeremies, D. Breite, B. Abel, B. Mahns, M. Knupfer, V. Matulis, O.A. Ivashkevich, B. Kersting, *Inorg. Chem.* 53 (2014) 10825.
- [39] K.V. Vivekananda, S. Dey, A. Wadawale, N. Bhuvanesh, V.K. Jain, *Eur. J. Inorg. Chem.* (2014) 2153.
- [40] C.-M. Che, C.-H. Li, S.S.-Y. Chui, V.A.L. Roy, K.-H. Low, *Chem. Eur. J.* 14 (2008) 2965.
- [41] S.E. Creager, C.M. Stieger, *Langmuir* 11 (1995) 1852.
- [42] J.D.E.T. Wilton-Ely, A. Schier, N.W. Mitzel, H. Schmidbaur, *J. Chem. Soc., Dalton Trans.* (2001) 1058.
- [43] K. Nomiya, S. Yamamoto, R. Noguchi, H. Yokoyama, N.C. Kasuga, K. Ohyama, C. Kato, *J. Inorg. Biochem.* 95 (2003) 208.
- [44] M. Contel, J. Fernandez-Gallardo, B.T. Elie, J.W. Ramos, *U.S. Pat. Appl. Publ.* (2015) US 20150353591 A1 20151210.

- 
- [45] J. Fernández-Gallardo, B.T. Elie, T. Sadhukha, S. Prabha, M. Sanaú, S.A. Rotenberg, J.W. Ramos, M. Contel, *Chem. Sci.* 6 (2015) 5269.
- [46] D. de Vos, D.R. Smyth, E.R.T. Tiekink, *Metal Based Drugs* 8 (2002) 303.
- [47] D.R. Smyth, B.R. Vincent, E.R.T. Tiekink, *Z. Kristallogr.* 216 (2009) 298.
- [48] **E.R.T. Tiekink, *Coord. Chem. Rev.* 275 (2014) 130.**
- [49] R. Noguchi, A. Hara, A. Sugie, K. Nomiya, *Inorg. Chem. Commun.* 9 (2006) 355.
- [50] J.D.E.T. Wilton-Ely, H. Ehlich, A. Schier, H. Schmidbaur, *Helv. Chim. Acta* 84 (2001) 3216.
- [51] Y.F. Mui, J. Fernández-Gallardo, B.T. Elie, A. Gubran, I. Maluenda, M. Sanaú, O. Navarro, M. Contel, *Organometallics* 35 (2016) 1218.
- [52] C. Domínguez, B. Heinrich, B. Donnio, S. Coco, P. Espinet, *Chem. Eur. J.* 19 (2013) 5988.
- [53] J.H. Waldo, *J. Am. Chem. Soc.* 53 (1931) 992.
- [54] J.H. Waldo, H.A. Shonle, H.M. Powell, *J. Bacteriol.* 21 (1931) 323.
- [55] E.R. Souza, J.H.S.K. Monteiro, I.O. Mazali, F.A. Sigoli, *J. Luminescence* 170 (2016) 520.
- [56] J. Cuan, B. Yan, *RSC Adv.* 3 (2013) 20077.
- [57] J. Cuan, B. Yan, *Micopor. Mesopor. Mater.* 183 (2014) 9.
- [58] U. Helmstedt, P. Lonneck, J. Reinhold, E. Hey-Hawkins, *Eur. J. Inorg. Chem.* (2006) 4922.
- [59] **J.P. Fackler Jr, R.J. Staples, A. Elduque, T. Grant, *Acta Crystallogr. C* 50 (1994) 520.**
- [60] Y. Liang, J.E. Thorne, B.A. Parkinson, *Langmuir* 28 (2012) 11072.
- [61] J.G.C. Veinot, J. Galloro, L. Pugliese, R. Pestrin, W.J. Pietro, *Chem. Mater.* 11 (1999) 642.

- 
- [62] D. Zhou, M. Lin, Z. Chen, H. Sun, H. Zhang, H. Sun, B. Yang, *Chem. Mater.* 23 (2011) 4857.
- [63] Z.-Y. Chen, H.N. Abdelhamid, H.-F. Wu, *Rapid Commun. Mass Spectrom.* 30 (2016) 1403.
- [64] J. Chang, H. Xia, S. Wu, S. Zhang, *J. Mater. Chem. C* 2 (2014) 2939.
- [65] G. Qian, Y. Lin, G. Wantz, A.R. Davis, K.R. Carter, J.J. Watkins, *Adv. Funct. Mater.* 24 (2014) 4484.
- [66] R.S. Dibbell, D.G. Youker, D.F. Watson, *J. Phys. Chem. C* 113 (2009) 18643.
- [67] N. Guijarro, Q. Shen, S. Giménez, I. Mora-Seró, J. Bisquert, T. Lana-Villarreal, T. Toyoda, R. Gómez, *J. Phys. Chem. C* 114 (2010) 22353.
- [68] Y. Liang, J.E. Thorne, M.E. Kern, B.A. Parkinson, *Langmuir* 30 (2014) 12551.
- [69] J. Wei, C. Zhang, Z. Du, H. Li, W. Zou, *J. Mater. Chem. C* 2 (2014) 4177.
- [70] T.-W. Duan, B. Yan, *CrystEngComm* 16 (2014) 3395.
- [71] Y. Zhao, B. Yan, *Photochem. Photobiol.* 88 (2012) 21.
- [72] G.J. Stasiuk, S. Tamang, D. Imbert, C. Gateau, P. Reiss, P. Fries, M. Mazzanti, *Dalton Trans.* 42 (2013) 8197.
- [73] C. Li, W.K. Leong, *J. Organomet. Chem.* 693 (2008) 1292
- [74] M. Brust, M. Walker, D. Bethell, D.J. Schiffrin, R. Whyman, *J. Chem. Soc., Chem Commun.* (1994) 801.
- [75] M. Brust, J. Fink, D. Bethell, D.J. Schiffrin, C. Kiely, *J. Chem. Soc., Chem. Commun.* (1995) 1655.
- [76] H. Qian, M. Zhu, Z. Wu, R. Jin, *Acc. Chem. Res.* 45 (2012) 1470.
- [77] N. Goswami, Q. Yao, T. Chen, J. Xie, *Coord. Chem. Rev.* 329 (2016) 1.
- [78] R. Jin, C. Zeng, M. Zhou, Y. Chen, *Chem. Rev.* 116 (2016) 10346.
- [79] H. Häkkinen, *Chem. Soc. Rev.* 37 (2008) 1847.

- 
- [80] R. Jin, *Nanoscale* 2 (2010) 343.
- [81] M. Giersig, P. Mulvaney, *Langmuir* 9 (1993) 3408.
- [82] O.M. Bakr, V. Amendola, C.M. Aikens, W. Wenseleers, R. Li, L. Dal Negro, G.C. Schatz, F. Stellacci, *Angew. Chem.* 121 (2009) 6035.
- [83] M.W. Heaven, A. Dass, P.S. White, K.M. Holt, R.W. Murray, *J. Am. Chem. Soc.* 130 (2008) 3754.
- [84] A. Tlahuice-Flores, R.L. Whetten, M. Jose-Yacaman, *J. Phys. Chem.* 117 (2013) 20867.
- [85] J. Jung, S. Kang, Y.-K. Han, *Nanoscale* 4 (2012) 4206.
- [86] Z. Luo, V. Nachammai, B. Zhang, N. Yan, D.T. Leong, D. Jiang, J. Xie, *J. Am. Chem. Soc.* 136 (2014) 10577.
- [87] A. Desireddy, B.E. Conn, J. Guo, B. Yoon, R.N. Barnett, B.M. Monahan, K. Kirschbaum, W.P. Griffith, R.L. Whetten, U. Landman, T.P. Bigioni, *Nature* 501 (2013) 399.
- [88] B.E. Conn, A. Desireddy, A. Atnagulov, S. Wickramasinghe, B. Bhattarai, B. Yoon, R.N. Barnett, Y. Abdollahian, Y.W. Kim, W.P. Griffith, S.R.J. Oliver, U. Landman, T.P. Bigioni, *J. Phys. Chem. C* 119 (2015) 11238.
- [89] L.G. Abdul Halim, S. Ashraf, K. Katsiev, A.R. Kirmani, N. Kothalawala, D.H. Anjum, S. Abbas, A. Amassian, F. Stellacci, A. Dass, I. Hussain, O.M. Bakr, *J. Mater. Chem. A* 1 (2013) 10148.
- [90] O.D. Villarreal, L.Y. Chen, R.L. Whetten, B. Demeler, *J. Phys. Chem. B* 119 (2015) 15502.
- [91] P.D. Jadzinsky, G. Calero, C.J. Ackerson, D.A. Bushnell, R.D. Kornberg, *Science* 318 (2007) 430.

- 
- [92] Y. Levi-Kalisman, P.D. Jadzinsky, N. Kalisman, H. Tsunoyama, T. Tsukuda, D.A. Bushnell, R. D. Kornberg, *J. Am. Chem. Soc.* 133 (2011) 2976.
- [93] S. Knoppe, O.A. Wong, S. Malola, H. Häkkinen, T. Bürgi, T. Verbiest, C.J. Ackerson, *J. Am. Chem. Soc.* 136 (2014) 4129.
- [94] Y. Li, G. Galli, F. Gygi, *ACS Nano* 2 (2008) 1896.
- [95] Y.-K. Han, H. Kim, J. Jung, Y. C. Choi, *J. Phys. Chem. C* 114 (2010) 7548.
- [96] M. Walter, J. Akola, O. Lopez-Acevedo, P.D. Jadzinsky, G. Calero, C.J. Ackerson, R.L. Whetten, H. Grönbeck, H. Häkkinen, *Proc. Nat. Acad. Sci.* 105 (2008) 9157.
- [97] H. Schnöckel, A. Schnepf, R.L. Whetten, C. Schenk, P. Henke, *Z. Anorg. Allg. Chem.* 637 (2011) 15.
- [98] E. Hulkko, O. Lopez-Acevedo, J. Koivisto, Y. Levi-Kalisman, R.D. Kornberg, M. Pettersson, H. Häkkinen, *J. Am. Chem. Soc.* 133 (2011) 3752.
- [99] C.L. Heinecke, W.W. Ni, S. Malola, V. Mäkinen, O.A. Wong, H. Häkkinen, C.J. Ackerson, *J. Am. Chem. Soc.* 134 (2012) 13316.
- [100] M.-C. Bowman, T.E. Ballard, C.J. Ackerson, D.L. Feldheim, D.M. Margolis, C. Melander, *J. Am. Chem. Soc.* 130 (2008) 6896.
- [101] O.A. Wong, C.L. Heinecke, A.R. Simone, R.L. Whetten, C.J. Ackerson, *Nanoscale* 4 (2012) 4099.
- [102] C.J. Ackerson, P.D. Jadzinsky, J.Z. Sexton, D.A. Bushnell, R.D. Kornberg, *Bioconjugate Chem.* 21 (2010) 214.
- [103] A. Gole, C.J. Murphy, *Chem. Mater.* 16 (2004) 3633.
- [104] M. Azubel, R.D. Kornberg, *Nano Lett.* 16 (2016) 3348.
- [105] L.M. Tvedte, C.J. Ackerson, *J. Phys. Chem. A* 118 (2014) 8124.
- [106] F. Reincke, W.K. Kegel, H. Zhang, M. Nolte, D. Wang, D. Vanmaekelbergh, H. Möhwald, *Phys. Chem. Chem. Phys.* 8 (2006) 3828.

- 
- [107] P.N. Njoki, I.-I.S. Lim, D. Mott, H.-Y. Park, B. Khan, S. Mishra, R. Sujakumar, J. Luo, C.-J. Zhong, *J. Phys. Chem. C* 111 (2007) 14664.
- [108] C. Song, J. Chen, Y. Zhao, L. Wang, *J. Mater. Chem. B* 2 (2014) 7488.
- [109] W. Xu, S. Xu, X. Ji, B. Song, H. Yuan, L. Ma, Y. Bai, *Colloids and Surfaces B: Biointerfaces* 40 (2005) 169.
- [110] S. Zong, Z. Wang, J. Yang, C. Wang, S. Xu, Y. Cui, *Talanta* 97 (2012) 368.
- [111] Z. Wang, H. Wu, C. Wang, S. Xu, Y. Cui, *J. Mater. Chem.* 21 (2011) 4307.
- [112] Z. Wang, S. Zong, W. Li, C. Wang, S. Xu, H. Chen, Y. Cui, *J. Am. Chem. Soc.* 134 (2012) 2993.
- [113] Z. Wu, Y. Liu, X. Zhou, A. Shen, J. Hu, *Biosensors and Bioelectronics* 44 (2013) 10.
- [114] C.G. Khoury, T. Vo-Dinh, *J. Phys. Chem. C* 112 (2008) 18849.
- [115] C. Hrelescu, T.K. Sau, A.L. Rogach, F. Jäckel, J. Feldmann, *Appl. Phys. Lett.* 94 (2009) 153113.
- [116] A.S.D.S. Indrasekara, S. Meyers, S. Shubeita, L.C. Feldman, T. Gustafsson, L. Fabris *Nanoscale* 6 (2014) 8891.
- [117] S.E. Hunyadi, C.J. Murphy, *J. Mater. Chem.* 16 (2006) 3929.
- [118] H. Feng, Y. Yang, Y. You, G. Li, J. Guo, T. Yu, Z. Shen, T. Wu, B. Xing, *Chem. Commun.* (2009) 1984.
- [119] F. Wang, R.G. Widejko, Z. Yang, K.T. Nguyen, H. Chen, L.P. Fernando, K.A. Christensen, J.N. Anker, *Anal. Chem.* 84 (2012) 8013.
- [120] Z. Li, V. Ravaine, S. Ravaine, P. Garrigue, A. Kuhn, *Adv. Funct. Mater.* 17 (2007) 618.
- [121] Y. Zhou, H. Zhao, Y. He, N. Ding, Q. Cao, *Colloids and Surfaces A: Physicochem. Eng. Aspects* 391 (2011) 179.
- [122] Y. Zhou, H. Zhao, C. Li, P. He, W. Peng, L. Yuan, L. Zeng, Y. He, *Talanta* 97 (2012) 331.

- 
- [123] Y.-Q. Dang, H.-W. Li, B. Wang, L. Li, Y. Wu, *Appl. Mater. Interfaces* 7 (2009) 1533.
- [124] S.-C. Liufu, L.-D. Chen, Q. Wang, Q. Yao, *Cryst. Growth Des.* 7 (2007) 639.
- [125] Y. Feng, Y. Wang, H. Wang, T. Chen, Y.Y. Tay, L. Yao, Q. Yan, S. Li, H. Chen, *Small* 8 (2012) 246.
- [126] D. Drescher, J. Kneipp, *Chem. Soc. Rev.* 41 (2012) 5780.
- [127] L. Liu, J. Du, S. Li, B. Yuan, H. Han, M. Jing, N. Xia, *Biosensors and Bioelectronics* 41 (2013) 730.
- [128] J. Bresee, K.E. Maier, C. Melander, D.L. Feldheim, *Chem. Commun.* 46 (2010) 7516.
- [129] A. Sharma, Z. Matharu, G. Sumana, P.R. Solanki, C.G. Kim, B.D. Malhotra, *Thin Solid Films* 519 (2010) 1213.
- [130] G. Zhang, G. Qu, Y. Chen, A. Shen, W. Xie, X. Zhou, J. Hu, *J. Mater. Chem. B* 1 (2013) 4364.
- [131] C. Li, W.Y. Fan, W.K. Leong, *J. Phys. Chem. C*, 113 (2009) 18562.
- [132] M. Wells, D.L. Dermody, H.C. Yang, T. Kim, R.M. Crooks, A.J. Ricco, *Langmuir* 12 (1996) 1989.
- [133] C.D. Zangmeister, R.D. van Zee, *Langmuir* 19 (2003) 8065.
- [134] J.V.M. Girón, E. Zelaya, A. Rubert, G. Benítez, P. Carro, R.C. Salvarezza, M.E. Vela, *J. Phys. Chem. C* 117 (2013) 24967.
- [135] A. Michota, J. Bukowska, *J. Raman Spectrosc.* 34 (2003) 21.
- [136] C.-H. Ho, S. Lee, *Colloids and Surfaces A: Physicochem. Eng. Aspects* 474 (2015) 29.
- [137] S.M. Rosendahl, I.J. Burgess, *Electrochim. Acta* 53 (2008) 6759.
- [138] E. Repo, E. Ahlberg, L. Murtomäki, K. Kontturi, D.J. Schiffrin, *Electrochim. Acta* 54 (2009) 6584.
- [139] L. Velleman, J.-L. Bruneel, F. Guillaume, D. Losic, J.G. Shapter, *Phys. Chem. Chem. Phys.* 13 (2011) 19587.

- 
- [140] C. Volcke, P. Simonis, F. Durant, P.A. Thiry, P. Lambin, C. Culot, C. Humbert, *Chem. Eur. J.* 11 (2005) 4185.
- [141] C. Salazar, J. Lach, F. Ruckerl, D. Baumann, S. Schimmel, M. Knupfer, B. Kersting, B. Büchner, C. Hess, *Langmuir* 32 (2016) 4464.
- [142] D.A. Winkler, M. Breedon, A.E. Hughes, F.R. Burden, A.S. Barnard, T.G. Harvey, I. Cole, *Green Chem.* 16 (2014) 3349.
- [143] T.G. Harvey, S.G. Hardin, A.E. Hughes, T.H. Muster, P.A. White, T.A. Markley, P.A. Corrigan, J. Mardel, S.J. Garcia, J.M.C. Mol, A.M. Glenn, *Corrosion Sci.* 53 (2011) 2184.
- [144] D.A. Winkler, M. Breedon, P. White, A.E. Hughes, E.D. Sapper, I. Cole, *Corrosion Sci.* 106 (2016) 229.
- [145] M. Breedon, M.C. Per, I.S. Cole, A.S. Barnard, *J. Mater. Chem A* 2 (2014) 16660.